CHEMICAL ANALYSIS OF DIESEL NANOPARTICLES USING A NANO-DMA/THERMAL DESORPTION PARTICLE BEAM MASS SPECTROMETER

Final Report

CRC Project No. E-43-4

Prepared by:

Principal Investigator
Professor Paul J. Ziemann
University of California-Riverside

Dr. Hiromu Sakurai
University of Minnesota

Subcontractor:
Peter H. McMurry
University of Minnesota

April 2002

Prepared for:

California Environmental Protection Agency

Air Resources Board
1001 I Street - Sacramento, California 95814

and

Coordinating Research Council, Inc.
3650 Mansell Road, Suite 140 - Alpharetta, Georgia 30022

CHEMICAL ANALYSIS OF DIESEL NANOPARTICLES USING A NANO-DMA/THERMAL DESORPTION PARTICLE BEAM MASS SPECTROMETER

Final Report

CRC Project No. E-43-4

Prepared by:
Principal Investigator

Professor Paul J. Ziemann
Air Pollution Research Center
University of California
Riverside, CA 92521
Phone: 909-787-5127
Fax: 909-787-5004
Email: paul.ziemann@ucr.edu

Dr. Hiromu Sakurai
Particle Technology Laboratory
Department of Mechanical Engineering
University of Minnesota
Minneapolis, MA 55455

Subcontractor

Peter H. McMurry
Particle Technology Laboratory
Department of Mechanical Engineering
University of Minnesota
Minneapolis, MA 55455

April 2002

TABLE OF CONTENTS

Page

TABLE OF CONTENTS

Page

1. SUMMARY

This report describes the results of Phase 2 of our project, “Chemical Analysis of Diesel Nanoparticles Using a Nano-DMA/Thermal Desorption Particle Beam Mass Spectrometer,” CRC Contract No. E-43-4. The project was a collaboration between the research groups of Professor Paul Ziemann at the University of California, Riverside (UCR) and Professor Peter McMurry at the University of Minnesota (UMN) and covered the period 9/8/2000-12/31/2001. Professor David Kittelson, also from UMN, was a key collaborator on the project but was not funded by this grant. The primary activities of Phase 2 involved two studies of diesel nanoparticles carried out at the University of Minnesota Center for Diesel Research (UMNCDR), one on a Caterpillar engine and the other on a Cummins engine. The studies were performed in approximately November 2000 and July 2001, respectively. The engines were operated on an EPA Pump fuel (360 ppm S), California fuel (50 and 96 ppm S), and Fischer-Tropsch fuel (< 1ppm S), and at different engine loads. The measurements included Nano-DMA/TDPBMS analyses of particle composition similar to those performed in Phase 1, as well as tandem differential mobility analyses (TDMA) of particle volatility and hygroscopicity (i.e., water uptake). Preliminary TDMA measurements were made in the Caterpillar study, followed by an extensive set of measurements in the Cummins study. The data analysis for both studies has been completed, and this document represents the final report on the results.

The primary objective of this project was to use the Nano-DMA/TDPBMS to obtain information on the chemical composition of diesel nanoparticles formed in a laboratory environment under various engine operating conditions. The focus was to be on the chemistry of nucleation-mode particles, but larger particles would also be analyzed for comparison. The goal was to use the composition data in conjunction with measured particle physical properties (e.g., size, concentration, etc.) to develop an understanding of the chemical mechanisms by which nanoparticles are formed in diesel exhaust. Such knowledge would be important for determining modifications in engine design, operation, fuel, lubricating oil, or after-treatment that might be made in order to ameliorate the problem of nanoparticle formation.

The general conclusion is that the studies have been a clear success. The primary objective of the project was achieved, in that a wealth of new and important information was obtained on diesel nanoparticle composition, particle properties, and formation processes. Most of the specific objectives of this project were either accomplished as planned or, when original methodologies proved inadequate, new approaches were developed to achieve the goals. This is the first time that particles in the nanoparticle size mode have been cleanly sampled from a diesel engine and chemically analyzed. These studies have clearly demonstrated the power of the Nano-DMA/TDPBMS and TDMA techniques for diesel particle analysis.

Some of the major conclusions from this work are that (1) the Nano-DMA/TDPBMS and TDMA are valuable analytical tools which can provide information on the size-dependent composition of diesel particles, their mixing characteristics, and particle formation processes. For the conditions investigated the results indicate that (2) the organic component of total diesel particles and nanoparticles is comprised predominantly of unburned lubricating oil, (3) low-volatility organic oxidation products (e.g., organic acids) and PAHs, which have been detected in low concentrations in previous GC-MS analyses by others, are only a minor component of the total particle and nanoparticle organic mass, (4) the major organic compound classes (alkanes, cycloalkanes, and aromatics) appear to be distributed relatively uniformly across the volatility spectrum, (5) nanoparticles formed with high sulfur EPA Pump fuel contain small amounts of sulfuric acid, which may enhance particle nucleation, whereas those formed with lower sulfur California fuel show no evidence for sulfuric acid, (6) nuclei-mode particles and accumulation-mode particles are externally mixed across a wide size range, with the chemical components being distributed between two particle types: (a) “less volatile” particles, comprised of a significant non-volatile core (probably elemental carbon) and an organic component, and (b) “more volatile” particles, containing predominantly organics and sometimes small amounts of sulfuric acid, with the volatile components contributing more than 99% of the “more volatile” nanoparticle mass, (7) residual species < 4 nm in diameter detected when “more volatile” particles are evaporated at high temperatures may be non-volatile cores (soot or metal oxide), or single molecules or molecular clusters of low-volatility organic compounds, and (8) the volatility of nanoparticle components exhibits no dependence on fuel or engine load.

The general model of diesel nanoparticle formation and chemistry that emerges from these results is that nucleation involves either a multicomponent mixture of some combination of low volatility organics, sulfuric acid, water, and ammonia, or formation of non-volatile nuclei of either elemental carbon or metal oxide. This still appears to be an open question, and both processes may be operating, depending on conditions. Once nucleation occurs, growth appears to involve condensation of organic compounds coming primarily from unburned lubricating oil. The resulting particles are an external mixture, some of which are nearly completely volatile (within detection limits), whereas others contain a significant non-volatile core. The resulting nuclei-mode particles are predominantly the “more volatile” particles, whereas the accumulation mode is predominantly the “less volatile” particles.

2. PROJECT BACKGROUND

Recent epidemiological studies have found an association between atmospheric fine particle (diameter < 2.5 μm) mass concentrations, and exacerbation of illness in people with respiratory disease and increased mortality among older people with respiratory and cardiovascular disease (1, 2). These studies have led the U.S. Environmental Protection Agency to promulgate a new fine particle standard, which is somewhat controversial and has been subjected to legal challenges. Unlike air quality standards for gaseous compounds such as ozone or carbon monoxide, the particle standard is based on particulate mass without regard to chemical composition. Because of the complex nature of atmospheric particulate matter, developing a possible mechanism for health effects will require more detailed knowledge of the size-dependent chemical composition of fine particles.

One important source of fine particles is combustion, which occurs both naturally and through human activities. Modern combustion engines burn cleaner and produce less particulate mass than older models, but it has also been observed that some engines, for example diesels, emit high concentrations of a subset of fine particles called nanoparticles (diameter < 50 nm) (3). The chemistry of nanoparticles may be worthy of special concern because some laboratory studies suggest an even stronger link between adverse health effects and smaller particles (4-7), and the strength of the response depends on composition (6). If it is concluded that nanoparticle emissions should be reduced, then a knowledge of nanoparticle composition will also be important for understanding the physical and chemical mechanisms by which they are formed.

Such information is necessary to help establish criteria for engine design, operation, fuel and lubricating oil modifications, and after-treatment that would help reduce nanoparticle formation. Unfortunately, due to the small size and low mass concentration of nanoparticles, chemical analysis of these species is difficult.

In an effort to further understand the problem of nanoparticle formation and develop reliable sampling and measurement techniques, the Coordinating Research Council recently funded a research project (CRC E-43) headed by the University of Minnesota Center for Diesel Research (UMNCDR), titled "Diesel Aerosol Sampling Methodology."

The major objectives of CRC E-43 were to:

1) Determine actual particle size distributions and particle number concentrations in the exhaust plume from heavy diesel vehicles operated on the road.

2) Compare that information with data generated in emission test facilities to determine if current sampling and analysis methods are adequate for characterizing particle size.

3) Examine particle transformations as the plume disperses downwind of the roadway in a typical urban situation. The goal of this objective is to determine the zone of influence of the ultrafine particle fraction of the emissions from the roadway.

4) Characterize the bulk diesel particulate matter chemical composition and to determine surface properties and composition.

The general approach used to meet these objectives was to first employ a mobile laboratory to measure the particle size distributions and number concentrations in the on-road exhaust plume from diesel test vehicles (from Cummins and Caterpillar), and then carry out laboratory experiments using a dilution system and wind tunnel facility to reproduce these distributions when the same vehicles/engines were run under similar operating conditions on a chassis dynamometer. In addition, a number of techniques were employed to obtain information on the chemical composition of the aerosol. The results of these experiments will be used to determine the major processes that influence the size distribution and number concentration of diesel exhaust particles, and to develop laboratory measurement techniques that will yield size distribution and concentration data that are representative of the on-road conditions. The results of the on-road measurements will also be used in models for understanding plume dispersion.

As originally planned, most of the aerosol measurements being made were to characterize physical properties of the particles, including the size distribution, number concentration, and surface area. Only limited data on chemistry (especially in real time) was to be obtained because of available sampling and analysis tools. The only real-time information on particle composition would come from a photoelectric aerosol sensor that is used to measure the surface-bound concentration of polycyclic aromatic hydrocarbons (PAHs). Some off-line chemical analyses for elemental and organic carbon, sulfate, and metals in particles collected using a microorifice uniform deposit impactor (MOUDI) (8) were also planned. It was also possible that gas chromatography-mass spectrometry (GC-MS) analysis would be performed to obtain more detailed information on organic speciation. One of the problems with this approach is that diesel nanoparticle samples collected using impactors are subject to artifacts, for a couple of reasons. Impactor stages having cut-points smaller than the mass median diameter of the sampled aerosol are particularly prone to errors associated with particle bounce. This is because bounce of even a small fraction of particles from larger stages can add significantly to the very small mass collected on the nanoparticle stage. In addition, the aerodynamic size of diesel chain agglomerates is much smaller than their mobility equivalent size. An investigation by the Kittelson group of MOUDI performance with diesel particles found much higher than expected concentrations of particles larger than 100 nm electrical mobility diameter downstream of the 56 nm stage of the MOUDI. This is believed to be due to a combination of particle bounce and the low effective densities of carbonaceous agglomerates. Furthermore, recent studies by the McMurry group comparing mass distributions of diesel nanoparticles using a tandem differential mobility analyzer, an aerosol particle mass analyzer, and a Nano-MOUDI show that the Nano-MOUDI stages are dominated by particle bounce. Therefore, particles collected on nanoparticle impactor stages may contain relatively large chain agglomerates as well as small droplets formed by condensation. Other sampling artifacts that arise during impactor sampling are adsorption of vapors and volatilization of collected particles (9, 10).

In an attempt to obtain compositional information on “clean” nanoparticle samples, the project described here used a nano-differential mobility analyzer (Nano-DMA) (11) to size-select nanoparticles produced from diesel engine exhaust for subsequent chemical analysis by thermal desorption particle beam mass spectrometry (TDPBMS) (12-15). The Nano-DMA provides high concentrations of size-selected nanoparticles without significant contamination from larger particles, and the TDPBMS can be used for real-time quantitative analysis of the organic composition of aerosols within the ~20-500 nm particle diameter size range (13).

3. OBJECTIVES

The primary objective of this project was to use the Nano-DMA/TDPBMS to obtain information on the chemical composition of diesel nanoparticles formed in a laboratory environment under various engine operating conditions. The focus was to be on the chemistry of nucleation-mode particles, but larger particles would also be analyzed for comparison. The goal was to use the composition data in conjunction with measured particle physical properties (e.g., size, concentration, etc.) to develop an understanding of the chemical mechanisms by which nanoparticles are formed in diesel exhaust. Such knowledge would be important for determining modifications in engine design, operation, fuel, lubricating oil, or after-treatment that might be made in order to ameliorate the problem of nanoparticle formation.

The specific objectives of this two-year research program were to:

1) Optimize operation of unipolar charger /Nano-DMA apparatus for obtaining size-selected diesel nanoparticles for TDPBMS analysis under various engine operating conditions.

2) Characterize particle beam focusing properties of aerodynamic lenses with spherical and diesel nanoparticles in order to determine size-dependent sampling efficiencies and gain information on diesel particle shape and its potential effect on sampling bias.

3) Characterize particle focusing properties of electrostatic and/or electrodynamic lenses with nucleation-mode size (<20 nm diameter) diesel nanoparticles in order to determine whether this lens system can improve the efficiencies with which nucleation-mode diesel particles can be sampled into the TDPBMS.

4) Determine the detection limits for TDPBMS analysis after the addition of an energy analyzer and new vaporizer.

5) Investigate the ability of temperature-programmed TDPBMS to analyze diesel fuel and lubricating oil, and investigate the use of high vaporization cell temperature and high electron energy to enhance the real-time TDPBMS signal intensity of PAHs relative to other species.

6) Use the Nano-DMA/TDPBMS to obtain real-time mass spectral/chemical composition data on diesel nanoparticles under various engine operating conditions.

7) Use temperature-programmed TDPBMS of collected size-selected particles to identify compounds present in diesel exhaust nanoparticles of complex composition. These measurements can also be used to estimate compound vapor pressures.

8) Identify the major PAHs in size-selected diesel nanoparticles by using high vaporization cell temperature and high electron energy to enhance the real-time Nano-DMA/TDPBMS signal intensity of PAHs relative to other species.

Objectives 1-3 were to be addressed by Professor Peter McMurry and coworkers at UMN, objectives 4-5 by Professor Paul Ziemann and coworkers at UCR, with objectives 6-8 involving measurements with the combined Nano-DMA/TDPBMS and the participation of both research groups.

4. APPROACH

The research program was designed to accomplish the objectives through a combination of instrument development and characterization studies at UMN and UCR, followed by a diesel particle emission study at UMNCDR. If Phase 1 was successful, it was planned that Phase 2 would take place. This was to involve participation in a Caterpillar study planned for Summer 2000 as part of the "Diesel Aerosol Sampling Methodology" study, and measurements in 2001 at the Cummins facilities. This approach was essentially followed, except that the Caterpillar and Cummins studies were performed at the UMNCDR, as described below.

5. SUMMARY OF PROGRESS ON PROJECT OBJECTIVES

Most of the specific objectives of this project were either accomplished as planned or, when original methodologies proved inadequate, new approaches were developed to achieve the goals. The primary objective of the project was clearly achieved, in that a wealth of new and important information was obtained on diesel nanoparticle composition, properties, and formation processes.

<u>Progress on the specific objectives of the project was as follows:</u>

1) Optimization of the unipolar charger /Nano-DMA apparatus for obtaining size-selected diesel nanoparticles for TDPBMS analysis was begun prior to the John Deere study in Phase 1 and completed prior to the Caterpillar study in Phase 2. This system was used in all three diesel studies.

2) The particle beam focusing properties of aerodynamic lenses with spherical and diesel nanoparticles was not investigated due to lack of time and access to the diesel engine. However, previous measurements on spherical nanoparticle focusing, and tandem differential mobility analysis (TDMA) of diesel particles made during the Cummins study in Phase 2 provided information on spherical (organic) and nonspherical (soot) nanoparticles for an evaluation of potential particle shape effects on sampling bias.

3) Evaluation of the particle focusing properties of electrostatic lenses with nucleation-mode size (<20 nm diameter) particles was begun prior to the John Deere study in Phase 1 and completed by the end of that study. It was determined that the lens system could not significantly improve the efficiencies with which nucleation-mode diesel particles could be sampled into the TDPBMS. Electrostatic focusing was therefore not employed in the diesel studies.

4) The detection limits for TDPBMS analysis using an energy analyzer and new vaporizer were evaluated prior to the John Deere study in Phase 1. It was determined that the detection limits should be adequate for analysis of diesel nanoparticles, although the new vaporizer did not improve the instrument performance. The detection limits proved to be sufficient for nanoparticle analysis in all three diesel studies.

5) The use of temperature-programmed TDPBMS for analysis of diesel fuel and lubricating oil, and the use of high vaporization temperature and high electron energy for PAH analysis were investigated before and during the John Deere study in Phase 1. It was determined that temperature-programmed TDPBMS could provide useful information on fuel and oil composition, but not PAHs because of their low concentrations. The technique was used to analyze fuel and oil in all three diesel studies.

6) The Nano-DMA/TDPBMS was sufficiently sensitive to obtain real-time mass spectral/chemical composition information on total diesel particles, but not size-selected nanoparticles. Real-time TDPBMS was used to analyze total diesel particles in all three diesel studies.

7) Temperature-programmed TDPBMS was sufficiently sensitive to obtain mass spectral chemical composition information on diesel nanoparticles. The technique was used in all three diesel studies to analyze total particles and size-selected nanoparticles. Information was obtained on various organic classes and sulfuric acid present in nanoparticles, and measurements on total particles were used to estimate compound vapor pressures.

8) Because the use of high vaporization temperature and high electron energy did not sufficiently enhance the signal of PAHs relative to other compounds (objective 5), this technique was not used during the diesel studies to identify the major PAHs in size-selected diesel nanoparticles.

In addition to the work described above, measurements of diesel particle volatility and water uptake were made by the McMurry group that were not part of the original proposal, but which added enormously to the success of the project. The volatility measurements provided information on nanoparticle composition and particle mixing characteristics (i.e., the extent to which volatile and non-volatile components are mixed in the aerosol), while water uptake measurements yielded information on sulfuric acid content.

<u>The additional measurements were as follows:</u>

1) The volatility and hygroscopicity (water uptake) of diesel particles (diameter 3-50 nm) were investigated using a Nano-Tandem Differential Mobility Analyzer. These measurements were paid for through the E-43-4 grant, but the development and characterization of the Nano-TDMA was supported in part by U.S. Department of Energy grant DOE DE-FG02-98ER62556 “Nucleation and Growth of Atmospheric Aerosols.”

2) The volatility and hygroscopicity of diesel particles (diameter 10-200 nm) were investigated using a Regular-Tandem Differential Mobility Analyzer-Aerosol Particle Mass Analyzer. These measurements were supported by the Environmental Protection Agency through Grant Number R 826372-01-0 to the Georgia Institute of Technology and GIT Subcontract Number G-35-W62-G1 to the University of Minnesota. This work has not been subjected to the Agency’s required peer and policy review and therefore does not necessarily reflect the views of the Agency and no official endorsement should be inferred.

5.1. SUMMARY OF PHASE 1 RESULTS

This project involved a collaboration between the research groups of Professor Paul Ziemann at the University of California, Riverside (UCR) and Professor Peter McMurry at the University of Minnesota (UMN). Phase 1 of the project covered the period 2/7/2000-9/7/2000, and included preliminary experiments at UCR and UMN, a one-month study of diesel nanoparticle chemistry carried out in collaboration with Professor David Kittelson and staff at the UMNCDR, and subsequent data analysis and writing. Phase 1 was a clear success. This was the first time that particles in the nanoparticle size mode had been cleanly sampled from a diesel engine and chemically analyzed, and much new information on nanoparticle composition was obtained. Using the Nano-DMA/TDPBMS for near-real time analysis, we were able to identify the major classes of organic components which make up the bulk of the nanoparticle mass, for aerosol samples down to ~25 nm mass median diameter (MMD). The organic mass spectra were similar for all sizes of diesel particles, and when compared to mass spectra of fuel and lubricating oil indicated that the source of particulate organics was primarily unburned oil. We were also able to detect low concentrations of sulfuric acid in particles as small as ~40 nm MMD. The results are consistent with a mechanism of diesel nanoparticle formation involving homogeneous nucleation of sulfuric acid and water followed by particle growth from condensation of organic species onto the sulfuric acid-water core. The results of the Phase 1 research have been presented previously in a journal article (16) and a CRC report (17).

6. PHASE 2 RESULTS

Phase 2 of this project continued the collaboration between the research groups of Professor Paul Ziemann at UCR and Professor Peter McMurry at UMN, and covered the period 9/8/2000-12/31/2001. The original plan for Phase 2 was that the Nano-DMA/TDPBMS diesel studies would be carried out at the Caterpillar and Cummins facilities. Following completion of the Phase 1 John Deere study at UMNCDR, however, Professor Kittelson strongly recommended that instead of taking the Nano-DMA/TDPBMS to the Caterpillar facility, we return to UMNCDR and sample from their recently-installed, modern Caterpillar engine. This approach was preferable for a number of reasons: (1) we had already performed a successful study at UMNCDR and were thoroughly familiar with the facilities and personnel, (2) the UMNCDR facility would provide a more flexible research environment, which we learned from the John Deere study could be critical for successful performance of the technically sophisticated Nano-DMA/TDPBMS, and (3) we would not be limited to the same two-week time frame as at the Caterpillar facility. The overall chances of success would therefore be greatly enhanced. The CRC and ARB were in favor of this approach, with the primary concern being that the work be performed within the original budget and not change in scope. Sufficient funds were provided by Caterpillar to run the engine using graduate students working in the UMNCDR. The same approach was taken for the Cummins study, in that the research was performed on a modern Cummins engine operated by UMNCDR. The entire project was completed with the original budget, without change in scope.

In addition to using the Nano-DMA/TDPBMS for diesel particle analysis in Phase 2, the McMurry group also performed measurements of particle volatility and water uptake using a tandem differential mobility analyzer (TDMA). The volatility measurements provided information on nanoparticle vapor pressures (and therefore composition), and particle mixing characteristics (i.e., the extent to which volatile and non-volatile components are mixed in the aerosol), while water uptake measurements yielded information on sulfuric acid content. The combination of Nano-DMA/TDPBMS and TDMA measurements provided important insights into the chemical mechanisms by which nanoparticles are formed in diesel exhaust.

6.1. PROJECT PERSONNEL

The faculty, postdocs, graduate students, and staff who participated in Phase 2 of this project are listed below:

University of California, Riverside (UCR)

Professor Paul Ziemann (PI)
Dr. Herbert Tobias (postdoc)
Kenneth Docherty (graduate student)

University of Minnesota (UMN)

Professor Peter McMurry (subcontractor)
Dr. Hiromu Sakurai (research associate)
Kihong Park (graduate student)[1]

Professor David Kittelson (collaborator and director of CDR)
Robert Waytulonis (associate director of UMNCDR)
Darrick Zarling (senior engineer at UMNCDR)
Qiang Wei (graduate student)
Alfred I. P. Ng (graduate student)
Tom M Jones (graduate student)
Kris H. Koenig (undergraduate student)
Michael F. McTigue (undergraduate student)

---

[1] Supported by the Environmental Protection Agency through Grant Number R 826372-01-0 to the Georgia Institute of Technology and GIT Subcontract Number G-35-W62-G1 to the University of Minnesota. This work has not been subjected to the Agency's required peer and policy review and therefore does not necessarily reflect the views of the Agency and no official endorsement should be inferred.

6.2. DIESEL NANOPARTICLE STUDIES AT UMNCDR

6.2.1. Methods

A schematic of the complete apparatus used in the diesel exhaust studies is shown in Figure 1. A Caterpillar or Cummins heavy duty diesel engine was used to generate diesel exhaust, which was diluted prior to analysis. A Nano-Scanning Mobility Particle Sizer (NSMPS) and conventional SMPS were used to measure particle size distributions. For mass spectral chemical analysis diesel exhaust particles were charged using a unipolar charger, size-selected using a Nano-Differential Mobility Analyzer (NDMA), and then analyzed using a Thermal Desorption Particle Beam Mass Spectrometer (TDPBMS). For volatility and water uptake measurements, particles were sampled after dilution into a Nano-Tandem Differential Mobility Analyzer (NTDMA) or Regular-TDMA-Aerosol Particle Mass Analyzer (RTDMA-APM). More detailed schematics of the TDPBMS and TDMA apparatus are shown in Figures 2-4.

6.2.1.1. Diesel Engine Exhaust Dilution

In the Caterpillar study, diesel exhaust was diluted using a Sierra Instruments BG-1 Micro-Dilution Test Stand. The typical procedure involved setup, calibration, and engine equilibration to stabilize exhaust and coolant temperatures. Engine exhaust was drawn from the stack and diluted and chilled with a measured amount of dry (RH < 5%), hydrocarbon free air. The dilution occurs in a chamber that consists of a porous stainless steel tube mounted concentrically within a stainless steel cylinder. During sampling, dilution air is introduced under pressure into the chamber through the walls of the porous tube. The air permeates the porous tube creating a virtual "wall" of hydrocarbon-free air. As a result, deposition of particulate on the walls is eliminated in the dilution chamber and the equilibration zone of the system is very short. About 11 [6] L/min of exhaust was mixed with 120 [125] L/min of dilution air to achieve the dilution ratio of 1:12 [1:20]. The temperature and RH of the diluted exhaust gases were ~30 ^{o}C and 5%. The dilution ratio was determined from the measured ratio of exhaust to diluted exhaust NO_x concentration.

In the Cummins study, diesel exhaust particles were sampled using the same procedure as in the Phase 1 John Deere study. Engine exhaust was diluted using a two stage, variable residence time, micro-dilution system (VRTDS). Briefly, the VRTDS consists of a primary dilution stage followed by a mixing tube, which has three sampling tubes located at different distances downstream of the primary dilution ejector. The residence time is determined by the choice of sampling tube. For these studies, aerosol was sampled directly after primary dilution to maximize particle concentrations so that subsequent chemical analysis could be performed above the detection limits of the instrumentation downstream of the VRTDS. The temperature and RH of the diluted sample after the primary stage was approximately 35 ^{o}C and 5%. The dilution air was 10 ^{o}C and the relative humidity (RH) was < 5%. About 20 [18] L/min of exhaust was mixed with 255 [335] L/min of dilution air to achieve the dilution ratio of 1:14 [1:20]. The dilution ratio was determined from the measured ratio of exhaust to diluted exhaust NO_x concentration.

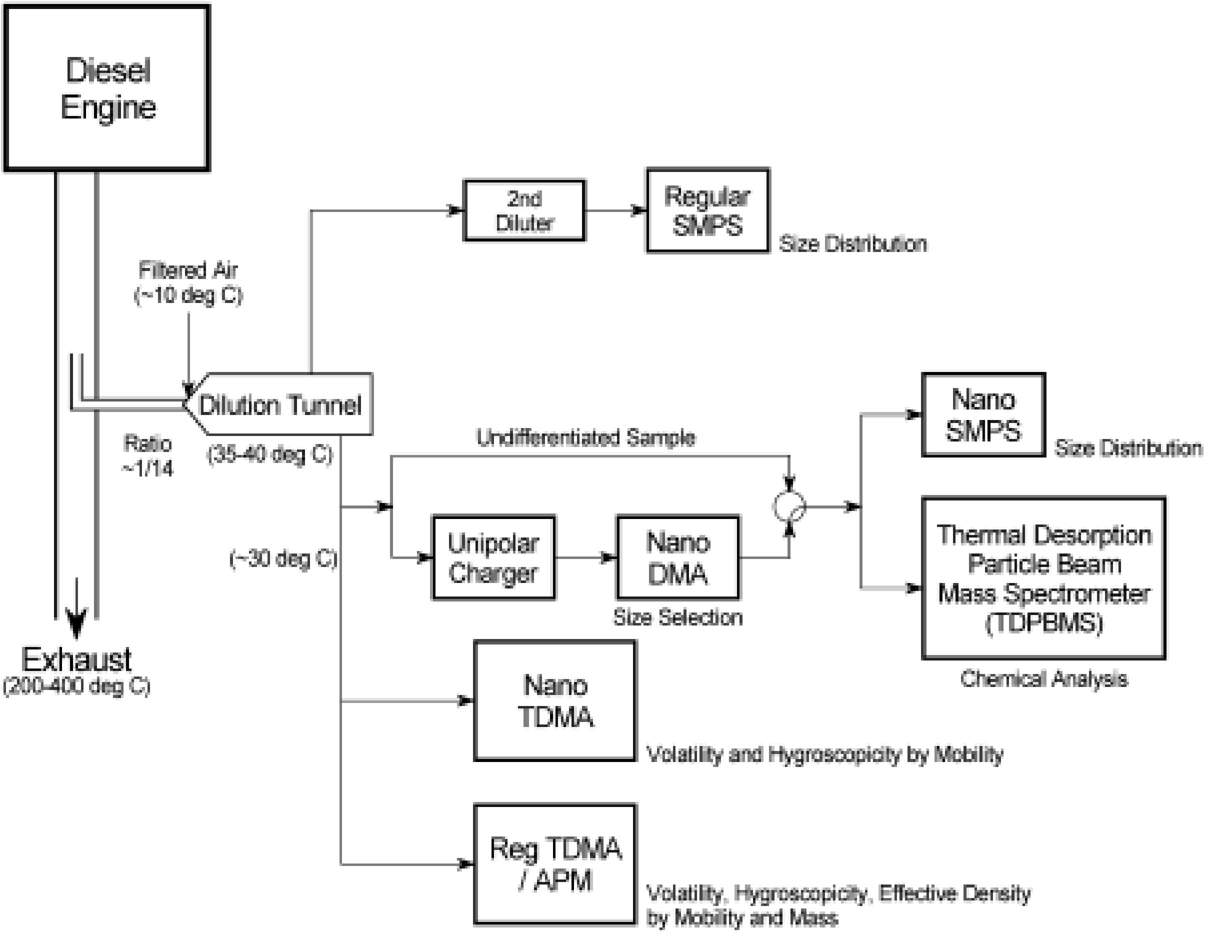

Figure 1. Schematic diagram of apparatus used for diesel exhaust particle studies.

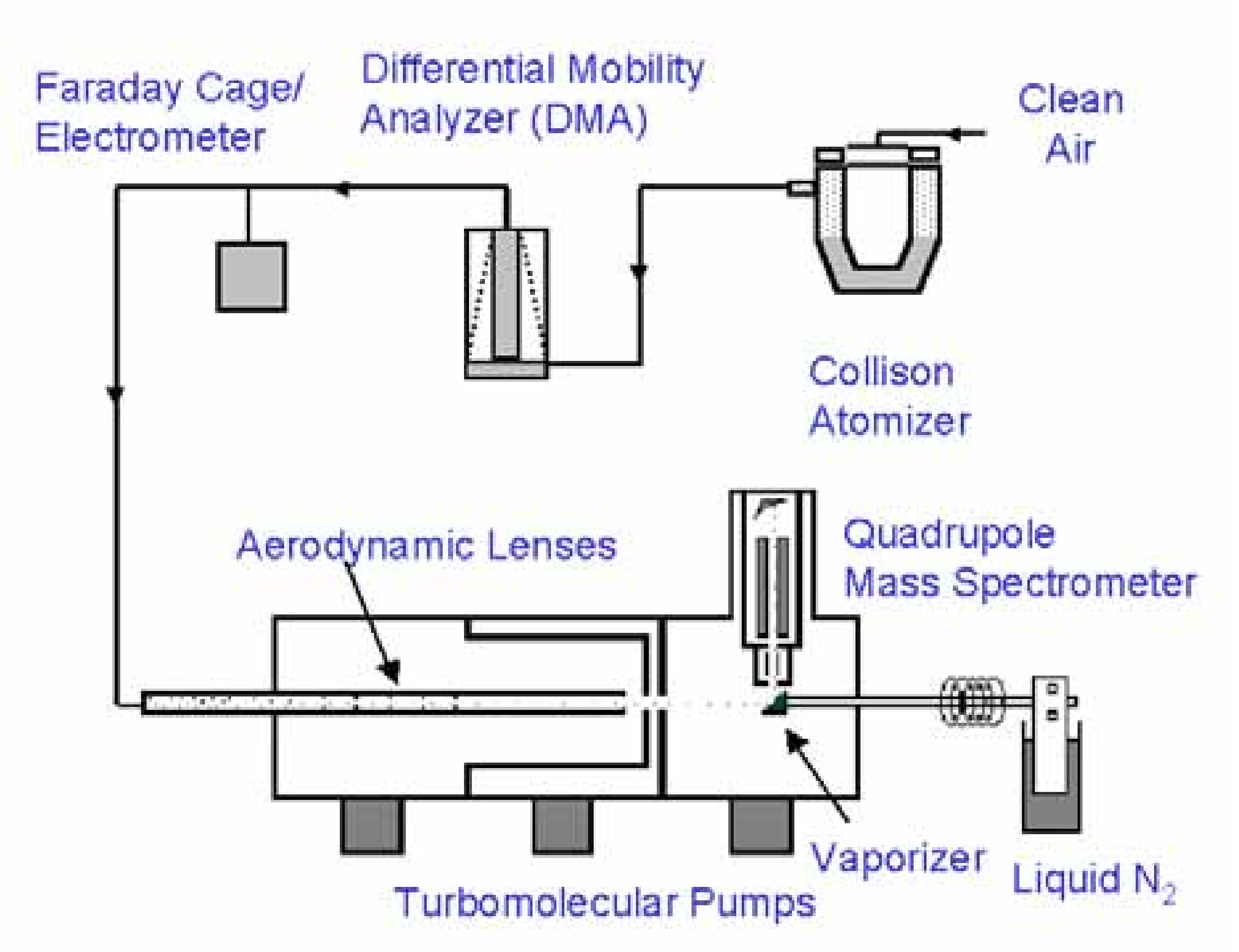

Figure 2. Thermal Desorption Particle Beam Mass Spectrometer (TDPBMS) and associated calibration apparatus.

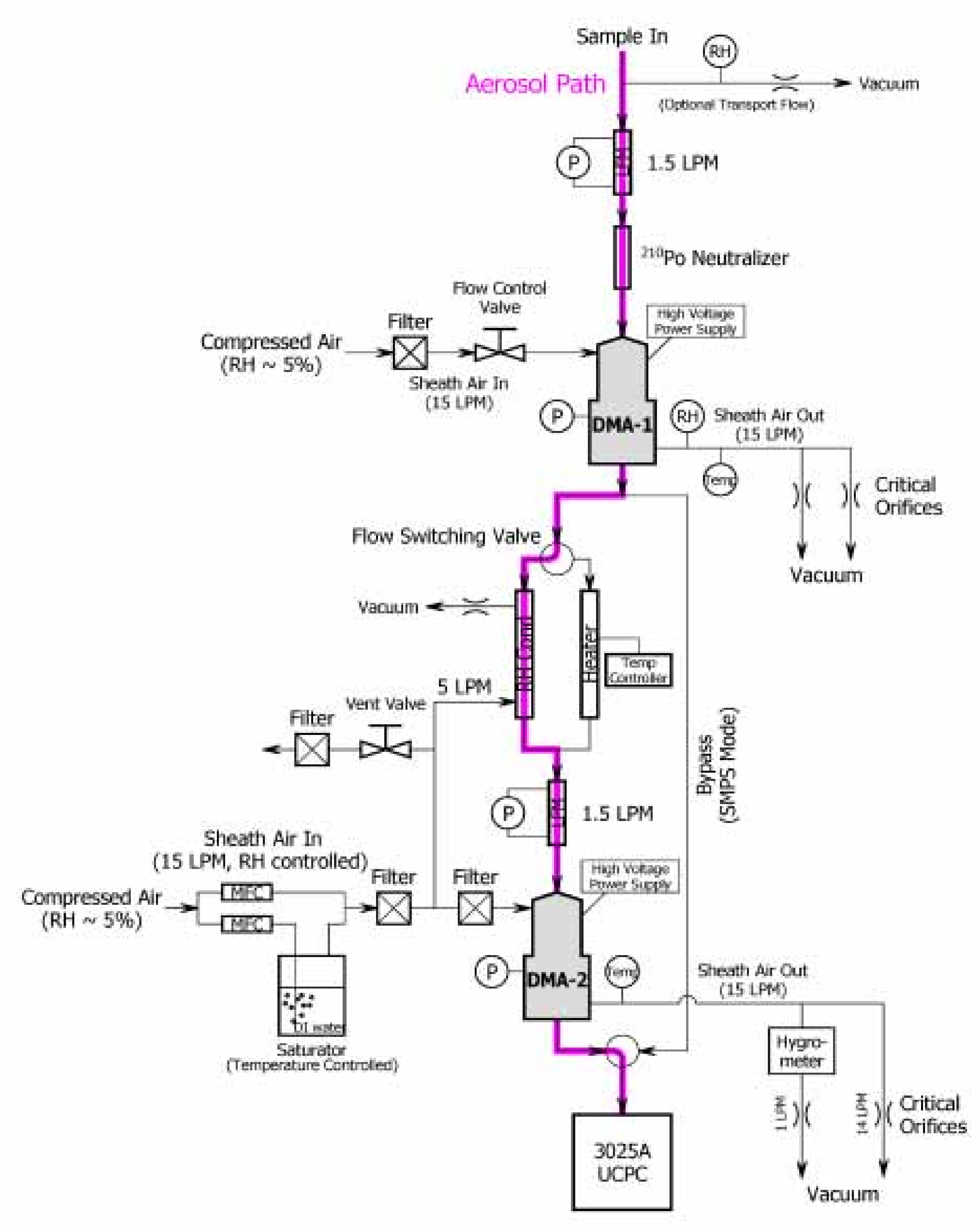

Figure 3. Nano-Tandem Differential Mobility Analyzer (NTDMA) apparatus used for measurements of diesel particle volatility and hygroscopicity.

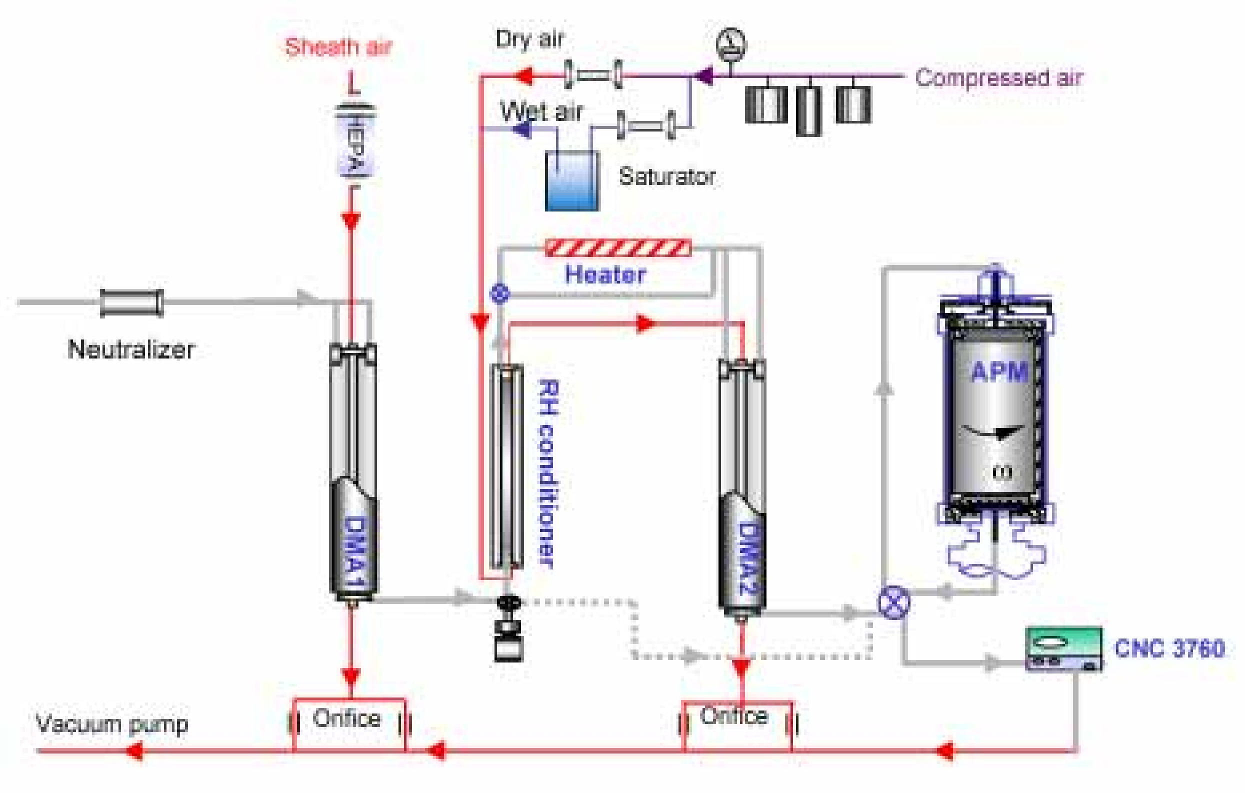

Figure 4. Regular-Tandem Differential Mobility Analyzer-Aerosol Particle Mass Analyzer (RTDMA-APM) used for measurements of diesel particle volatility and hygroscopicity.

6.2.1.2. Particle Size Selection and Size Distribution Measurements

After dilution, particles were size-selected for analysis prior to entering the TDPBMS. We also analyzed total particles without size-selection by sampling diluted exhaust directly into the TDPBMS. For size selection, particles were sampled into a unipolar charger, followed by a NDMA. The unipolar charger (18) charges nanoparticles with high efficiency because ions of only a single polarity are present, and it reduces particle loss by directing the flows of ions and charged aerosol in an electric field. A sheath flow can be added to increase throughput of small particles, but was not used because it dilutes the aerosol and is not necessary for the sizes sampled here. The high charging efficiency of the unipolar charger increases the concentration of charged particles and therefore the sensitivity of nanoparticle measurement, but can also generate a significant number of larger, multiply charged particles that can pass through the NDMA and contribute to the nanoparticle sample. These particles shift the sampled mass distribution to larger sizes. For these studies, a voltage in the unipolar charger was adjusted to increase the concentration of unipolar ions for smaller particles and decrease the concentration for larger particles. Voltages were selected for different sizes so that the fraction of large multiply charged particles did not exceed ~10-20% of the total mass concentration. For particles 40 nm or larger, the voltage was turned off so that the charger operated in the bipolar mode.

A NDMA (TSI Model 3085) (11) was used downstream of the charger for particle size selection. The NDMA separates charged nanoparticles according to their electrical mobilities and can provide accurate, high-resolution, size selection of particles in the 3-60 nm diameter range. In a NDMA, a short path length and high inlet flow are used to reduce particle residence time and improve nanoparticle throughput, since diffusional losses during aerosol transport are significant for nanometer size particles. For our application, however, high-resolution was sacrificed by operating the NDMA with a somewhat broadened transfer function (aerosol to sheath flow ratio of 1/3) in order to increase the mass concentration of nanoparticles entering the TDPBMS. The resolution was still high enough that if multiply charged particles were present, they could be observed with the NSMPS (see next paragraph) and the unipolar charger voltage adjusted to minimize their contribution. In all experiments the aerosol flow rate was 1.6 L/min, with ~0.1 L/min flowing to the TDPBMS and 1.5 L/min to an ultrafine condensation particle counter (TSI Model 3025 UCPC), and the sheath air flow rate was 4.5 L/min. Under these conditions, the half-width of the size distribution is ~20% of the selected diameter. TDMA measurements made by placing a second NDMA downstream of the first showed no significant tailing of the transfer function into larger sizes. The only particles outside the selected size window that passed through the NDMA were those with multiple charges.

The size distribution of particles entering the TDPBMS from the NDMA was measured with a Nano-Scanning Mobility Particle Sizer (NSMPS) consisting of a bipolar charger, NDMA (TSI Model 3085), and UCPC (TSI Model 3025). The same instrument was used to measure the size distribution from 3-60 nm for particles exiting the VRTDS. The aerosol flow rate in the NSMPS was 1.5 L/min and the sheath air flow rate was 15 L/min. The size distribution of particles exiting the VRTDS in the 10-320 nm range was measured using a conventional SMPS consisting of a bipolar charger, a DMA (19, 20) similar in design to the TSI Model 3934, and a TSI Model 3010 CPC. The aerosol flow rate was 1.0 L/min and the sheath air flow rate was 10 L/min.

The particle mobility distributions measured with the NSMPS and SMPS were inverted to obtain particle size distributions. The procedure included corrections for particle charging, the DMA transfer function, particle loss by diffusion in the DMA, diffusional broadening of the transfer function, and the CPC and UCPC counting efficiencies. Details of the general inversion procedure are described in the literature (21). Data from experimental and numerical studies (11) were used to correct for size-dependent diffusional loss and transfer function broadening in the NDMA, and CPC and UCPC counting efficiencies were obtained from the TSI manual. The size-dependent charge fractions were calculated using Fuchs' theory for bipolar diffusion charging (22).

6.2.1.3. TDPBMS Particle Sampling and Fast-TPTD Analysis

Techniques for real-time (13) and temperature-programmed thermal desorption (TPTD) (12) analyses of aerosols using TDPBMS have previously been described in detail, but are used with several modifications in hardware and procedure for this work (16, 17). The TDPBMS is shown in Figure 2. Particles are sampled into the TDPBMS through a 100 micron orifice at 0.075 L/min, which reduces the pressure from atmospheric to ~2 torr. Using aerodynamic lenses (23, 24), particles are then focused into a tight particle beam and transported through two flat-plate skimmers separating three differentially pumped chambers. They enter a high-vacuum chamber at a pressure of ~3 x 10^{-7} torr and reach a particle vaporizer with ~40-100% efficiency. Vacuum is maintained by turbomolecular pumps mounted on each chamber and backed by an oil-free mechanical scroll pump to reduce organic vapor contamination. All focused particles impact onto the inside walls of a v-shaped molybdenum foil vaporizer that is attached to a copper rod and is situated just outside the mass spectrometer ionizer. The particles were either continuously vaporized for real-time analysis by resistively heating the foil at ~200-250^{o}C, or cryogenically collected for TPTD analysis by cooling the foil to -50^{o}C using an external liquid nitrogen bath. The temperature is monitored using a chromel-alumel thermocouple placed in contact with the foil. The desorbing molecules are ionized by 70 eV electrons and mass analyzed using a MEXM 500 quadrupole mass spectrometer (ABB Extrel, Pittsburgh, PA) and detected using a conversion dynode/pulse counting detector. The mass spectrometer was equipped with a tandem energy analyzer (ABB Extrel, Pittsburgh, PA) that reduces background noise by a factor of ~100 and signal by a factor of ~3, resulting in a signal-to-noise (S/N) improvement of ~30 compared to operation without the energy analyzer.

The particle mass flux was sufficient for real-time TDPBMS analysis of total diesel particles, but not for nanoparticles. Therefore only TPTD was used for nanoparticle analysis. In previous laboratory studies, TPTD was used to separate, identify, and estimate vapor pressures of individual compounds in aerosols comprised of a few components. In this work, slightly longer particle collection times and an ~50 times faster desorption rate were used to enhance S/N over that of real-time analysis. This allowed us to obtain full mass spectra and identify a few compound classes in the diesel particles, which are comprised of many components. We refer to this analytical procedure as fast-TPTD. Particles sampled from a particular size mode were cryogenically collected onto the cold foil. After collection, the components of the sample were desorbed according to their vapor pressures and therefore separated to some degree in time. During fast-TPTD, the foil was resistively heated from approximately -50 to + 400^{o}C over 5 min using a linear temperature ramp supplied by a high current power supply controlled using

Labview software. For some experiments on total diesel particles and standards the ramp rate was lowered to ~5^{o}C/min (referred to here as slow-TPTD), to allow for slower, more controlled evaporation and more accurate vapor pressure and carbon number estimation. Throughout the desorption period, the mass spectrometer samples a portion of the evaporating molecules for mass analysis. The signal due to background gases was determined by sampling diesel exhaust under the same conditions as for the nanoparticles, except that the NDMA was set at 0 volts to allow only diesel exhaust gases to pass. Background gases were cryogenically collected and then analyzed using the TPTD procedure.

6.2.1.4. Mass Spectral Analysis: Full Scan or Five-Mass SIM

Mass spectral analysis of collected particles was conducted either by continuous scanning over an appropriate mass range or by single-ion monitoring (SIM) of five mass-to-charge ratios (*m/z*). Full mass spectra were scanned from *m/z* 45-450 in 8 s, with 1 amu step size, and with detector dwell times of 15 ms at each *m/z*. For certain sampling conditions, collecting sufficient nanoparticle mass for full mass spectral analysis was not feasible, so instead, SIM of five *m/z* signals was used to enhance S/N. This allowed for longer dwell times (2000 ms) at each mass, compared to the scanning mode (15 ms), and provided sufficient S/N to distinguish low nanoparticle signal from the background. The five masses used in the SIM method were chosen to represent hydrocarbons and sulfuric acid: *m/z* 69 for cycloalkanes, *m/z* 85 for alkanes, *m/z* 95 for "non-specific" hydrocarbons, and *m/z* 81 and 98 for sulfuric acid.

6.2.1.5. TDPBMS Calibration and Standards Analysis

The TDPBMS was calibrated with standard compounds to identify fuel and oil contributions to the diesel particles and estimate carbon numbers and vapor pressures of the components. Aerosol standards were generated using a Collison atomizer (25). A solution of ~0.2% (w/w) pure organic compound, diesel fuel, or lubricating oil in hexane (HPLC Grade; Fisher Scientific) was atomized using clean air and sent though an activated charcoal diffusion drier to evaporate hexane solvent. The submicron dried aerosol was then passed through a bipolar charger and DMA to select ~100 nm particles. The particle current exiting the DMA was measured using a Faraday cage and electrometer to determine the particle concentration, which was used with the known size, density, and sampling rate to calculate the particle mass flux (13). Aerosol was analyzed in real time or cryogenically collected on the foil in the TDPBMS high-vacuum chamber and then analyzed using the slow- or fast-TPTD procedure. Mass spectral analysis was performed by scanning from *m/z* 45-300 for fuel and lubricating oil standards. Pure organic standards were analyzed using SIM of *m/z* 85 for the n-alkanes eicosane [$C_{20}H_{42}$], tetracosane [$C_{24}H_{50}$], octacosane [$C_{28}H_{58}$], dotriacontane [$C_{32}H_{66}$], and hexatriacontane [$C_{36}H_{74}$].

6.2.1.6. Method of TDPBMS and TPTD Data Analysis

The approach used here to interpret TDPBMS and TPTD mass spectra is based on the following assumptions.

1) The mass spectra are representative of diesel particulate components that evaporate at temperatures less than ~200-400 ^{o}C. This means that no information is obtained for refractive materials such as soot (elemental carbon) or metal oxides. This assumption is based on the fact that the TDPBMS vaporizer is operated at temperatures of ~200-400 ^{o}C, and so compounds that do not evaporate in this temperature range will not be detected. These temperatures are sufficiently high to volatilize all organics and sulfuric acid. In these studies, the mass spectra of diesel particulate matter are compared to standards vaporized at similar temperatures, in order to minimize the effect of temperature on mass spectra. This precaution is barely necessary, however, as shown in Figure 5. The real-time TDPBMS mass spectra of fuel and oil obtained with the vaporizer at the typical temperature of ~200-250 ^{o}C are not significantly different from those obtained by summing the TPTD scans over the entire desorption profile from ~-50-400 ^{o}C.

2) The contribution of diesel exhaust gases to the mass spectra are negligible. This is regularly validated during diesel studies. Examples of real-time TDPBMS mass spectra, TPTD mass spectra, and SIM scans of diesel exhaust gases are shown in Figure 6. These are obtained by setting the voltage on the Nano-DMA to zero, which removes all particles and allows only gases to be sampled. The signal intensities are all negligible compared to signal intensities obtained when particles are sampled (e.g., compare with Figures 10A, 11A, 12A, and 13). The major peaks observed in Figures 6A and 6B are from the tungsten filament (*m/z* 182, 183, 184, 186) used for ionization and slight contamination from cadmium (*m/z* 110, 112, 114), which is quite volatile at these temperatures.

3) Evaporative losses of diesel particulate matter inside the TDPBMS are negligible. This assumption is discussed in detail section 6.2.3.5.3. and shown to be valid.

4) The major components that may contribute to the mass spectra are unburned fuel, unburned oil, oxidized organic combustion products, and sulfuric acid. This assumption is based on the results of numerous previous studies by others using primarily GC-MS to analyze diesel particulate matter, as well as the results of our Phase 1 study.

5) Unburned fuel, unburned oil, oxidized organic combustion products, and sulfuric acid have characteristic mass spectra that can be used to identify these components by comparing to diesel particle mass spectra. This assumption is equivalent to the basic assumption made in GC-MS, which is that the individual compounds that have been separated by gas chromatography have characteristic mass spectra which can be used for identification by comparing with standard mass spectra. Figure 7 shows mass spectra of CA fuel and oil used in the Cummins study, palmitic acid, and sulfuric acid. The fuel and oil have complex spectra because they are composed of many compounds, including branched and cyclic alkanes and aromatics. They also have significant signal at most of

the same masses, because they both contain the same classes of hydrocarbons. The important feature for identification purposes is that the relative intensities of many neighboring peaks in the spectra are consistently different between fuel and oil. Comparing the relative intensities of peaks more distant from each other is less reliable because of possible fluctuations in conditions during a mass scan. Note, for example, the intense low-mass peaks in the fuel spectrum at *m/z* 71 and 85, and the intense high-mass peaks at 141, 155, 169,…, 197. By contrast, in the oil spectrum intense low-mass peaks occur at *m/z* 69 and 81 and intense high-mass peaks occur at 165, 179, and 191, while an obvious 141, 155, 169,…, 197 series is absent. Also note that *m/z* 95 and 97 and *m/z* 109 and 111 are more similar in intensity in oil than in fuel, and *m/z* 97 is much larger than *m/z* 99 in oil than fuel. The mass spectrum of oil does not change with use, as shown in Figure 8. The similar mass spectra of new and used oil shows that the oil mass spectrum is not altered by pyrolysis or possible differential losses of compound classes during engine operation. In other words, the oil mass spectrum is conserved throughout the combustion process, and can therefore be use as a tracer of unburned oil. The mass spectrum of palmitic acid (Figure 7C) is typical of monocarboxylic acids, which are the major oxidized organic combustion products found in diesel particles by GC-MS analysis. The *m/z* 60 and 73 peaks are always the major peaks in the monocarboxylic acid mass spectra, and can therefore be used as markers for oxidized organic combustion products. The mass spectrum of sulfuric acid (Figure 7D) is relatively simple and has a peak at *m/z* 64, which is not abundant in fuel, oil, or carboxylic acids, and therefore serves as an indicator (sometimes in conjunction with *m/z* 81 and 98) of this compound.

6) The relative amounts of the major components of diesel particulate matter can be estimated by comparing diesel particle mass spectra to mass spectra created by mixing different fractions of standard component mass spectra. This assumption is equivalent to that used in any type of spectral analysis (e.g., Fourier Transform Infrared Spectroscopy, FTIR), which is that a complex spectrum can be decomposed into its component spectra. In practice, this amounts to weighting the contributions of the components such that the sum of the weighted spectra matches the complex spectrum. The weight of each component is then used to determine its contribution (in terms of mole or mass fraction) to the mixture. The only difference between quantitative FTIR spectral analysis and the approach used here is that instead of matching the diesel particle mass spectra to molecular components, the components used for matching are the unburned fuel, unburned oil, oxidized combustion products, and sulfuric acid. One technique for quantifying the similarity of mass spectra is to calculate, for example, the sum of squares difference between particle and standard spectra of fuel and oil mixtures. The mixture which minimizes this quantity would then be the best match. When this approach was used, it was found that the best fit for a diesel particle spectrum was always a standard pure oil spectrum. Because this was not always the conclusion reached on the basis of a visual comparison (a few spectra clearly appeared to have a fuel contribution), we have not used this computational matching approach. Instead, we used a more subjective, but, we think convincing, visual comparison to set lower limits on the contribution of oil to particles. A statistical approach will be developed in the future when more time is available for necessary method evaluation.

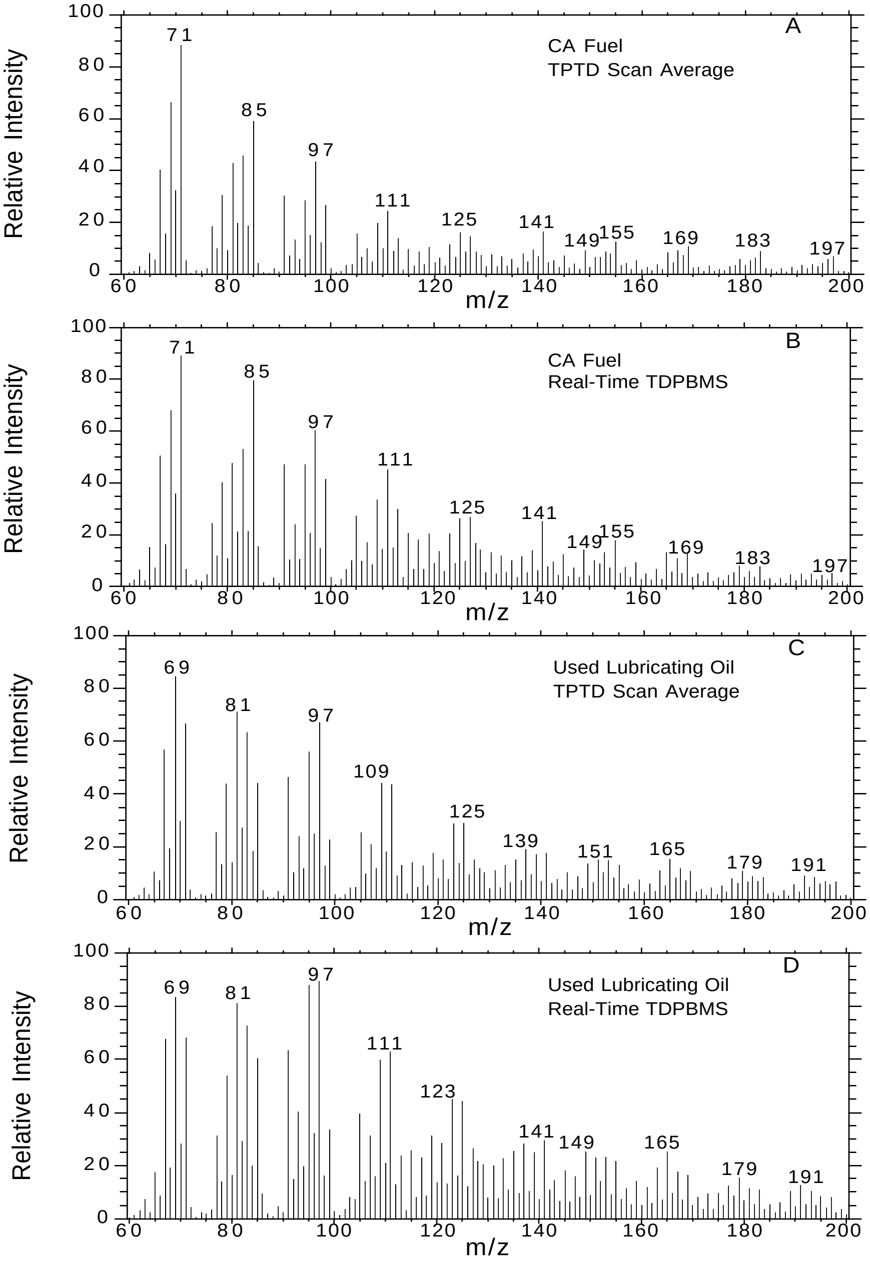

Figure 5. (A) Mass spectra of CA fuel measured by (A) fast-TPTD and (B) real-time TDPBMS, and mass spectra of used oil measured by (C) fast-TPTD and (D) real-time TDPBMS. Fast-TPTD mass spectra obtained by averaging all scans of fuel and used oil samples collected for 4 min. The fuel and oil are those used in the Cummins study.

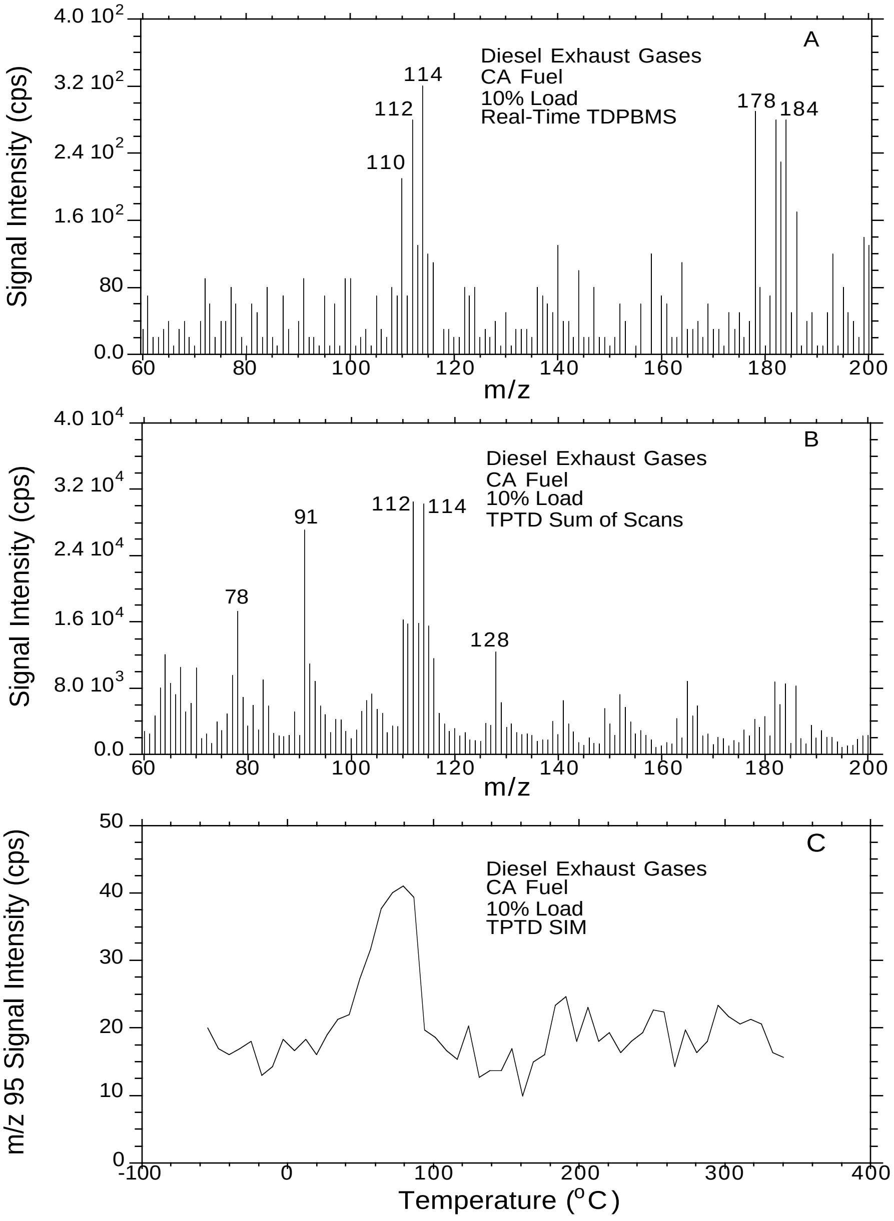

Figure 6. Background mass spectra of diesel exhaust gases obtained by setting Nano-DMA voltage to zero, which removes all particles. (A) Real-time TDPBMS, (B) Fast-TPTD mass spectrum obtained by summing all scans, for 25 min sample collection, and (C) Fast-TPTD SIM profile for 62 min sample collection.

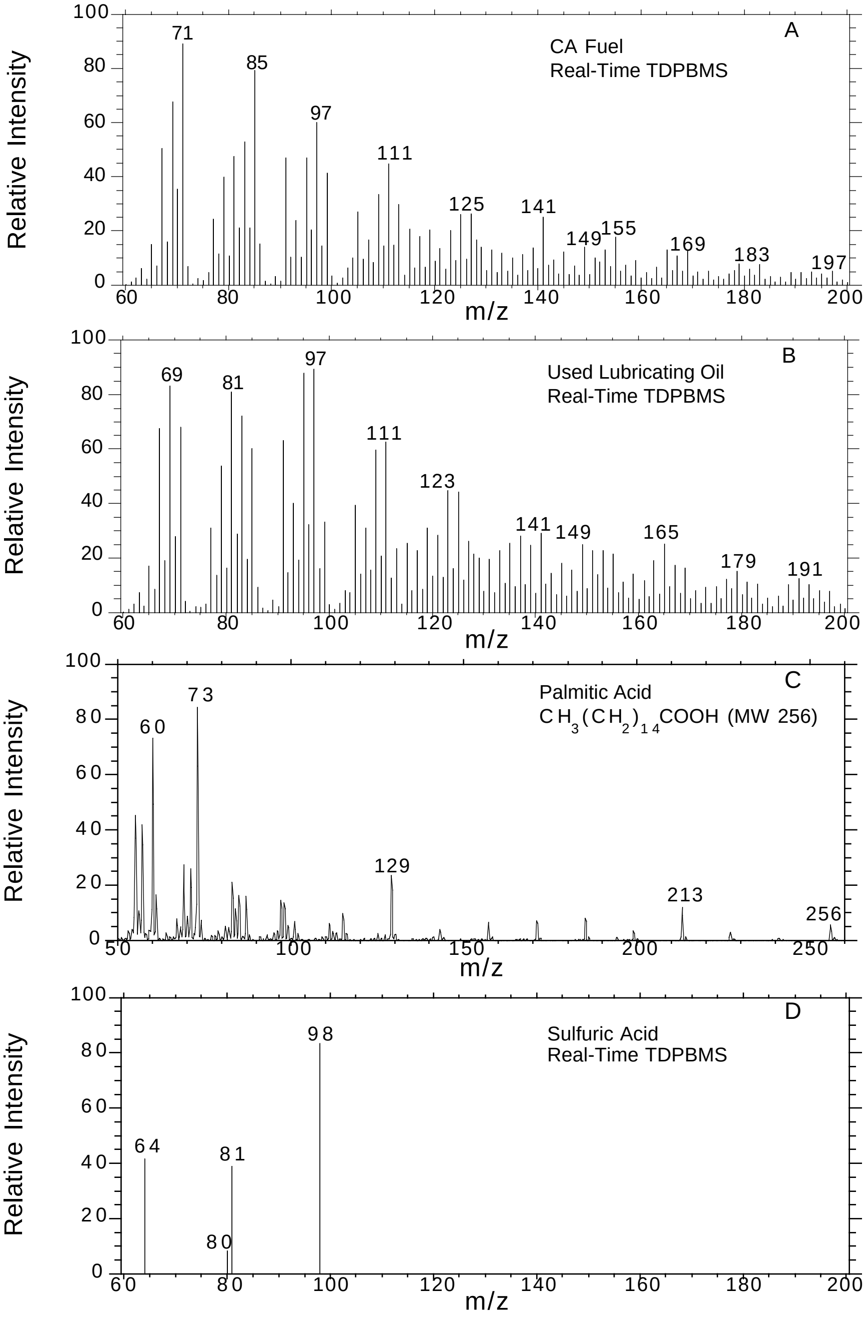

Figure 7. Real-time TDPBMS mass spectra of (A) CA fuel and (B) oil used in the Cummins study, (C) palmitic acid (a surrogate for monocarboxylic acids/oxidized organic combustion products), and (D) sulfuric acid.

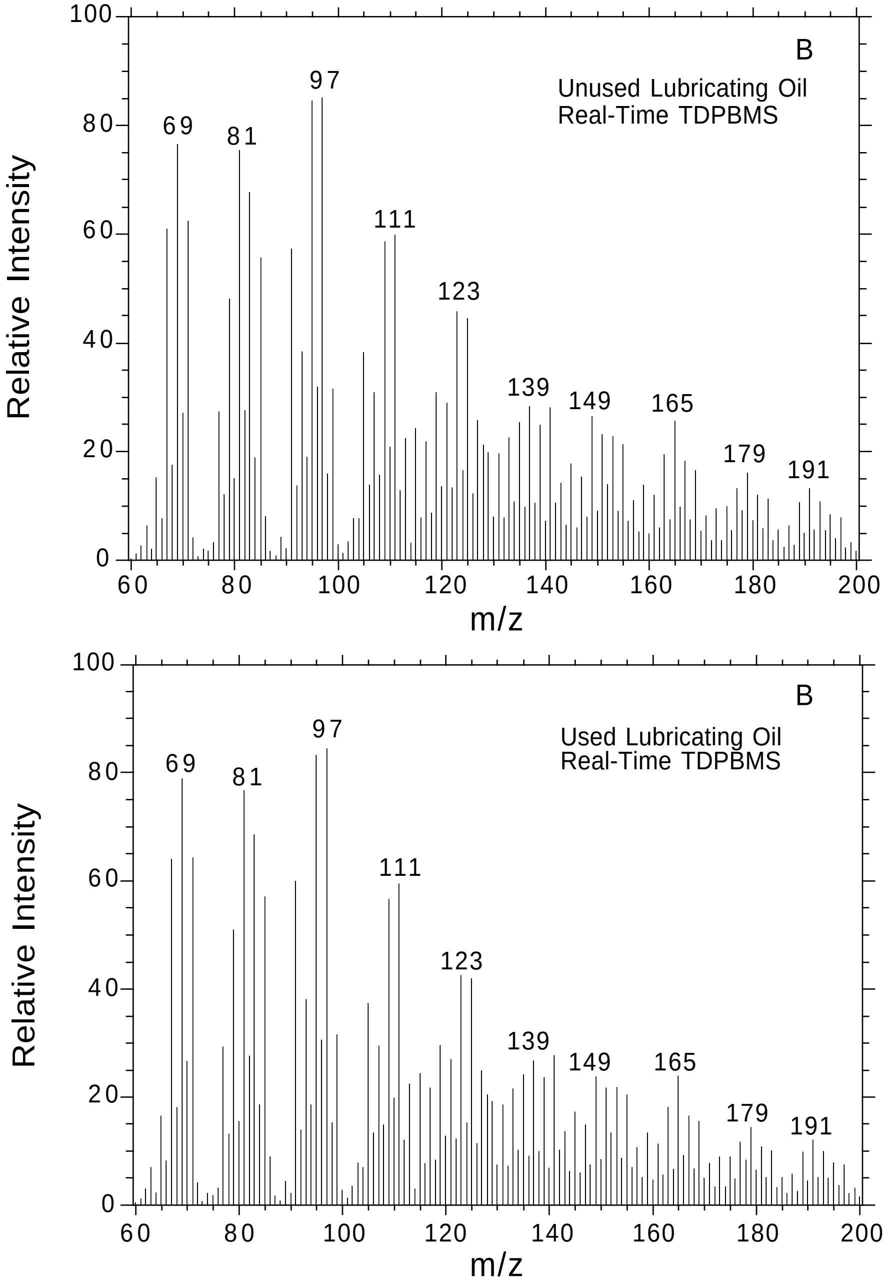

Figure 8. Real-time TDPBMS mass spectra of (A) unused oil and (B) used oil (109 hr) from the Cummins engine.

At the beginning of Phase 2, it was also assumed that TPTD desorption profiles could be used to obtain information on the volatility of diesel particle compounds, but, as will be shown below, that is only true in some circumstances. Fortunately, tandem differential mobility analysis provides this information.

6.2.1.7. Gas Chromatographic Analysis of Fuel and Oil

Gas chromatography with flame ionization detection (GC-FID) was used to analyze Fischer-Tropsch and California fuel, and used oil from the Cummins engine. Sample solutions were prepared by dissolving 0.5 mL of fuel or oil in cyclohexane to achieve a final volume of 100 mL. A solution containing 0.033% each of C14, C15, and C16 *n*-alkanes in hexane was also analyzed in order to determine equivalent alkane carbon numbers of fuel and oil components by comparing retention times with alkane standards. Samples were analyzed using an HP 6890 GC with an FID detector. The column was an HP-1 Methyl Siloxane capillary column (Model No. HP 19091Z-413, column length = ~30 m, diameter = .32 mm, film thickness = .00025 mm). Approximately 2 uL samples were injected into the GC inlet, which was operated in splitless mode and maintained at 0 ^{o}C throughout the analysis. The oven was maintained at 50 ^{o}C during sample injection and for an additional 8 minutes (inlet hold time). The oven temperature was then ramped at a rate of 15 ^{o}C/min to a final temperature of 325 ^{o}C. The run time for an analysis was ~34 minutes.

An attempt was also made to analyze diesel particle filter samples collected by UMN-CDR staff and Soxlet extracted at UCR. Unfortunately, the sample concentrations were below the detection limit of the GC-FID and so could not be analyzed.

6.2.1.8. NTDMA and RTDMA-APM Analysis of Particle Volatility and Water Uptake

A simplified schematic of the NTDMA and RTDMA-APM systems are shown in Figures 3 and 4. We used the two TDMA systems to cover both the nuclei and accumulation modes of diesel exhaust particles; 3-50 nm with the NTDMA and 10-200 nm with the RTDMA-APM. Details of the TDMA theory can be found elsewhere (26) and only brief description is given here. The recently built NTDMA was equipped with two TSI Model 3085 NDMA columns (27) (NDMA-1 and NDMA-2) and a TSI Model 3025A UCPC, which improved the transmission and detection efficiencies of particles smaller than 20 nm in diameter. The aerosol and sheath air flow rates were maintained at 1.5 and 15 L/min in the NTDMA. The RTDMA-APM system was composed of two conventional-size DMA columns (RDMA-1 and RDMA-2), a TSI Model 3760 CPC, and an Aerosol Particle Mass Analyzer (APM) manufactured by Kanomax Japan, Inc. The aerosol flow rate was 1.5 L/min throughout this system and the sheath air flow rates were 15 and 6.9 L/min in RDMA-1 and RDMA-2, respectively. Sampled aerosol particles first passed through a Po-210 bipolar charger in which an equilibrium charge distribution was achieved. The particles then entered DMA-1, which was used to select monodisperse particles of the size of interest. The monodisperse aerosol then entered one of two types of aerosol conditioners; one was a heated tube in which volatile aerosol components evaporated, while the other was a tube in which the aerosol was exposed to low or high relative humidity. The aerosol heaters are similar to one developed and characterized by Orsini et al., (28). The heaters consist of a 1/4”-O.D., ~50-cm long stainless steel tube wrapped with a 200-W heating tape. Temperature controllers maintain the temperature within ±1 °C of the desired value. The temperatures used in this study ranged from ~30 °C (room temperature) to ~450 °C, and the residence time of aerosol particles in the heaters was about 0.25 s. In the humidity conditioner tube, particles from DMA-1 were exposed to high humidity in order to evaluate their ability to uptake water. The relative humidity in the RH conditioner (and downstream) was set at either 6-7% (dry mode) or 80-85% (wet mode). Particles passing through either the heated tube or the humidity conditioner then entered DMA-2 and the CPC (the APM of the RTDMA-APM system was bypassed in this case) and were re-sized to determine the change in particle size due to evaporation (shrinkage) or water uptake (growth). The voltage on DMA-2 was scanned through a wide range of values to measure the entire size distribution of the conditioned particles, which was often wider and shifted compared with the distribution prior to conditioning. The size distribution data (dN/dDp vs Dp) were corrected for loss in the DMA-2 columns, broadening of the DMA transfer functions by diffusion, and reduced detection efficiencies of the CPCs at the lower end of their detectable size range. Particle sizes studied with the TDMA systems were ~6 (water uptake experiment only), 12, and 30 nm with the NTDMA, and 70, 120, and 200 nm with the RTDMA-APM system, with several other sizes added occasionally depending on the diesel aerosol size distribution.

In the volatility experiments, another mode of operation of the RTDMA-APM system was to use the APM to measure the mass of particles exiting RDMA-2. A schematic of the APM is shown in Figure 4. A detailed description of this instrument is given elsewhere (29). Briefly, the APM consists of two cylindrical electrodes which rotate at the same angular speed. Aerosol particles are introduced axially into a small annular gap between the electrodes and rotate at the same speed as the electrodes as they travel downward through the gap. A negative voltage was applied to the inner electrode while the outer electrode was grounded, which generated a radial electric field. Particles in the gap experienced an outward centrifugal force and an inward electrostatic force, since the particles from RDMA-2 were positively charged. When these forces were balanced, particles penetrated through the gap without impacting on the electrodes and were detected by the CPC. By controlling the rotation speed and voltage, the APM classifies particles of a desired mass. It should be noted that mass classification by the APM is accomplished without effects from particle shape. This is in contrast to size classification by the DMA, which separates particles according to their electrical mobility, a property which depends on particle shape. In these experiments, particles which exited the heater were size-selected by RDMA-2 and then delivered to the APM for mass measurement. By doing this, only particles of a certain volatility were mass analyzed. This was important because the diesel particles studied here were an external mixture of particles of different volatility and hence different composition.

6.2.1.9. TDMA Calibration and Standards Analysis

Standard particles for the RTDMA-APM were generated by atomizing 0.1% (wt/wt) solutions of dotriacontane or engine oil in hexane (Optima Grade; Fisher), which were then dried in a pair of diffusion driers containing activated carbon. The lubricating oil was taken from the oil reservoir of the engine after ~109 hours of use during the Cummins study. Dotriacontane particles for the NTDMA experiments were generated by the evaporation-condensation technique to avoid contamination by use of solvent. In this technique, the alkane was vaporized into flowing air in a tube furnace at ~120 °C, and then mixed with clean, room temperature air to induce particle formation of pure dotriacontane particles by homogeneous nucleation.

6.2.2. Results of the Caterpillar Study

6.2.2.1. Summary of Activities

The Caterpillar engine study was carried out from 11/11/00 –12/02/00. The TDPBMS was shipped from Los Angeles to Minneapolis on 11/3. The UCR group arrived on 11/10 and from 11/11-11/20 the TDPBMS was assembled and leak tested, baked, and calibrated in preparation for experiments. At the same time, the McMurry group set up the unipolar charger/NDMA for sampling size-selected diesel nanoparticles into the TDPBMS, a NSMPS for measuring diesel nanoparticle size distributions, and a NTDMA for measuring nanoparticle volatility and water uptake. The period from 11/21-11/28 was primarily spent troubleshooting and bringing graduate students up to speed on the operation of the new engine and the new dilution system. Only a limited amount of useful TDPBMS data was acquired during this time due to problems with unstable engine exhaust flows, unstable exhaust temperatures, and problems with the diesel engine. Unfortunately, on 11/28 the diesel engine dynamometer deteriorated to the point where engine loads greater than 20% could not be attained. Before this occurred, however, some data were acquired at 50% engine load using CA fuel. After 11/28/00, TDPBMS data were acquired for 10% and 20% engine loads using CA and EPA Pump fuel. All but one day of experiments were performed using the CA fuel. After completing all the experiments that had been planned for the CA fuel, we decided that it would be worthwhile to run at least a few experiments on high sulfur (estmimated S~300 ppm, not measured) EPA Pump fuel. The data would be valuable in making a connection between this study and the previous one that employed a John Deere engine with high sulfur (410 ppm S) fuel. Both fuels have very similar TDPBMS thermal desorption profiles and mass spectra, but differ by ~6x in sulfur content. A few NTDMA measurements were made in parallel with TDPBMS measurements, but were very preliminary in nature and served only as preparation for the later Cummins study. During the study, students, staff, and PIs met daily to evaluate results and plan upcoming experiments. The engine specifications and operating conditions, exhaust sampling conditions, and a summary of particle analyses is given below.

6.2.2.2. Caterpillar Diesel Engine Specifications, Operating Conditions, and Exhaust Sampling Conditions

Caterpillar Diesel Engine Specifications

Caterpillar Model C-12
Year 1998
6 cylinder, 4 cycle
12-L engine displacement
Rated speed: 2100 rpm
1650 lb-ft (= 2244 N-m) @ 1200 rpm (peak torque)
430 hp @ 2100 rpm (max power)

Caterpillar Diesel Engine Operating Conditions

Speed: 1200 rpm
Load: 10% (165 lb-ft), 20% (330 lb-ft), and 50% (825 lb-ft)
Fuel: CA (50 ppm S) and EPA Pump (meets ASTM D 975 No. 2-D or ASTM D 975 Low Sulfur No. 2-D specifications (S < 500 ppm, typically 282-338 ppm))
Lubricating Oil: Caterpillar Diesel Engine Oil SAE 15W-40

Caterpillar Diesel Engine Exhaust Sampling Conditions

Sample temperature in VRTDS after dilution: ~30 ^{o}C
Sample relative humidity in VRTDS after dilution: ~5%
Primary dilution ratio: 12:1 and 20:1
No secondary dilution
Dilution tunnel residence time: Not known
Engine room (same as particle analysis room) temperature ~20 ^{o}C

6.2.2.3. Caterpillar Study Data Summary

6.2.2.3.1. TDPBMS Data

The following is a summary of the TDPBMS data acquired during the Caterpillar study.

SIM/TPTD analyses of collected particles

(a) CA fuel, 10% load, 12:1 dilution ratio, particle size (nm): total, 75, 38, 23, 17, background
(b) CA fuel, 10% load, 20:1 dilution ratio, particle size (nm): total, 200, 130, 40, 25, 18
(c) CA fuel, 50% load, 12:1 dilution ratio, particle size (nm): total, 26
(d) EPA Pump fuel, 10% load, 20:1 dilution ratio, particle size (nm): total, 40, 25, 17, 15
(e) EPA Pump fuel, 20% load, 20:1 dilution ratio, particle size (nm): total, 75, 38, 23, 17

Full mass spectra/TPTD of collected particles

(a) CA fuel; 10% load; 12:1 dilution ratio; particle size (nm): total, 75, 25, background
(b) CA fuel; 50% load; 12:1 dilution ratio; total particles, background

Full mass spectra and SIM/TPTD of particle standards

(a) Fuels: CA, EPA Pump
(b) Oil: Caterpillar Diesel Engine Oil SAE 15W-40, new and used
(c) Alkanes: C20, C24, C28, C32, C36
(d) Sulfuric acid

6.2.2.4. Results of TDPBMS Analyses

The most useful TDPBMS data obtained in this study were the TPTD full mass spectra and SIM desorption profiles. TPTD mass spectra of the fuel and lubricating oil standards used in this study are shown in Figure 9. Total diesel particle mass spectra obtained with CA fuel at 10% and 50% load are shown in Figures 10 and 11, respectively, and the mass spectra of size-selected, 25 nm, diesel nanoparticles obtained with CA fuel at 10% load are shown in Figure 12.

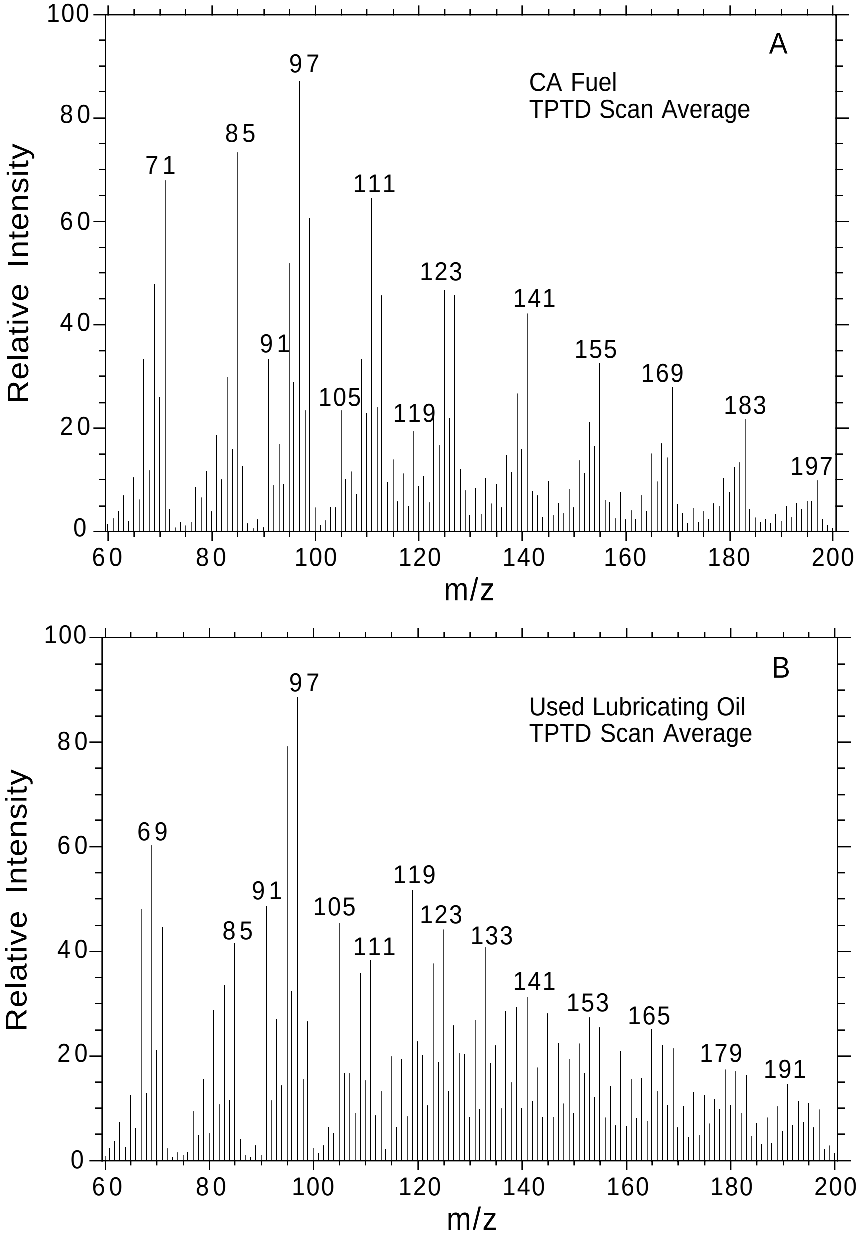

Figure 9. Fast-TPTD mass spectra of (A) CA fuel and (B) oil used in the Caterpillar study, obtained by averaging all scans, for 4 min sample collection.

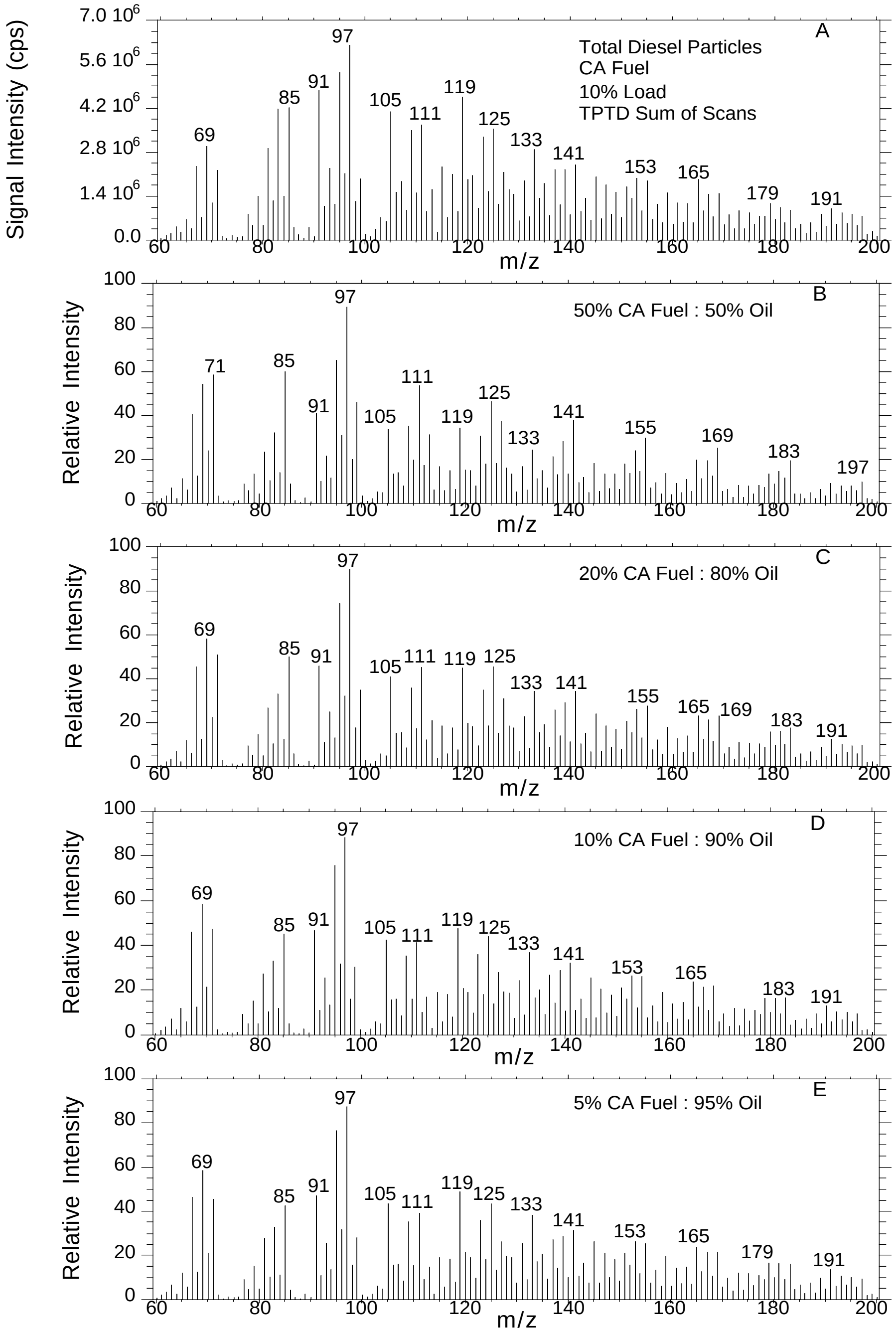

Figure 10. (A) Fast-TPTD mass spectrum of total diesel particles obtained by summing all scans, for 20 min sample collection from the Caterpillar engine with CA fuel at 10% load. (B-E) synthesized mass spectra obtained by mixing fractions of the fast-TPTD mass spectra of CA fuel and used oil from Figure 9.

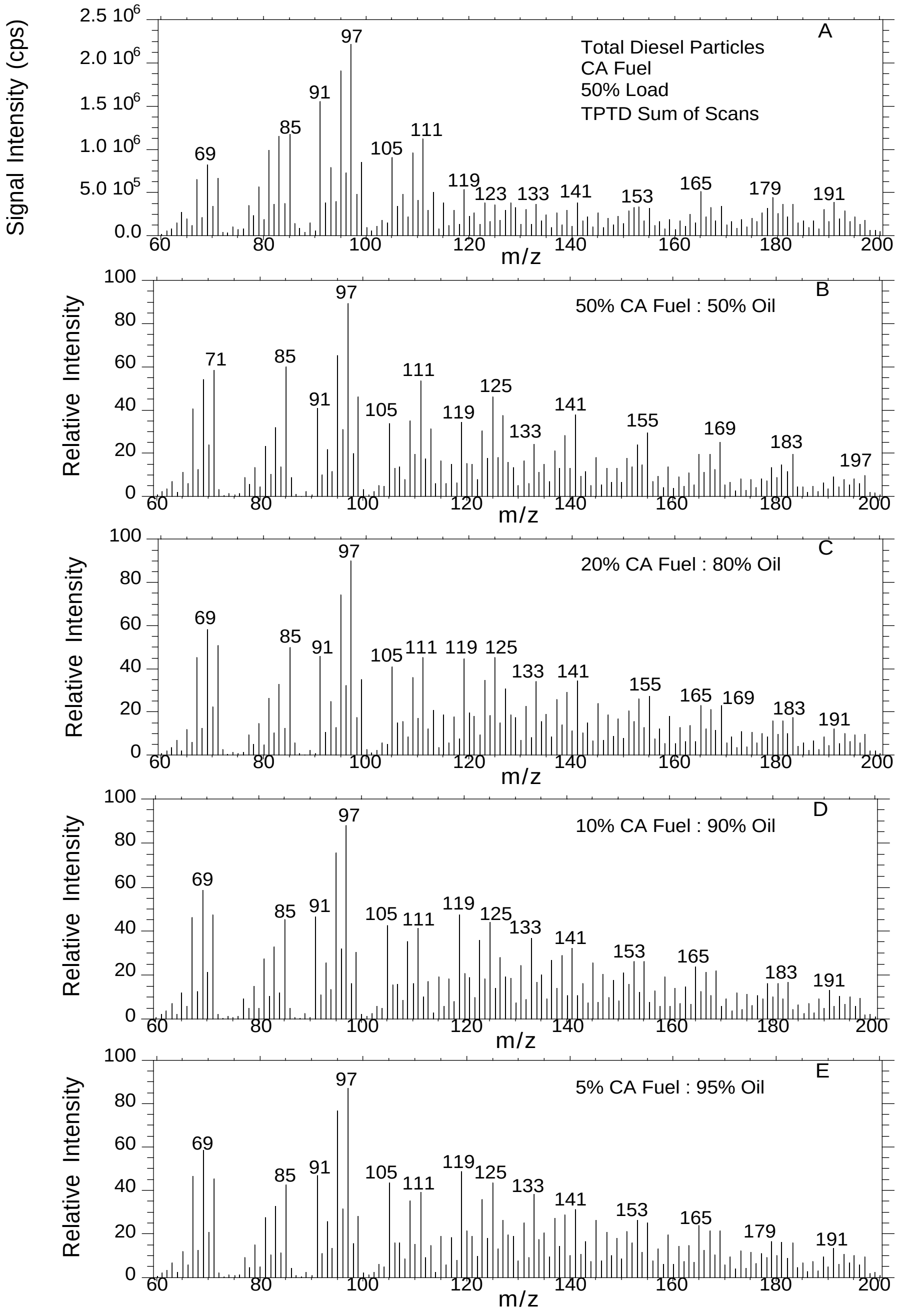

Figure 11. (A) Fast-TPTD mass spectrum of total diesel particles obtained by summing all scans, for 20 min sample collection from the Caterpillar engine with CA fuel at 50% load. (B-E) synthesized mass spectra obtained by mixing fractions of the fast-TPTD mass spectra of CA fuel and used oil from Figure 9.

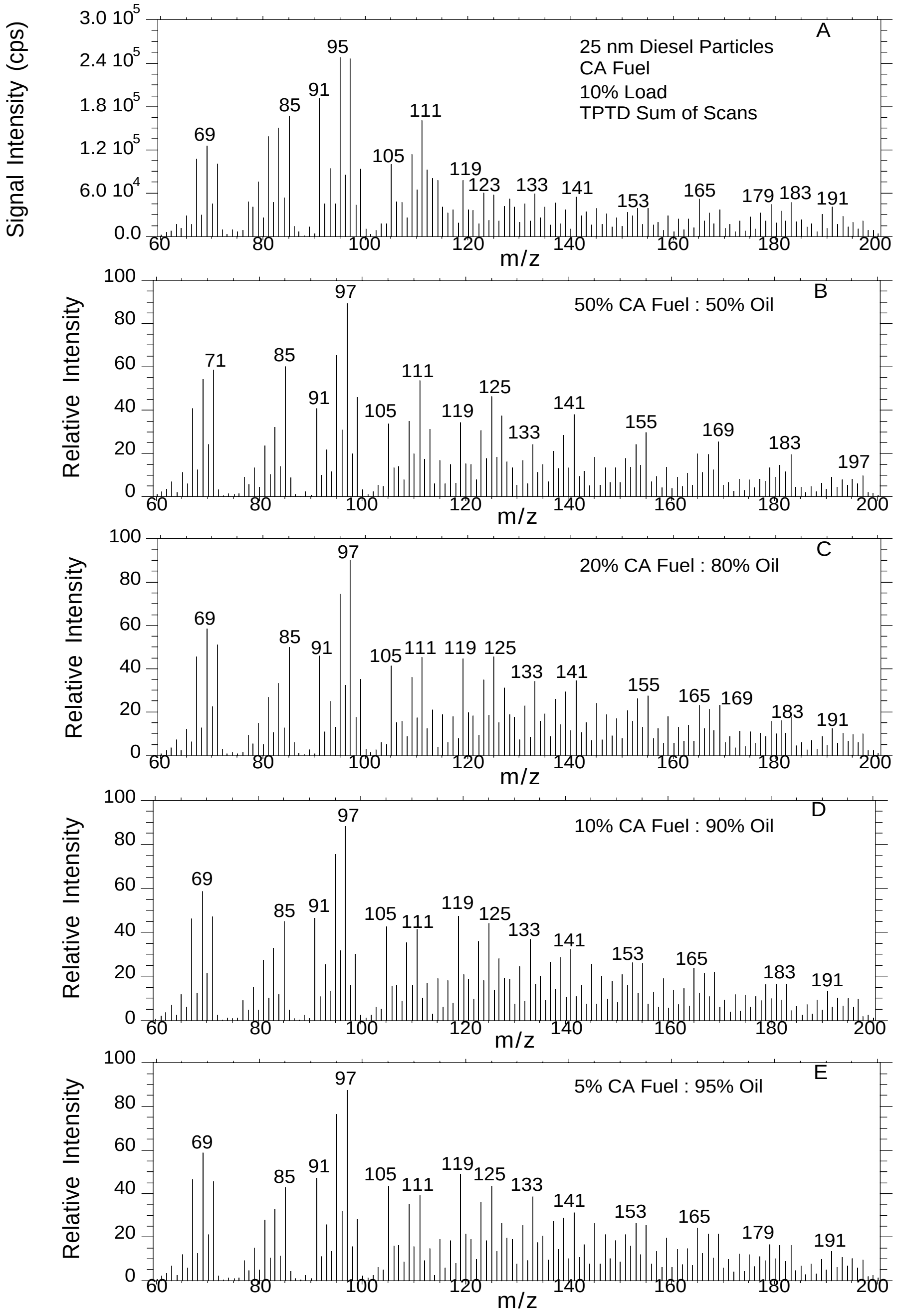

Figure 12. (A) Fast-TPTD mass spectrum of 25 nm diesel particles obtained by summing all scans, for 30 min sample collection from the Caterpillar engine with CA fuel at 10% load. (B-E) synthesized mass spectra obtained by mixing fractions of the fast-TPTD mass spectra of CA fuel and used oil from Figure 9.

Also shown are standard mass spectra obtained by mixing various fractions of the normalized fuel and oil spectra. Because the total mass spectral signal obtained from hydrocarbons is proportional to the mass of sample (i.e., the total signal/hydrocarbon mass is constant) (30) the component spectra are normalized by dividing the signal at each mass by the total signal. The total signal is obtained by summing from *m/z* 60-200 in order to avoid contributions from gases such as CO_2, O_2, N_2, and H_2O, and the hexane solvent used for the standards. This covers most of the organic signal, and should scale approximately linearly with the total hydrocarbon signal. Adding together two component spectra (e.g., 20% fuel spectrum and 80% oil spectrum) then yields the normalized mass spectrum that should be obtained for particles having those mass fractions of components. This approach must be used because, as will be shown below, the high volatility of many fuel components makes it impossible to prepare standard mixtures of particles having known amounts of fuel and oil.

Note first that in all the particle mass spectra the signals at *m/z* 60 and 73 (markers for oxidized organic combustion products, Figure 7C), and at *m/z* 64 (marker for sulfuric acid, Figure 7D) are negligible, indicating that these species are only minor contributors to the diesel particle mass. The major components are therefore some combination of unburned fuel and oil.

The total diesel particle mass spectra (Figures 10 and 11) are similar at the two loads, although the intensity of the higher mass fragments (above ~*m/z* 111) are somewhat lower at 50% load. This may due to enhanced thermal cracking of organics at the higher engine temperatures. The total diesel particle (Figure 10 and 11) and 25 nm nanoparticle (Figure 12) mass spectra are clearly different from that of a 50:50 mixture of fuel and oil, as indicated by the different patterns and relative intensities in the *m/z* 67-71 and 81-85 regions, and the pronounced *m/z* 141, 155, 169, 183, 197 series that appears in the mixture, but not the particles. The mass spectrum of a 20:80 mixture looks more similar to the particles in the low-mass region, although the intensity of *m/z* 85 relative to *m/z* 83 and 81 is still much higher in the mixture than in the particles. Furthermore, the high-mass *m/z* 165, 179, 191 series that predominates in the particles is equal to or less prominent than the *m/z* 141, 155, 169, 183 series that is indicative of a fuel component. As the oil component of the standard increases the mass spectrum looks more similar to that of the particles, and only when the mixture reaches ~90-95% oil are all the predominant peaks in the particle and mixture mass spectra the same. We therefore conclude that for these conditions total diesel particles and nanoparticles are at least 90-95% unburned oil, which is the limit with which we are confident distinguishing particle and standard mass spectra.

The fast-TPTD SIM (selected ion monitoring) profiles of diesel nanoparticles and total particles obtained with CA fuel at 10% load are shown in Figure 13. The profiles were obtained by monitoring *m/z* 69, but profiles for *m/z* 81, 85, 95, and 98 were similar. The similarity in the profiles for *m/z* 69, 85, and 95, which are markers for organics, and *m/z* 81 and 98, which are markers for organics and sulfuric acid, indicates that the sulfuric acid content of these particles is below the detection limit of the TPTD technique. In the John Deere study using high sulfur fuel (410 ppm S), the TPTD profiles of *m/z* 69, 85, and 95 exhibited a single desorption peak, due to organics, whereas *m/z* 81 and 98 exhibited two peaks, one from organics and the other from sulfuric acid. It appears that the lower sulfur content of the CA fuel, and perhaps the lower engine load (sulfuric acid was observed at 40% and 50% load in the John Deere study), greatly reduced sulfuric acid formation. When little sulfuric acid is present, particle nucleation may involve organic compounds. There are very low volatility organics present in the particles and lube oil, and these may be the nucleating species for nanoparticle formation in these experiments.

The TPTD profiles shown in Figure 13 raise an interesting question regarding the volatile components of the diesel particles. As the particle size decreases, the volatility of the aerosol appears to decrease, as indicated by the increasing desorption temperature. Previously we interpreted this shift as an indication of changing composition, such that the smaller particles were enriched in lower volatility components relative to larger particles. But the problem is that none of the size-selected particles contain the highest volatility components, which desorb at ~55°C in the total particles. Because the 75 nm particles are close to the mass median diameter of the distribution, it is expected that they would contain some of the high volatility compounds. The total particles therefore appear to contain components which are not present in any of the single size fractions. The reason for this discrepancy, which turns out to be an analytical artifact of TPTD desorption profiles measured for small samples, was not understood until the Cummins study, and so will be discussed in that section.

6.2.2.5. Results of TDMA Analyses

Preliminary particle water uptake measurements were made on nanoparticles sampled from the Caterpillar engine operating on CA and EPA fuel. Because organic compounds should take up negligible amounts of water, measurable uptake of water can be used to estimate the amount of sulfuric acid present in the nanoparticles. Although the results looked promising, the measurements were very preliminary in nature, and so will not be discussed in greater detail. They served primarily as preparation for the Cummins study, in which they yielded valuable information on nanoparticle sulfuric acid content.

6.2.3. Results of the Cummins Study

6.2.3.1. Summary of Activities

The Cummins engine study was carried out from 7/13/01–8/9/01. The TDPBMS was shipped from Los Angeles to Minneapolis on 7/13. The UCR group arrived on 7/15 and from 7/16-7/22 the TDPBMS was assembled and leak tested, baked, and calibrated in preparation for experiments. At this time the McMurry group set up the unipolar charger/NDMA for sampling size-selected diesel nanoparticles into the TDPBMS, a NSMPS for measuring diesel nanoparticle size distributions, and a NTDMA and RTDMA-APM for measuring particle volatility and water uptake. Measurements were performed over a range of engine loads from 10-50% using California (CA), Fischer-Tropsch (FT), and EPA Pump (EPA) fuels. The engine was operated by staff at the UMN-CDR. Measurements were performed from 7/23-8/3 using all instruments, and then continued from 8/6-8/9 with UMN instruments after the UCR group returned to California on 8/6. During the study, students, staff, and PIs met daily to evaluate results and plan upcoming experiments. Later in August, filter samples were collected under various engine conditions with all fuels by UMN-CDR staff for GC-FID analysis by the UCR group. After the Cummins study, the UCR group investigated the volatilities of fuels, oil, and standards using TPTD and performed GC-FID analysis on the fuel, oil, and diesel particle filter samples. The UMN group investigated the volatility and water uptake of standard compounds for comparison with the diesel exhaust particles. Data analysis was also performed. The engine specifications, operating conditions, exhaust sampling conditions, and a summary of particle analyses is given below.

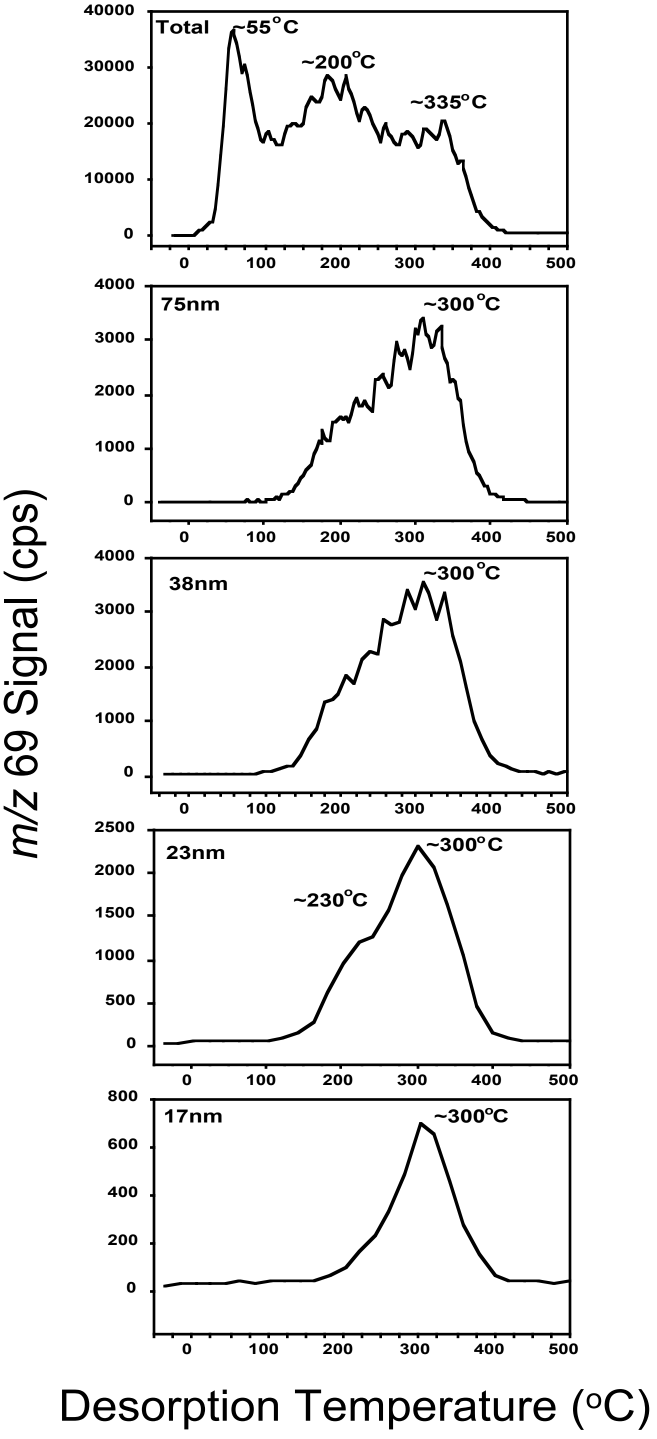

Figure 13. Fast-TPTD desorption profiles of 17 nm, 23 nm, 38 nm, 75 nm, and total diesel particles collected for 45, 15, 10, 13, and 3 min, respectively, from the Caterpillar engine with CA fuel at 10% load.

6.2.3.2. Cummins Diesel Engine Specifications, Operating Conditions, and Exhaust Sampling Conditions

Cummins Diesel Engine Specifications

Cummins ISM Engine
Year 1999
6 cylinder, 4 cycle
10.8-L engine displacement
Rated speed:
1350 lb-ft (= 1831 N-m) @ 1200 rpm (peak torque)
386 hp @ 1800 rpm (max power)

Cummins Diesel Engine Operating Conditions

Speed: 1400 rpm
Load: 10% (142 lb-ft), 20% (270 lb-ft), and 35% (510 lb-ft)
Fuel: CA (96 ppm S), FT (<1 ppm S), and EPA (360 ppm S)
Lubricating Oil: John Deere Plus 50 Supreme SAE 15W-40

Cummins Diesel Engine Exhaust Sampling Conditions

Sample temperature in VRTDS after dilution: ~35 ^{o}C
Sample relative humidity in VRTDS after dilution: ~5%
Primary dilution ratio: 14:1 and 20:1
Secondary dilution ratio: 27:1
Dilution tunnel residence time: 1.8 s (14:1 primary dilution ratio) and 1.4 s (20.1 primary dilution ratio)
Engine room temperature: ~35 ^{o}C
Particle analysis room temperature: ~30 ^{o}C

6.2.3.3. Cummins Study Data Summary

6.2.3.3.1. TDPBMS Data

The following is a summary of the TDPBMS data acquired during the Cummins study.

Full mass spectra of real-time particles

(a) CA fuel; 20% load; 14:1 primary dilution ratio; total particles; thermodenuder temperatures (^{o}C): 30, 50, 70, 80, 90, 150, 190, 300
(b) CA fuel; 35% load; 14:1 primary dilution ratio; total particles; thermodenuder temperatures (^{o}C): 40, 50, 70, 90, 190, 300
(c) FT fuel; 10% load; 14:1 primary dilution ratio; total particles; thermodenuder temperatures (^{o}C): 30, 50, 70, 90, 110, 190, 300
(d) FT fuel; 20% load; 14:1 primary dilution ratio; total particles; thermodenuder temperatures (^{o}C): 30, 50, 70, 90, 110, 190, 300

Full mass spectra/TPTD of collected particles

(a) CA fuel; 20% load, 14:1 primary dilution ratio; total particles; 4 min collection time

SIM/TPTD analyses of collected particles

(a) CA fuel; 20% load; 14:1 primary dilution ratio; total particles; collection times (min): 5, 19; fast-TPTD
(b) CA fuel; 20% load; 14:1 primary dilution ratio; total particles; collection times (s): 5, 15, 30, 60, 240; fast-TPTD
(c) CA fuel; 20% load; 14:1 primary dilution ratio; particle size (nm): total, 250, 150, 70, 40; collection times (min): 5, 15, 20, 30, 60; fast-TPTD
(d) CA fuel; load (%): 20, 35, 50; 14:1primary dilution ratio; total particles; 60 min collection time; slow-TPTD
(e) FT fuel; 20% load; 14:1 primary dilution ratio; total particles; 60 min collection time; slow-TPTD

Full mass spectra and SIM/TPTD (fast and slow) of standards

(a) Fuels: CA, FT, EPA
(b) Oils: John Deere Plus 50 Supreme SAE 15W from Cummins engine, new and used
(c) Alkanes: C20, C24, C28, C32, C36
(d) Sulfuric acid

6.2.3.3.2. NTDMA and RTDMA-APM Data

The following is a summary of the TDMA data acquired during the Cummins study. The dilution ratio was 14:1, except for the 35% load condition in which it was 20:1.

Volatility data

(a) CA fuel; load (%) 20, 35; NTDMA particle size (nm): 12, 30, 50 nm; RTDMA-APM particle sizes (nm): 70, 120, 200
(b) FT fuel; load (%): 10, 20; NTDMA particle size (nm): 12, 30, 50; RTDMA-APM particle size (nm): 70, 120, 200
(c) EPA fuel; 35% load; NTDMA particle size (nm): 12, 30, 50; RTDMA-APM particle size (nm): 70, 120, 200

Water uptake data

(a) CA fuel; load (%): 20, 35; NTDMA particle size (nm): 7, 12, 30; RTDMA-APM particle size (nm): 50, 60, 70, 100, 120, 150
(b) EPA fuel; load (%) 20, 35; NTDMA particle size (nm): 12, 30, 50; RTDMA-APM particle size (nm): 70, 120, 200

6.2.3.4. Results of Particle Size Distribution Measurements

Figure 14 shows the size distributions of exhaust particles from the Cummins engine after primary dilution for CA, FT, and EPA fuels and operation at different engine loads, while the engine speed was maintained at 1400 RPM. The primary dilution ratio was 14:1, except for CA fuel at 35% load, for which it was 20:1. The secondary dilution was 27:1. NSMPS (2.9-50 nm) and RSMPS (30-275 nm) systems were used to cover the size range shown in the figure. As a baseline comparison among the three fuels, at 20% load the number concentrations between 2.9 and 275 nm were dominated by the nuclei-mode particles, with the accumulation mode particles being less abundant. For example, the size distribution for the CA fuel did not have a distinct accumulation mode peak, but showed merely a shoulder which started at ~70-80 nm. Particle number concentrations decreased in the order EPA (1.1 x 10^8/cm^3) > CA (3.3 x 10^7/cm^3) > FT (8.9 x 10^6/cm^3) fuel. The peak in the number distributions occurred at 28, 50, and 22 nm for the CA, FT, and EPA fuels, respectively. As the engine load was increased to 35%, the nuclei mode obtained for each fuel shifted to smaller sizes and the number concentration decreased, while the concentration of accumulation mode particles increased. In the size distributions for the CA fuel at 35% load, for example, the nuclei mode became very weak and was apparent only as a shoulder at about 10-20 nm, while the accumulation mode increased to become the overall peak in the size distribution at about 50-70 nm.

In order to put these observations in the context of E-43 on-road studies, where bimodal distributions were clearly observed, we note that the two-stage dilution system used has a fairly wide range of residence times in the first stage where most nanoparticles form and grow. This leads to a slightly broader nuclei mode that is a little less distinct than in some of the on-road measurements. Despite this the nuclei mode is very clear with the EPA fuel for 20 and 35% load (light and medium load cruise) and for the CA fuel at 20% load. It is harder to see with the Fischer-Tropsch fuel, but that fuel might not have made much of a nuclei mode on-road either, although it was not tested. The broadening of the nuclei mode is due to physical processes (coagulation, condensation, etc.) and should not significantly alter its chemical composition. Furthermore, while the E-43 program showed that it was difficult to match specific real world on-road conditions in the laboratory, composite average on-road size distributions were very similar in shape to corresponding measurements in the laboratory.

In several instances a distinct peak was observed at the lower end of the NSMPS scan (Figure 14). The presence of this peak has not been previously reported. The peak was most prominent when the engine was operated with EPA fuel at 35% load, appearing at about 4.3 nm, but was absent at 20% load. The peak was also present with the CA fuel, but in this case at ~3.3 nm and at all engine loads. The peak appears to be real, based on the numbers of particles detected repeatedly in the 3-5 nm range, which were used to calculate the concentrations shown in the plots. Measurements in this size range are difficult, however, because of sharp drops in the performance of the UCPC and NDMA. Calculation of particle concentrations include corrections for the lowered efficiencies of the two instruments, but add considerable uncertainty to the absolute concentration of this peak in the plot. In addition, the cut-off at 3 nm may not be real, and the peaks may be wider and extend further toward smaller sizes. For the FT fuel, although the size distribution curves have some structure at ~3-4 nm, the numbers of particles detected in this size range were too low to ascertain the presence of the peak. The relative concentration of particles at this peak compared to the nuclei mode peak was highest (~2.7 %) for EPA fuel at

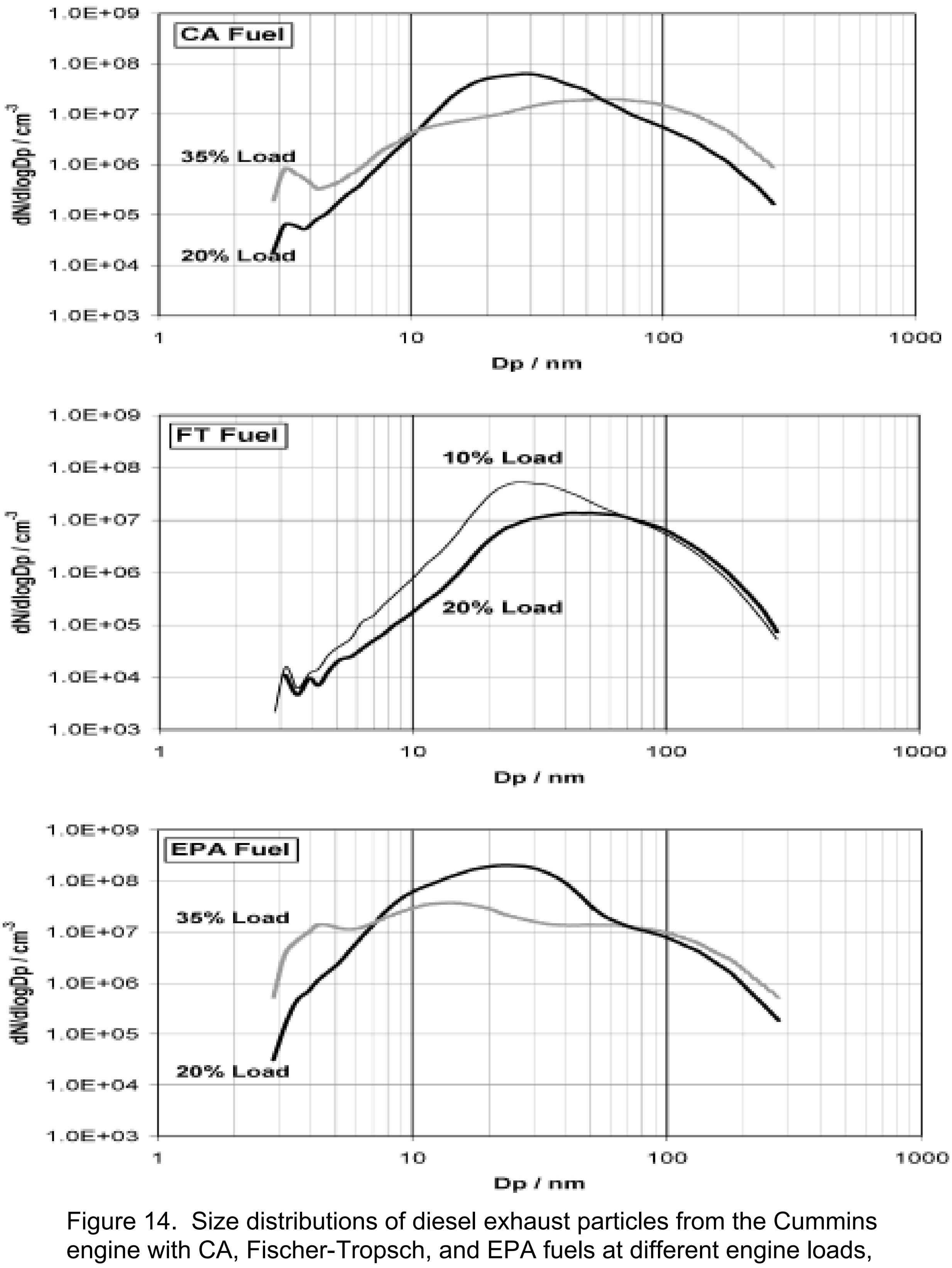

Figure 14. Size distributions of diesel exhaust particles from the Cummins engine with CA, Fischer-Tropsch, and EPA fuels at different engine loads, measured using two SMPS systems. Each curve is an average of several scans.

35% load and lowest (~0.1 %) for the CA fuel at 20% load. To the best of our knowledge, these are the first measurements in which a NSMPS has been used to characterize size distributions of diesel nanoparticles. It is clear from the interesting observations made here that this new instrument system is a powerful tool for diesel nanoparticle studies.

6.2.3.5. Results of TDPBMS Analyses

6.2.3.5.1. Fast-TPTD Analysis and Potential Desorption Artifacts

The results of the Caterpillar study raised an important question with regards to the volatility profiles of the diesel particles. TPTD analysis of total particles showed the presence of components that desorbed at temperatures between ~25-400 °C. But analysis of size-selected particles as large as 75 nm, which was approximately the mass median diameter, showed no components desorbing below ~125 °C. In an effort to determine the particle size mode in which the most volatile components resided, TPTD analyses were performed in the Cummins study for a range of particle sizes. The results were similar to those shown in Figure 13 for the Caterpillar study. It was then noticed that the amount of sample collected (as indicated by the TDPBMS signal) increased with selected particle size, as would be expected from the particle mass distribution and constant collection time. To further investigate this observation, analyses were performed on total particles collected for decreasing periods of time. The results are shown in Figure 15. It then became apparent that the volatility of the particles (as indicated by desorption temperature) was not correlated with particle size, but with sample size. This led to the hypothesis that the particle desorption behavior was being influenced by adsorption of compounds to diesel soot particles that had coated the vaporizer. Apparently, as compounds evaporated from the organic particle matrix, they first adsorbed onto elemental carbon present in the deposits. The strong adsorption to this material then delayed evaporation until the vaporizer reached much higher temperatures. For sufficiently large samples, the soot surface became completely coated during desorption and compounds began to evaporate at lower temperatures, thus shifting the desorption profile. To test this theory we performed fast-TPTD analysis on fuel, oil, and single-compound standards during the Cummins study. The desorption behavior was similar to that of diesel particles. Soon after returning to UCR we removed the vaporizer and noted that it had a very grainy appearance, which we had not noticed in the past. We replaced this with a new vaporizer of the same design (which had a smooth, shiny appearance) and analyzed a variety of standards by fast-TPTD. The high-temperature desorption peaks observed with the soot-covered vaporizer dramatically decreased in intensity, although they were sometimes still apparent with very small samples. An example is shown in Figure 16, in which dioctyl sebacate (MW 426 organic ester) SIM profiles are displayed for analysis of similar size samples on the soot-covered vaporizer and clean vaporizer. The two peaks observed for this single compound (Figure 16A) on the soot-covered vaporizer cannot be due to desorption of multiple compounds with different vapor pressures, as one might presume for a mixture such as diesel particles. Since the high temperature peak nearly disappears when a clean vaporizer is used, we conclude that the second peak is due to adsorption on soot. The slight tailing observed with the clean vaporizer may be due to adsorption onto the metal surface or evaporation of small amounts of residual material from regions of the vaporizer mount that heat more slowly than the vaporizer. Because the V-shaped vaporizer is mounted with the two legs of the V facing the

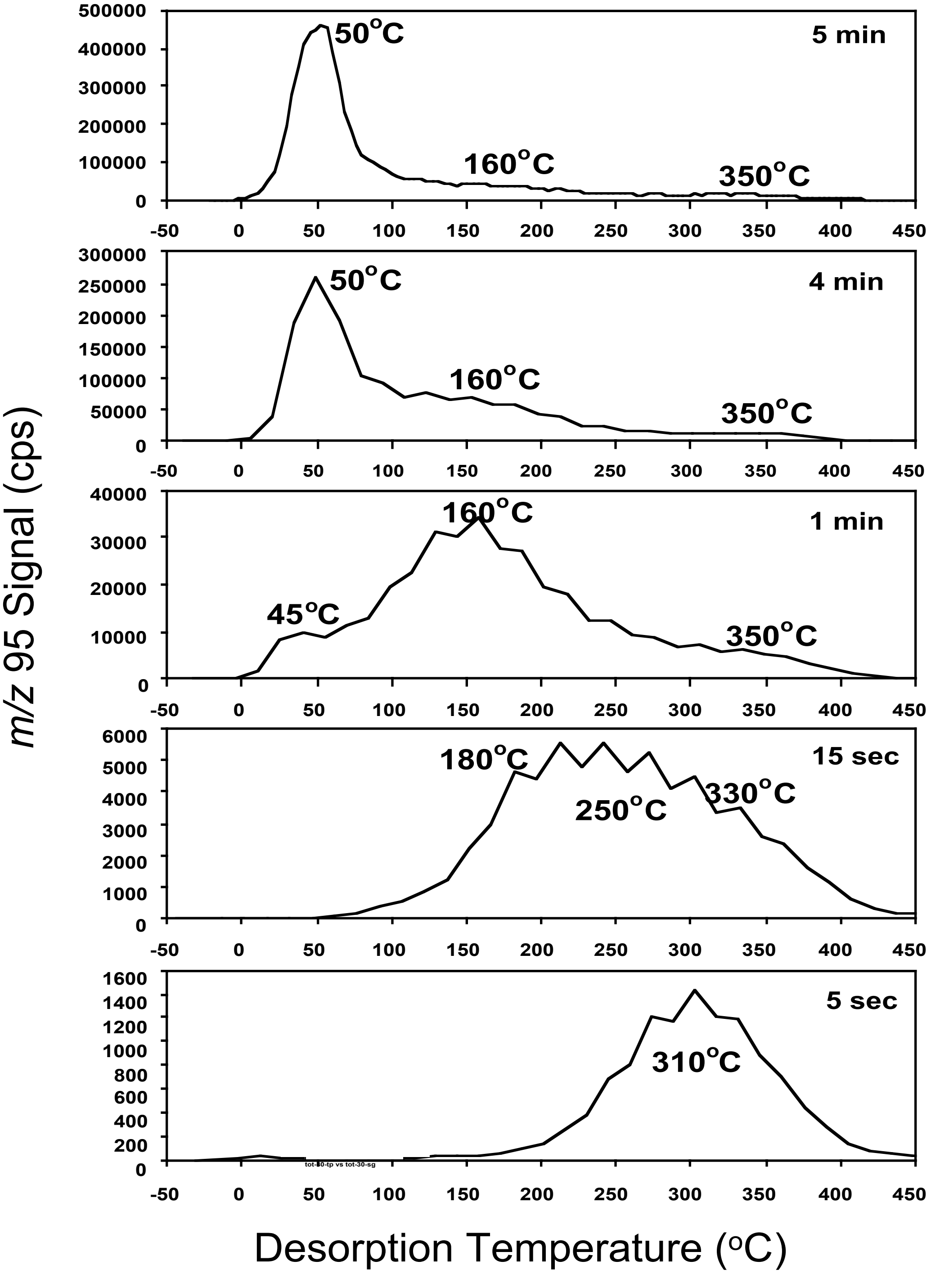

Figure 15. Fast-TPTD desorption profiles of total diesel particles collected for 5 min, 4 min, 1 min, 15 s, and 5 s, from the Cummins engine with CA fuel at 20% load.

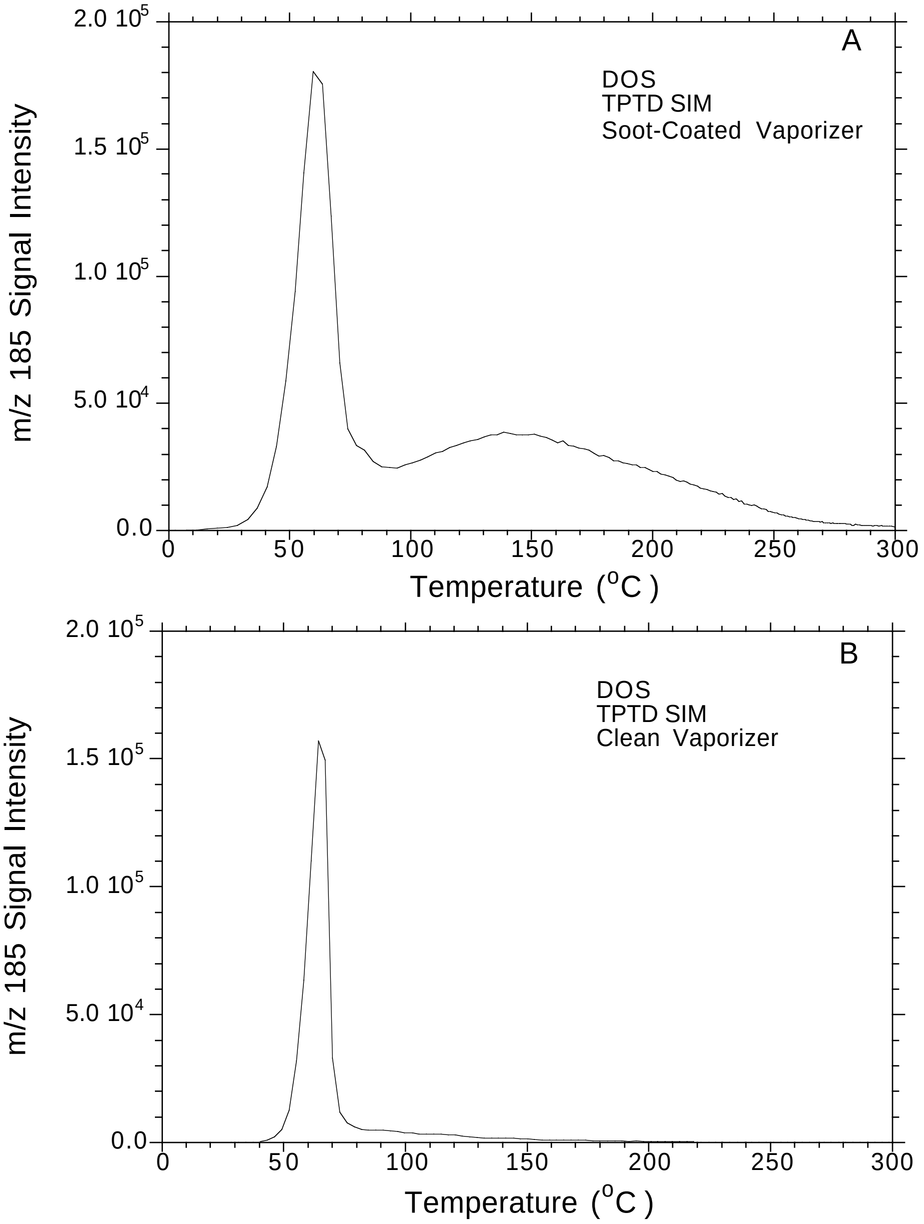

Figure 16. Fast-TPTD desorption profiles of dioctyl sebacate (DOS) particles (A) collected for 1.5 min on a soot-coated vaporizer during the Cummins study and (B) collected for 1 min on a clean vaporizer.

particle beam, and only a bottom surface which is perpendicular to the V faces the mass spectrometer, a large fraction (at least ~85% based on the orientation of vaporizer surfaces relative to the mass spectrometer opening) of the evaporating molecules that are eventually analyzed will strike other surfaces of the vaporizer before entering the mass spectrometer. All these observations are therefore consistent with the theory that soot adsorption is responsible for the desorption profiles. In addition, soot adsorption provides an explanation for the desorption temperatures of small samples, which are too high (up to 300-400 ^{o}C) to be explained by the vapor pressures of fuel, oil, or oxidized organic combustion products. From the desorption calibration curve in Figure 23, which is discussed later, a hydrocarbon would need to contain ~60 carbon atoms to desorb at 300 ^{o}C (note that this curve is for slow-TPTD, but fast-TPTD desorption temperatures are only ~17 ^{o}C higher).

This result is unfortunate, because it makes our use of desorption temperature as an indicator of particle volatility unreliable for small particle samples. The effect was not noticed in TPTD analyses prior to the diesel studies, probably because the vaporizer had not been exposed to soot particles, and because larger samples were used for analysis. This result impacts some of the conclusions of our Phase 1 study on the John Deere engine. There we observed two peaks in the TPTD desorption profiles and concluded that this was probable due to contributions from fuel and oil. Now we conclude that the low temperature peak probably represents evaporation of organics from the organic matrix, while the high temperature peak represents desorption from elemental carbon. The nanoparticle desorption profiles do not provide information on whether these components originated from fuel or oil. The mass spectrum, however, which is not influenced by the adsorption effect, indicates that the material is derived primarily (and perhaps completely) from oil. The nanoparticle desorption profiles also cannot be used to determine the effect of engine load and particle size on particle volatility, as was done in the John Deere study. Fortunately, TDMA analyses of particle volatility performed in the Cummins study were not subject to adsorption artifacts, and so filled this gap in measurement capabilities. Finally, our previous conclusions regarding the presence of sulfuric acid in nanoparticles is also not affected by soot adsorption. This is because the conclusions were based on comparisons of desorption profiles of two *m/z* ratios from the same nanoparticle sample. The profile for *m/z* 69 (and 85 and 95), which are markers for organics, showed a single desorption peak at ~150-180 ^{o}C. The profile for *m/z* 98 (and 81), which are markers for organics and sulfuric acid, showed desorption peaks at ~150-180 ^{o}C and at ~22-43 ^{o}C. If these peaks were due to desorption of organics from an organic matrix and soot, then all five peaks would be affected. Since only those that could come from organics and sulfuric acid showed two peaks, it is valid to conclude that the high temperature peak is due to organics, and the low temperature peak to sulfuric acid.

6.2.3.5.2. Diesel Nanoparticle Composition

Because the mass spectra obtained in previous studies had provided strong evidence that the organic component of nanoparticles came primarily from unburned oil, and because of the problem we discovered regarding nanoparticle TPTD desorption profiles, in the Cummins study we focused on analysis of total particles. We did perform TPTD analyses of nanoparticle samples to ascertain the possible presence of sulfuric acid, but found no evidence for this compound.

6.2.3.5.3. Total Diesel Particle Composition: Fuel and Oil Contributions

An important objective of this project was to investigate the relative contributions of fuel and lubricating oil to the diesel particle organic fraction. The approach was to compare the mass spectra of diesel particles with the mass spectral standards of fuel and oil mixtures. As discussed previously, the mass spectra of diesel nanoparticles analyzed in both the John Deere (Phase 1 Final Report; Figures 3 and 4) and the Caterpillar (Figure 12) studies were similar to the mass spectra of the oil, and in the Caterpillar study we estimated that unburned oil comprised at least 90-95% of the organic matter. In the Cummins study we again used the CA fuel, but also ran the engine on a Fischer-Tropsch (FT) fuel. This is a synthetic fuel containing mostly alkanes, which has a much simpler mass spectrum than the CA fuel and is therefore even more easily distinguished from oil. For the Cummins study, we also focused on total diesel particles because the larger sample sizes made possible more thorough mass analysis in real-time and by TPTD.

The mass spectra of the CA fuel, FT fuel, and used lubricating oil taken from the Cummins engine are shown in Figure 17. The CA and FT fuels both have a strong series of alkane peaks at *m/z* 57, 71, 85, 99, … 197. But whereas these are the dominant peaks in the FT spectrum, the CA fuel mass spectrum contains additional series of peaks with significant intensity due to other compounds. The mass spectrum of the lubricating oil is different from those of both fuels in aspects that were noted above for the Caterpillar study, although the differences are more obvious with the FT fuel.

Figure 18 shows the real time-mass spectra of the organic component of total diesel particles when the engine was running on CA fuel. Also shown are mass spectra of synthesized fuel and oil mixtures. The absence of *m/z* 60, 64, and 73 again indicates that oxidized organic combustion products and sulfuric acid are minor components, and that the particles are primarily comprised of some combination of unburned fuel and oil. The particle mass spectrum is similar to all the standards shown with respect to the relative intensities of *m/z* 165, 179, and 191 in the high-mass range. In the low-mass range, there are obvious differences between *m/z* 67-71 until the mixture becomes 30:70, and between *m/z* 81-85 until the composition reaches 80% oil. Further addition of oil does not significantly change the standard mass spectrum. We therefore conclude that for these conditions the total diesel particles are at least 80% unburned oil.

Under these conditions, the real-time mass spectra of diesel particles are clearly dominated by unburned lubricating oil, but in an attempt to gain more detailed composition information the particles were also analyzed using fast-TPTD. This allowed mass spectra to be obtained for components of different volatilities. The first four scans for which signal was observed and the sum of all scans obtained in the analysis of particles sampled when the engine was running on CA fuel are shown in Figure 19. The average fast-TPTD temperature during each scan and the equivalent slow-TPTD temperature are given in the caption. The equivalent slow-TPTD temperature was calculated by subtracting 17 ^{o}C from the measured fast-TPTD temperature. This value was obtained by comparison of the desorption temperatures of standards analyzed by both methods. The desorption temperature increases with increasing ramp rate because the fraction of material that evaporates in a given temperature interval is proportional to the product of the vapor pressure (which increases with temperature) and the evaporation time. As the ramp rate increases, the amount of time particles are exposed to a given temperature decreases. In other words, because during fast-TPTD the sample is desorbed in less time than in slow-TPTD, the average temperature to which the sample is exposed is higher.

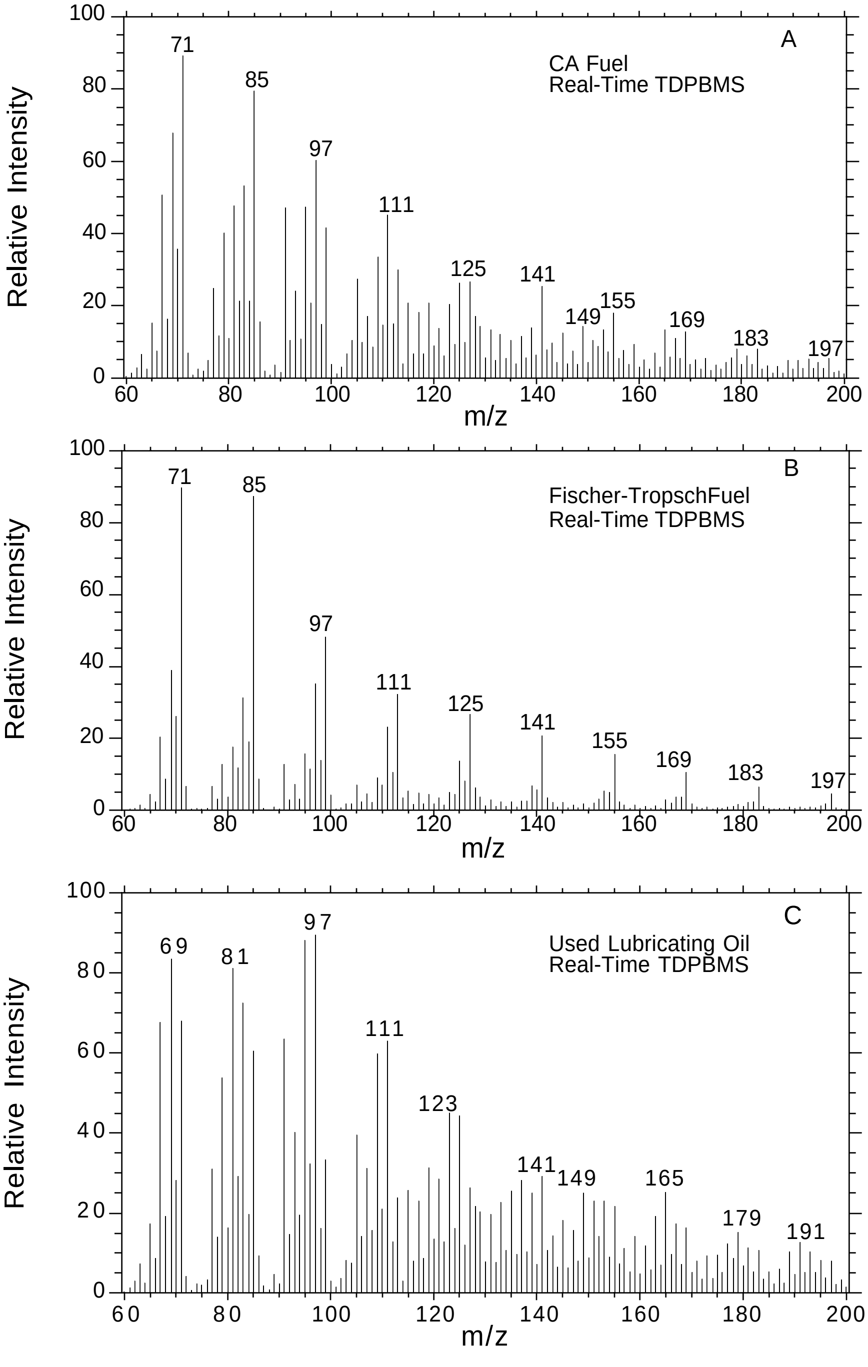

Figure 17. Real-Time TDPBMS mass spectra of (A) CA fuel, (B) Fischer-Tropsch fuel, and (C) used oil.

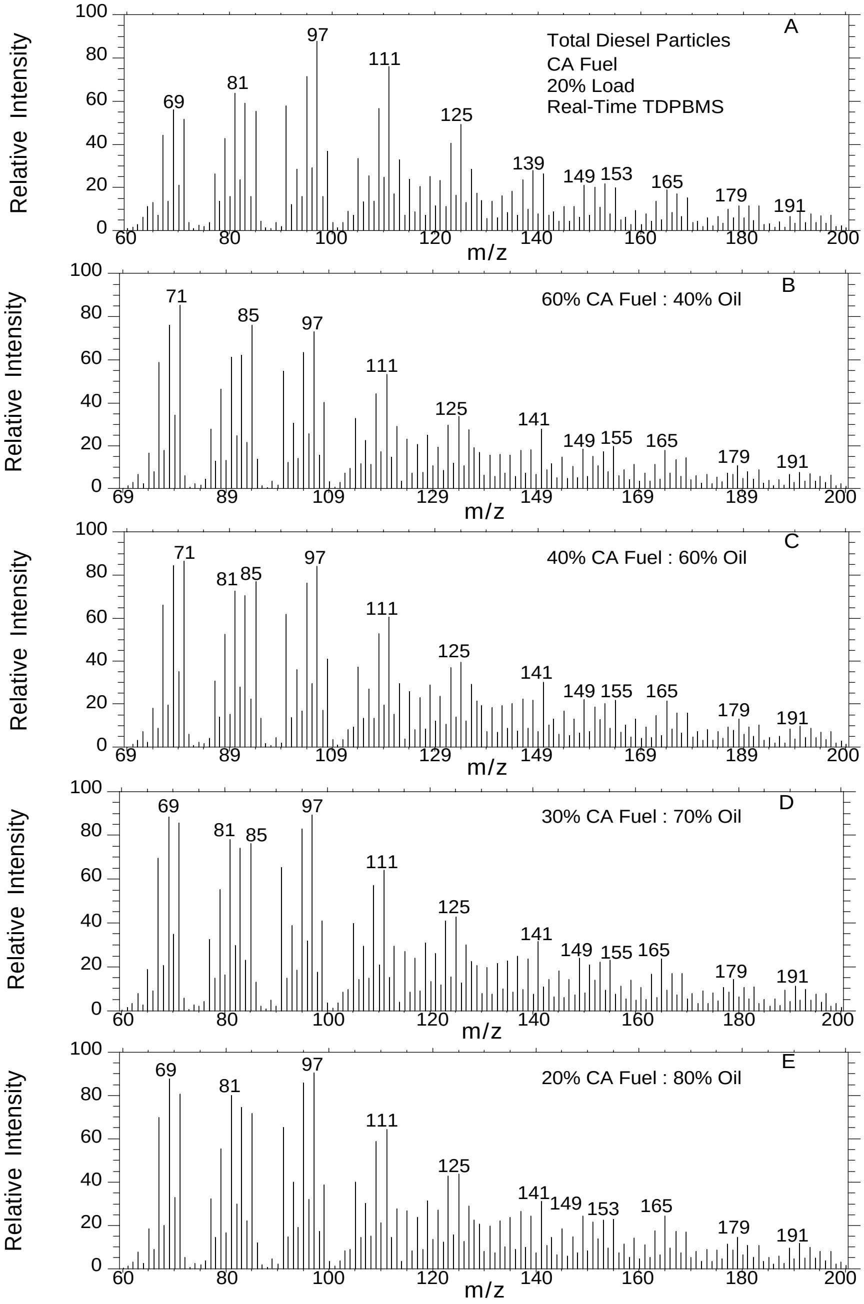

Figure 18. (A) Real-Time TDPBMS mass spectrum of total diesel particles obtained from the Cummins engine with CA fuel at 20% load and (B-E) synthesized mass spectra obtained by mixing fractions of the real-time TDPBMS mass spectra of CA fuel and used lubricating oil from Figure 17.

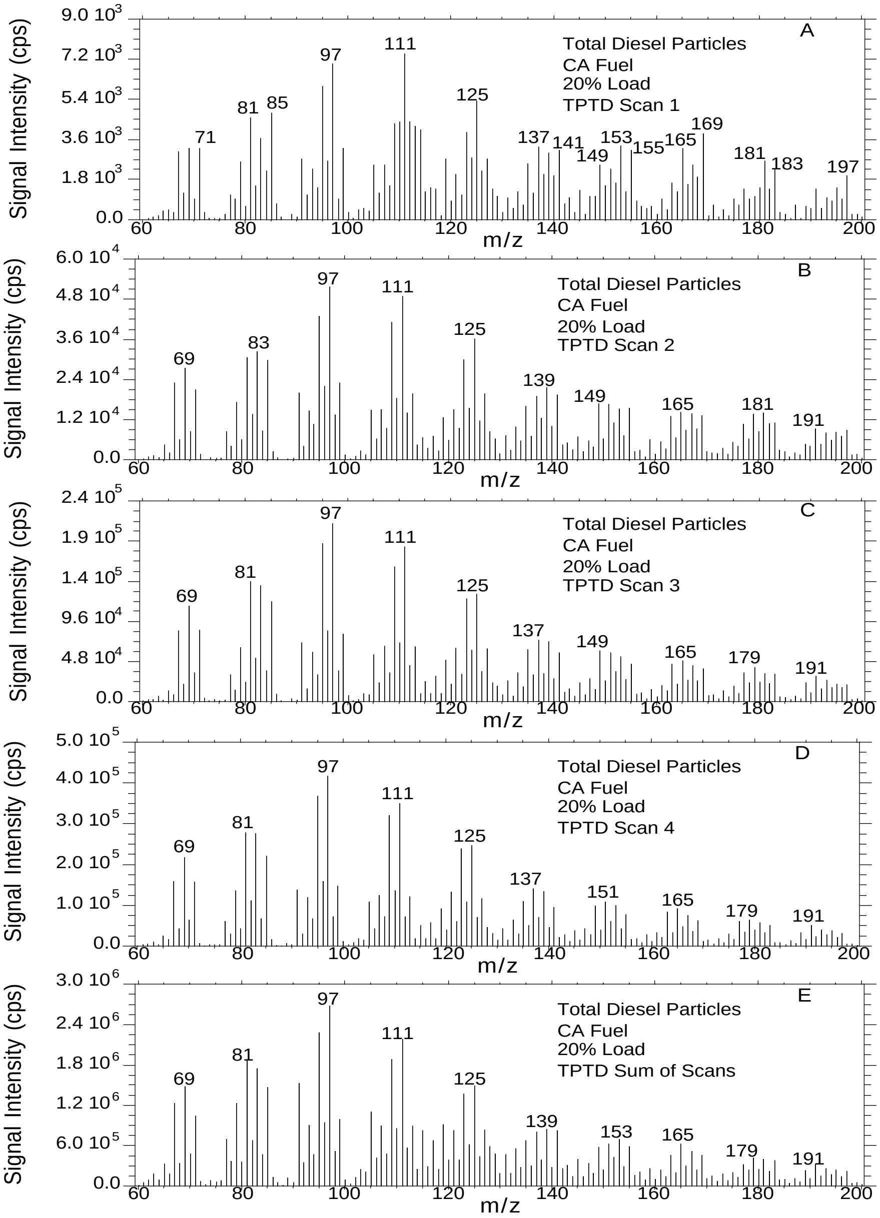

Figure 19. Fast-TPTD mass spectra of total diesel particles collected for 4 min from the Cummins engine with CA fuel at 20% load. The first scan in which signal was observed is (A) Scan 1, (B-D) are spectra from the next three scans, and (E) is the sum of all scans. The peak signal occurred at scan 4. The average temperatures (^{o}C) during each scan are approximately (A) 20 [3], (B) 40 [23], (C) 60 [43], and (D) 80 [63], with the equivalent slow-TPTD temperatures shown in brackets (see text for calculation details). The width of each scan is ~20 ^{o}C.

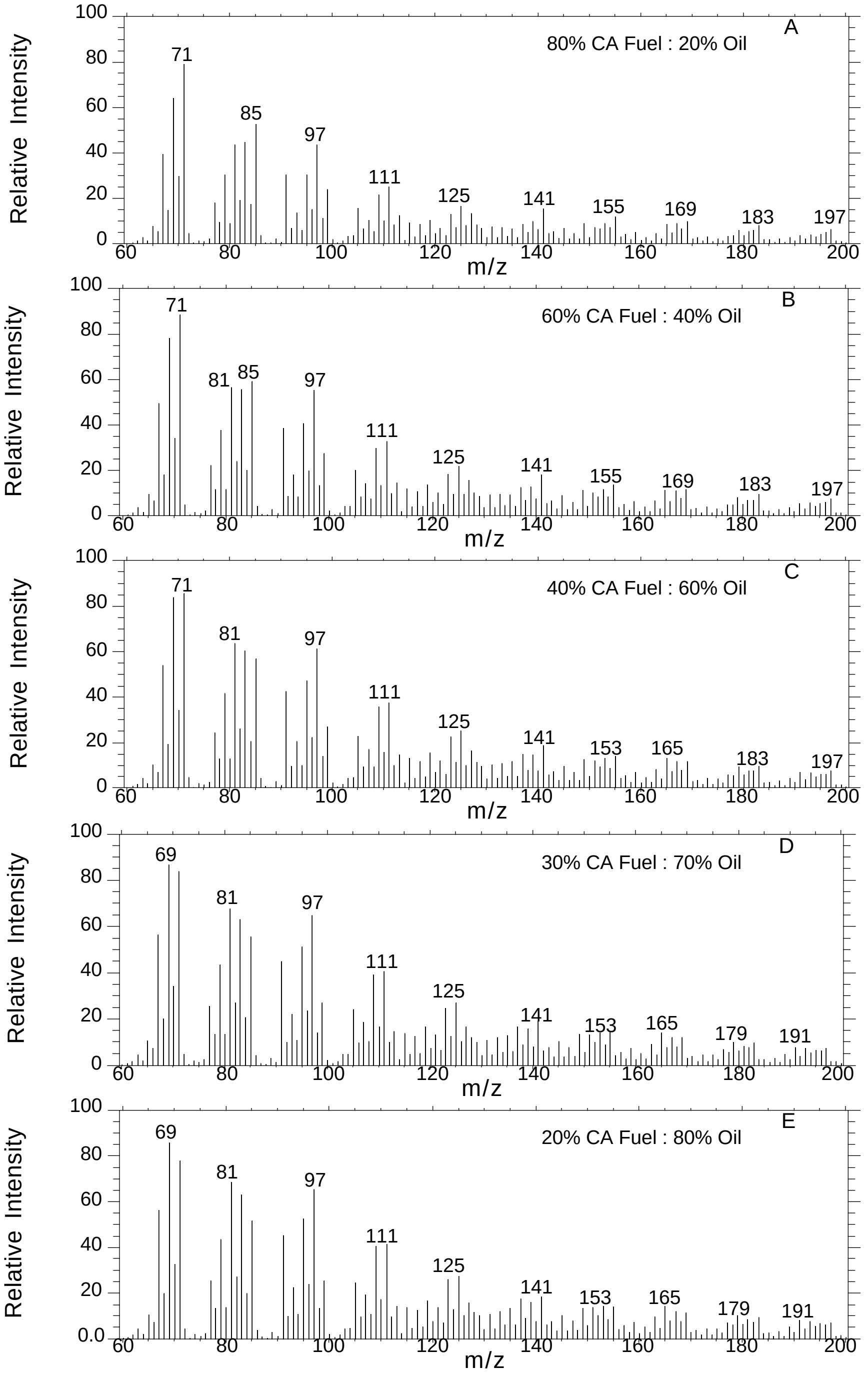

Figure 20. Synthesized mass spectra obtained by mixing fractions of the fast-TPTD mass spectra of CA fuel and used oil from Figure 5.

Figure 20 shows the mass spectra of fuel and oil mixtures synthesized from the fast-TPTD spectra shown earlier in Figure 5. Figure 19A is a mass spectrum of the most volatile components of the particles, which were the first to desorb when the sample was heated. This spectrum looks similar in many respects to the standard spectrum of a 60:40 mixture of fuel and oil (Figure 20B), especially the *m/z* 81-85 region and the intense *m/z* 141, 155, 169, 183, 197 series. The mass spectra of the second scan (Figure 19B) also shows contributions from fuel, but looks much more like oil than the first scan. The first two scans cover the equivalent slow-TPTD temperature range from ~-7 to 33 ^{o}C. Comparing these temperatures with the calibration curve shown below in Figure 22 indicates that the first two scans cover the carbon number range from ~C16-C26, which from the chromatograms shown in Figure 24A and 24C are consistent with a fuel and oil mixture. Later scans (Figures 19C and 19D) and the sum of all scans (Figure 19E) look like the pure oil mass spectrum, but cannot be distinguished from standards containing up to 30% fuel. On this basis we conclude that for these conditions the total diesel particles are comprised of 70% or more oil. Because the obvious contributions of fuel to the mass spectrum disappear after the second scan, however, and the desorption temperatures of later scans correspond to carbon numbers beyond those which can come from fuel, the scans beyond the second must correspond to oil. Assuming that 50% of the material in the first two scans is from fuel, on the basis of the fraction of the total signal in these scans we conclude that unburned fuel comprises only ~1 % of the total diesel particles. Figure 21 shows the real time-mass spectra of the organic component of total diesel particles sampled when the engine was running on Fischer-Tropsch fuel, and also the synthesized mass spectra of fuel and oil mixtures. Because of the much simpler mass spectrum of this fuel compared to the CA fuel, it is easier to distinguish fuel and oil contributions to the diesel particles. The absence of *m/z* 60, 64, and 73 again indicates that oxidized organic combustion products and sulfuric acid are only minor components, and that the particles are primarily comprised of some combination of unburned fuel and oil. The particle mass spectra and standards only become indistinguishable in the high-mass range for mixtures containing at least 80-90% oil, at which point the *m/z* 141, 155, 169, 183 series becomes less strong than the *m/z* 165, 179, and 191 peaks. In the low-mass range, however, it is not until the standard contains 95% oil that the differences between mass spectra disappear, especially in the m/z 81-85 region. From this we conclude that under these conditions the total diesel particles contain at least 95% unburned oil.

In addition to comparing mass spectra, the organic components of diesel particles were analyzed by comparing the TPTD desorption profiles of particles with those of the fuels, oil, and alkane standards. These are large samples, and therefore the desorption profile is not significantly impacted by adsorption to soot. The measured relationship between alkane carbon number and TPTD desorption temperature is shown in Figure 22. The equivalent alkane carbon numbers of the components of fuel, oil, and diesel particles were estimated by comparing the desorption profile of the sample with the standard curve. The results of TPTD analyses of CA and FT fuel, oil, and diesel particles are shown in Figure 23. The fuels and oil were also analyzed by gas chromatography with flame ionization detection (GC-FID). The chromatograms are shown in Figure 24. An attempt was also made to analyze filter samples of diesel particles, but the amount of collected material was below the detection limits of the GD-FID measurement.

From the gas chromatograms it can be seen that particle components with carbon numbers less than ~C15 must come from fuel, those with carbon numbers greater than ~C25 must come from oil, and those between ~C15 and C25 could come from either fuel or oil.

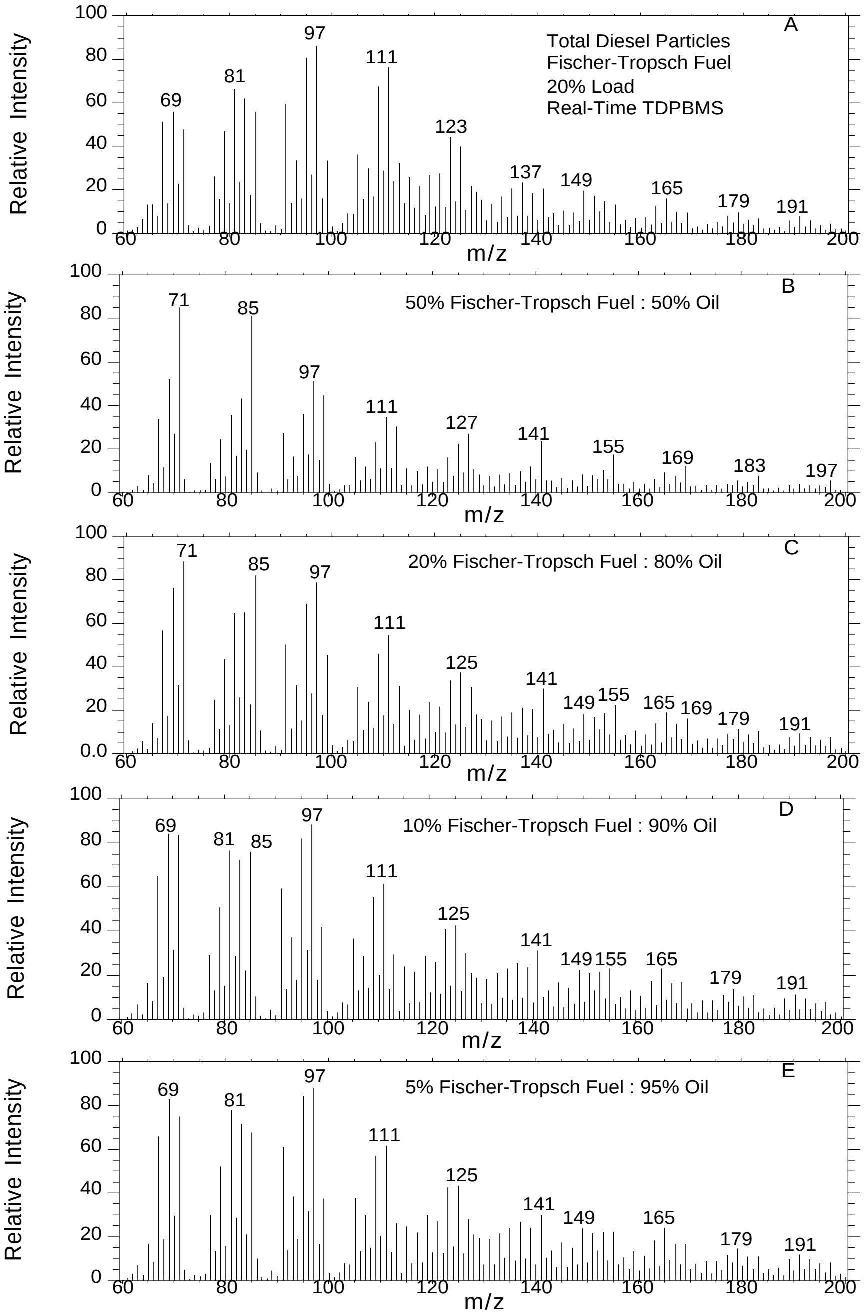

Figure 21. (A) Real-Time TDPBMS mass spectrum of total diesel particles obtained from the Cummins engine with Fischer-Tropsch fuel at 20% load and (B-E) synthesized mass spectra obtained by mixing fractions of the real-time TDPBMS mass spectra of Fischer-Tropsch fuel and used oil from Figure 17.

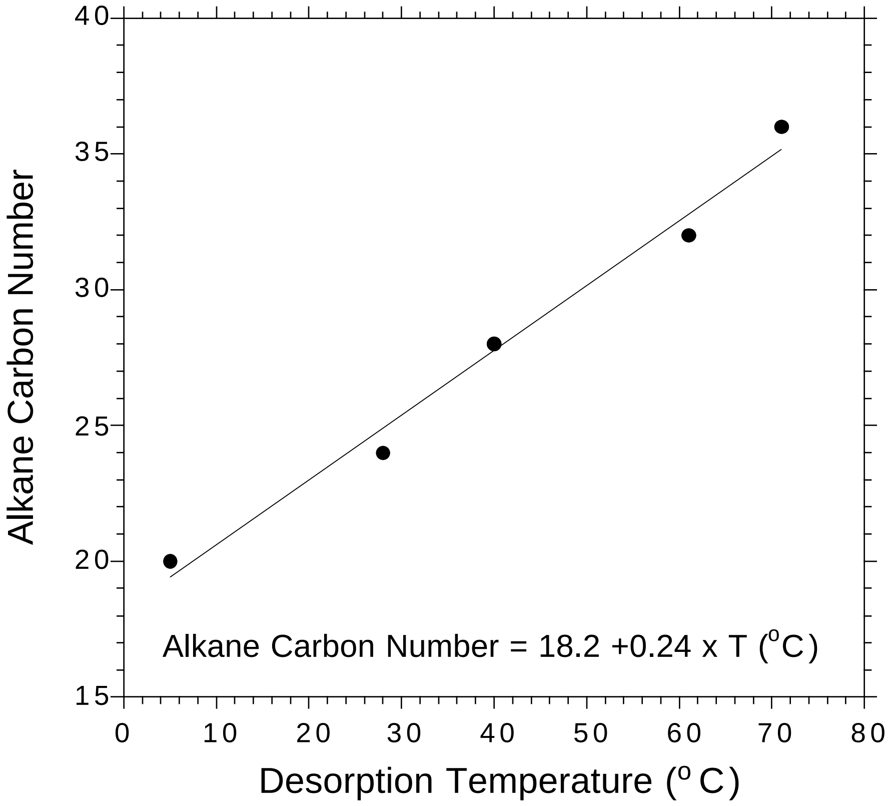

Figure 22. Calibration curve relating alkane carbon number and slow-TPTD desorption temperature.

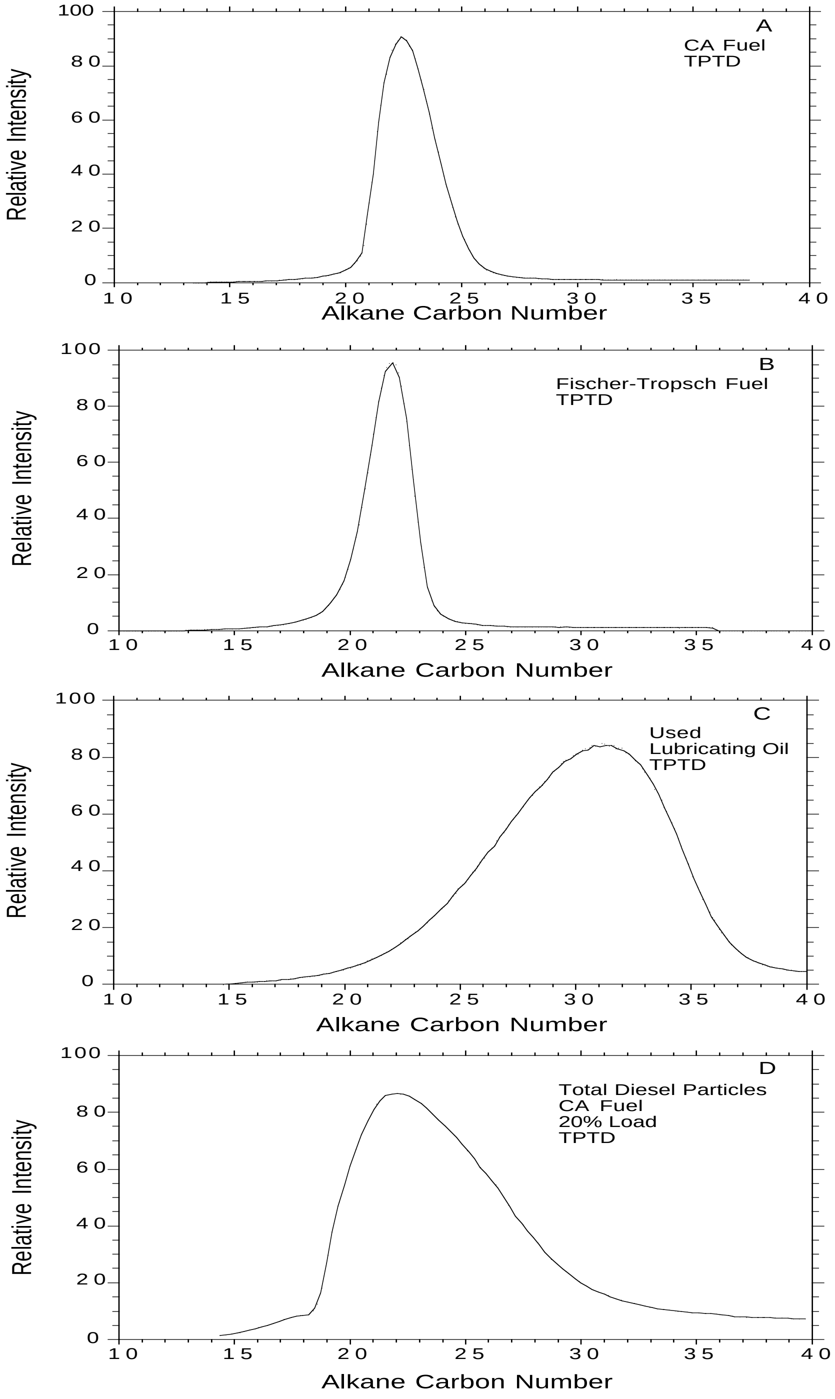

Figure 23. Slow-TPTD SIM desorption profiles of (A) CA fuel, (B) Fischer-Tropsch fuel, (C) used oil, and (D) total diesel particles obtained from the Cummins engine with CA fuel at 20% load. The *m/z* 95 signal is shown. Fuel and oil were each collected for 15 min and the total diesel particles for 65 min.

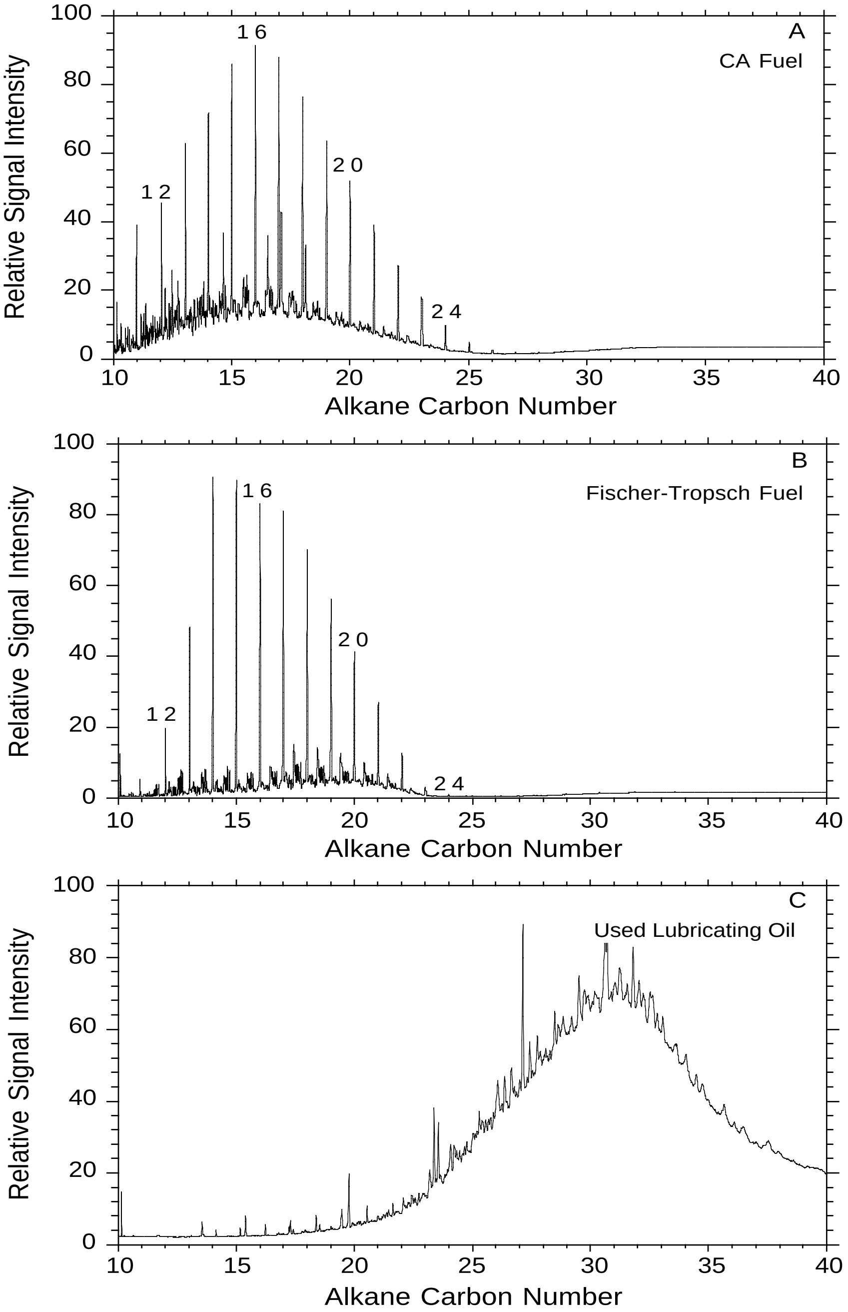

Figure 24. Gas chromatograms (GC-FID) of (A) CA fuel, (B) Fischer-Tropsch fuel, and (C) used oil.

The TPTD desorption profile of the diesel particles formed with the engine running on CA fuel (Figure 23C) indicates that nearly all the organic compounds in these particles have carbon numbers ≥ C20, with a small fraction of lighter compounds. Comparison of this profile with those of CA fuel (Figure 23A) and oil (Figure 23C) shows that all these compounds could come from oil, as indicated by the mass spectra. Although there is a significant overlap between the diesel particle and fuel TPTD profiles, the mass spectra indicate that the fuel components do not contribute significantly to the particle mass.

One observation to note is that the carbon number distributions obtained from the TPTD profiles of the CA and FT fuels are different from the GC-FID chromatograms. Whereas the GC profiles peak at ~C14-C16, the TPTD profiles peak at ~C22-C23. One possible explanation that was considered was that the TPTD calibration was wrong, and that the fuel desorption profiles are shifted from their true alkane carbon numbers. This is not the case, however, as shown by the mass spectra taken at the peak of the CA and FT fuel TPTD desorption profiles (Figure 25). The alkane carbon numbers determined from the most intense peaks in the high-mass range agree very well with the values obtained using the TPTD temperature calibration. Furthermore, the agreement between the GC and TPTD profiles for oil is excellent. The most likely explanation for the discrepancy between TPTD and GC analyses is therefore that compounds smaller than ~C22 undergo significant evaporation during TDPBMS analysis of standards.

Before discussing further the analysis of standards, we first address a more important question, which is how evaporation might affect diesel particle analyses. As can be seen in the apparatus schematic shown in Figure 2, particle standards could evaporate prior to analysis in any of three regions: (a) between the atomizer and DMA inlet, (b) between the DMA inlet and TDPBMS sampling orifice, and (c) between the TDPBMS sampling orifice and the vaporizer. Diesel particles, however, could only evaporate in the latter of these regions. We are neglecting here possible evaporation in the tubing between the dilution tunnel and the TDPBMS sampling orifice. When diesel particles are sampled from the dilution tunnel, they pass through tubing on their way to the TDPBMS. The particles should be exposed to approximately the same concentrations of vapors as when in dilution tunnel, so changes that occur in this region should be similar in character to those in the dilution tunnel. The same assumption is made for measurements of particle size distributions or for filter or impactor sampling, so this is not an issue specific to the TDPBMS. Once particles pass through the TDPBMS sampling orifice, however, they will be exposed to vacuum conditions for ~0.2 s. Some evaporation could occur in this region, but it will be slowed due to cooling of particles in the supersonic gas jet downstream of the orifice, and also evaporative cooling if particles begin to evaporate in vacuum. Evaporation does not occur after the particles deposit on the substrate, which is cooled to –50^{o}C.

To help evaluate the potential effect of particle evaporation on sampling losses, the evaporative lifetimes for 0.2 μm, C16, C20, and C24 alkane particles calculated (31) using literature values for alkane vapor pressures at 25^{o}C (32) are listed in Table 1. The values have been corrected for the Kelvin effect, evaporative cooling, and transition-regime evaporation (Fuchs correction), and it was assumed that the partial pressure of the vapor was zero. These values are similar (at least within a factor of 2) to those calculated for evaporation in vacuum. Comparison of the evaporative lifetimes with the residence time in the TDPBMS before deposition on the vaporizer indicates that both diesel and standard particles should undergo little evaporation inside the TDPBMS for alkanes larger than ~C16. Evaporation in the TDPBMS is therefore not responsible for the discrepancy between GC and TPTD analyses of fuel.

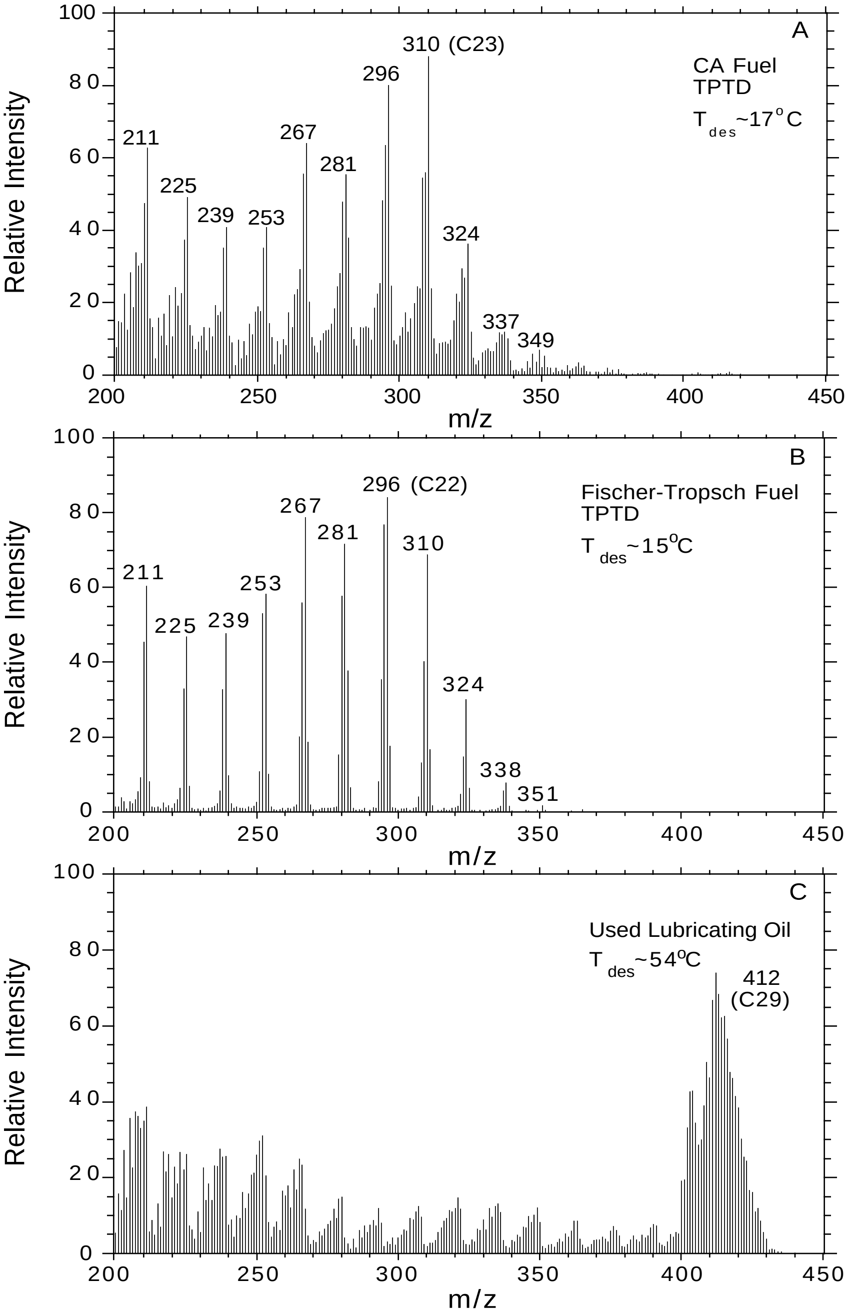

Figure 25. Slow-TPTD mass spectra of (A) CA fuel, (B) Fischer-Tropsch fuel, and (C) used oil, obtained at the peak desorption temperature, T_{des}. Fuel and oil were each collected for 15 min.

Table 1. TDPBMS Sampling Efficiencies and Evaporative Lifetimes for 0.2 µm Alkane Particles

Alkane Carbon Number	Relative Sampling Efficiency	Evaporative Lifetime (s)
C16	-----	0.1
C20	1.00	10
C24	0.36	1000
C28	0.32	--------
C32	0.37	--------
C36	0.37	--------

As mentioned above, standard particles could also evaporate between the atomizer and DMA, or between the DMA and TDPBMS. The residence times in these regions are ~15 s and ~1 s, respectively. Comparison of the calculated evaporative lifetimes of alkane particles (Table 1) with the sampling residence times indicates that only in the region between the atomizer and the DMA is the residence time for C20 and smaller alkanes comparable to, or larger than the evaporative lifetime, thus allowing evaporation to occur. To verify this assertion, the amount of evaporation that occurs between the DMA and the TDPBMS was evaluated by comparing the TDPBMS sampling efficiencies of standard alkane compounds. The alkanes all have similar mass spectral abundance patterns, with the most intense peaks occurring in the low-mass range ($m/z < 100$) due to fragmentation. The ion signal per unit mass is approximately the same for all compounds (30). Using the m/z 85 peak intensity integrated over the desorption period [alkane signal (m/z 85)] as a measure of the deposited mass, and the mass of sampled particles obtained from the DMA settings and the measured concentration of particles leaving the DMA [DMA mass], we calculate the sampling efficiencies, relative to C20, for alkane standards with carbon numbers Cx as

$$\frac{[\text{Cx alkane signal } (m/z\ 85)]/[\text{Cx DMA mass}]}{[\text{C20 alkane signal } (m/z\ 85)]/[\text{C20 DMA mass}]} \tag{1}$$

The relative sampling efficiencies for C20, C24, C28, C32, and C36 are given in Table 1. The values for the C24-C36 alkanes are similar, but with that of C20 being larger by a factor of 3. This difference may be due to particle shape effects, since regularly shaped particles focus better in the aerodynamic lens than do irregularly shaped ones. These compounds are all solids at room temperature, and appear to form flaky crystals, which could have quite different focusing properties. But without particle shape information, we cannot be certain if this is the cause of the higher C20 efficiency. Regardless of the reason for this difference, however, the results show that C20 and larger alkanes are sampled from the DMA to the vaporizer with similar efficiencies. This indicates that alkanes down to at least C20 do not evaporate significantly between the DMA and the vaporizer, since otherwise the C20 efficiency would be much less than for the other alkanes.

The discrepancy between the GC and TPTD analyses of fuel samples must therefore be caused by evaporation of compounds smaller than ~C22 between the atomizer and the DMA. The experimental observations on the analysis of fuel and alkane standards can be explained as follows: when pure C20 alkane particles are generated by atomization, they undergo partial evaporation before reaching the DMA. But the 0.15 μm particles that are selected for analysis are still pure C20 alkane, and are transported from there to the vaporizer without further evaporation. The sampling efficiency of C20 alkanes should therefore be comparable to that of larger alkanes, as was the case. Conversely, when fuel particles are generated and the C20 and smaller alkanes evaporate between the atomizer and DMA, the 0.15 μm particles that are selected are depleted in these compounds relative to the original fuel, as was observed in the TPTD and GC analyses.

In order to further investigate the possible evaporation of particles during TDPBMS sampling we performed an experiment in which the C15 alkane, pentadecane ($CH_3(CH_2)_{13}CH_3$), was added to a 7000 L smog chamber and allowed to condense onto C28 octacosane ($CH_3(CH_2)_{26}CH_3$) seed particles. The aerosol was sampled into the TDPBMS before and after addition of pentadecane, and when a filter was placed in line the signal dropped back to background levels, showing that the pentadecane being analyzed was in the particles. The mass spectra are shown in Figure 26. The mass concentration of pentadecane in the aerosol was determined by using the mass spectral signals and the concentration of octacosane, which is present entirely in the particle phase because of its low vapor pressure (~10^{-9} torr). As noted above, for hydrocarbons the total mass spectral signal per unit mass is constant. The measured mass concentration of pentadecane in particles in the chamber is then

$$[\text{Pentadecane}]_{\text{particles}} = [((P+O)_{50} - O_{50})/O_{50}][(P+O)_{214}/O_{214}][\text{Octacosane}]_{\text{particles}} \qquad (2)$$

where O and (P + O) correspond to octacosane and octacosane + pentadecane, and the subscripts 50 and 214 correspond to the sum of all mass spectral signal in the range *m/z* 50-400 and 214-400, respectively. The first quantity in brackets is the ratio of mass spectral signals for pentadecane and octacosane, which is equal to the ratio of the mass of pentadecane and octacosane reaching the mass spectrometer. The second quantity in brackets is the ratio of mass spectral signals for octacosane in seed particles and when mixed with pentadecane. This is equal to the ratio of the transport efficiencies of the pure seed particles and the mixed particles. The third quantity in brackets is the mass concentration of octacosane added to the chamber. Previous measurements show that wall losses of particles in the chamber are less than ~5% during an experiment of this timescale (~20 min). In this experiment, $[\text{Octacosane}]_{\text{particles}} = 1$ mg/m^3, $[((P+O)_{50} - O_{50})/O_{50}] = 28$, and $[(P+O)_{214}/O_{214}] = 0.65$, yielding $[\text{Pentadecane}]_{\text{particles}}$ ~18 mg/m^3. This value can be compared with the particulate mass concentration of pentadecane expected in the chamber from the difference between the amount added and the amount in the gas phase

$$[\text{Pentadecane}]_{\text{particles}} = [\text{Pentadecane}]_{\text{total}} - [\text{Pentadecane}]_{\text{gas}}$$

$$= [\text{Pentadecane}]_{\text{total}} - [(P)(MW)10^3]/[(760)RT] \qquad (3)$$

The gas is assumed to be in equilibrium with the particles, so its concentration is determined by the pentadecane vapor pressure, P. In this equation $[\text{Pentadecane}]_{\text{total}}$ is the concentration of added pentadecane, MW is the molecular weight of pentadecane, R is the ideal gas constant

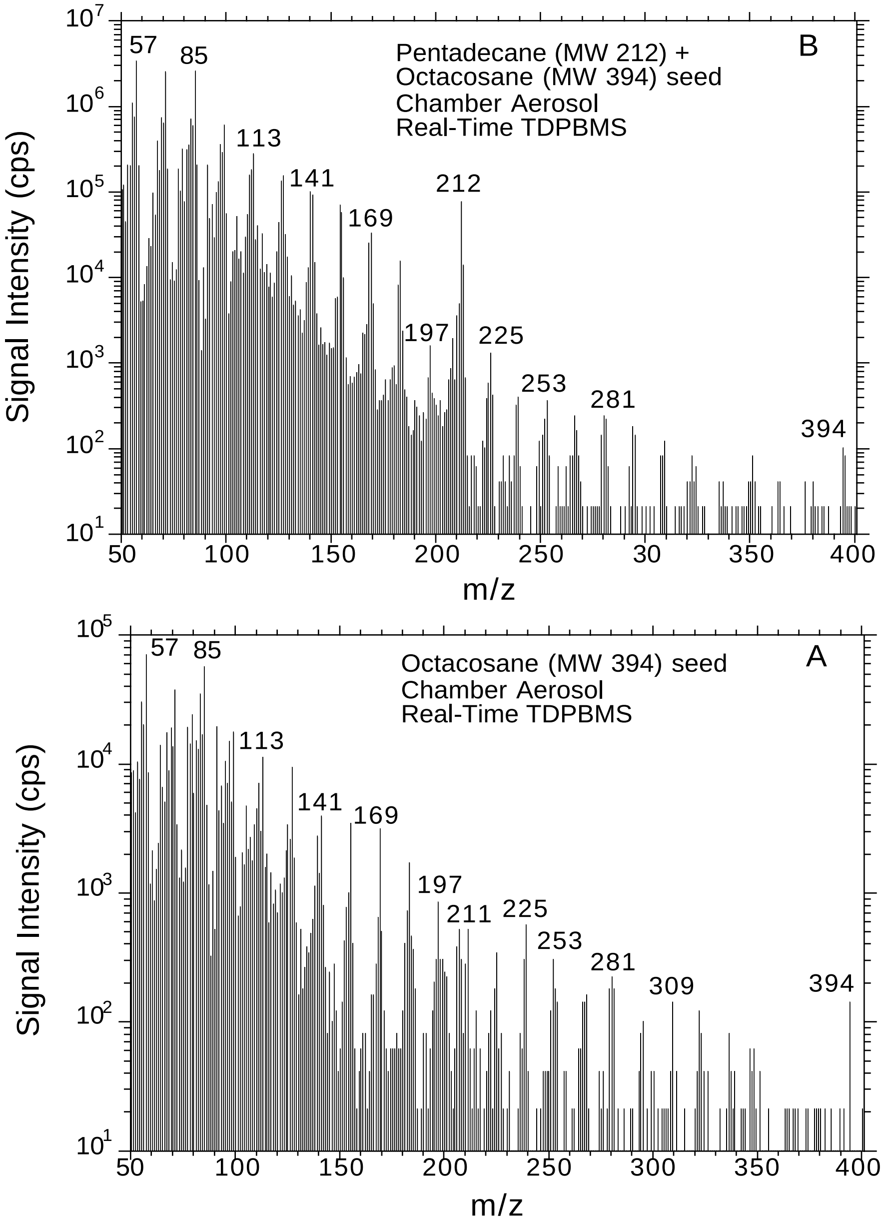

Figure 26. Real-time TDPBMS mass spectra of (A) octacosane ($CH_3(CH_2)_{26}CH_3$) seed particles and (B) pentadecane ($CH_3(CH_2)_{13}CH_3$) plus octacosane particles after addition to smog chamber by evaporation-condensation.

(8.206×10^{-5} m^3-atm/mol-K), and T is temperature (K). Using $[\text{Pentadecane}]_{\text{total}} = 120$ mg/m^3,T = 298 K, MW = 142 g/mol , and P = 1.2×10^{-2} torr (33), we obtain $[\text{Pentadecane}]_{\text{particles}}$ ~28 mg/m^3. Considering the uncertainties, this result is in good agreement with the TDPBMS value, indicating little evaporative loss during sampling. Even if the discrepancy is real, the mass fraction lost by evaporation should decrease from ~35% for C15 to ~10% for C16 and ~3% for C17, since the vapor pressure decreases by a factor of ~3 for each additional carbon number. The reason compounds evaporate less than predicted by the evaporation calculations in Table 1 is probably that the particles are strongly cooled during the supersonic expansion into vacuum, which effectively stops evaporation. It is well known that the adiabatic expansion in a supersonic jet typically cools molecules to temperatures on the order of 50-100 K, so it is reasonable that the particles would also be quite cold. This effect was not included in the evaporation calculations.

It is worth noting at this point that the evaporative losses in the TDPBMS are probably much less than those that occur in MOUDI samplers, which have significant pressure drops, especially across the lower stages. Particles exposed to undersaturated air in such a sampler will evaporate at nearly the same rate as they would in a vacuum (31), and the samples are collected for much longer times than the ~0.2 s particles have to evaporate in transit to the TDPBMS vaporizer. The TDPBMS is also not subject to sampling artifacts from adsorption of vapors, as are MOUDIs. Filter samplers suffer from evaporation and adsorption artifacts as well, so the TDPBMS samples are expected to be more accurate than samples collected by these standard methods.

An important conclusion that can be drawn from these results is that the sharp reduction in signal in the TPTD desorption profile of diesel particles between ~C18-C23 (Figure 23D) is not a sampling artifact. As shown above, compounds down to at least ~C15 do not appear to undergo significant evaporation during TDPDMS sampling from a smog chamber, which is equivalent to sampling diesel particles from a dilution tunnel. Our conclusion that the organic component of the diesel particles is comprised almost entirely of unburned oil is therefore not affected by particle sampling issues. The near-absence of compounds lighter than ~C20 in fresh diesel exhaust particles should not be surprising, considering their high volatility. As indicated by the calculations in Table 1, they are even less likely to remain in particles after entering the atmosphere unless they are strongly adsorbed to soot. For example, particles collected in a Los Angeles roadway tunnel contained no alkanes lighter than C17, and those from C17-C20 comprised only ~10% of the total particulate alkanes (34).

Studies by others have often yielded results similar to those observed here (35-37). For example, the diesel particle carbon number distribution obtained by TPTD is similar to distributions observed in a number of other studies which used gas chromatography to analyze filter samples of diesel particle emissions. Profiles are often bimodal, with the first peak at ~C18-C22, and a second peak at ~C26-C30. The usual interpretation is that the first peak is from fuel and the second from oil. The TPTD profile in Figure 23D is not bimodal, but the distribution is skewed beyond the peak at ~C22 with a slight shoulder at ~C26. In some GC studies hydrocarbons as light as C14 have been detected in filter samples, clearly suggesting the presence of fuel in the particles. Because of the serious artifacts associated with filter sampling of semi-volatile compounds, however, one cannot rely on these analyses to be representative of the actual particle composition. It is also not surprising that oxidized organic combustion products are only a minor fraction of the organic matter. For example, in one study (37) using GC-MS to analyze filter samples of particles from a heavy-duty diesel engine it was found that

~1% of the total elutable organic components were monocarboxylic acids. Approximately 90% of the elutable mass was unresolved unbranched and cyclic alkanes.

Although the mass spectra indicate that the source of the organic component of diesel particles is primarily oil, the TPTD profile of the particles (Figure 23D) is shifted to lower temperatures compared to the oil (Figure 23C). If the oil that composes the particles entered the exhaust by atomization from the cylinder wall, then one would expect that the two profiles would be similar. It may be that in this case the major mechanism by which oil enters the exhaust is by evaporation from the cylinder walls, which should lead to enrichment of the more volatile oil components, as is observed in the TPTD profiles. The peak in the distribution might be primarily from evaporation, and the shoulder from atomization.

6.2.3.5.4. Total Diesel Particle Composition: Effect of Engine Load and Volatility

Experiments were also performed to gain information on possible changes in diesel particle composition with changes in engine load and with component volatility. Total particle samples were analyzed in real time by TDPBMS after passing through a thermodenuder at temperatures ranging from 30-300 ^{o}C. The thermodenuder is a heated tube used to evaporate volatile components from the particles. Depending on the thermodenuder temperature, components with vapor pressures higher than a particular value were evaporated from the particles, leaving less volatile components behind for subsequent TDPBMS analysis. By analyzing particles over a wide temperature range, differences in the composition of more and less volatile components could be ascertained. The measurements were also made for a range of engine loads to evaluate the effect of this parameter on particle composition.

The results of thermodenuder/TDPBMS analyses performed with CA fuel at 20% and 35% engine load, and with FT fuel at 10% and 20% load, are shown in Figures 27-30, respectively. The top plot in each figure shows the dependence of the total particle signal on thermodenuder temperature. In all cases the signal decreases sharply between 30^{o}C (room temperature) and ~70-80^{o}C due to particle evaporation. Evaporation either increases slightly or does not change at higher temperatures. The curves do not go to zero, but reach constant values corresponding to ~20-30% of the original signal for 10% and 20% engine load, and ~60% at 35% load. The TDPBMS vaporizer was set at 220 ^{o}C in these experiments, so the signal observed at 300^{o}C thermodenuder temperature cannot be from organic compounds that do not evaporate at 300^{o}C. This temperature should be high enough to quickly evaporate all organics. The components observed at 300^{o}C are therefore due to re-condensation of organics onto soot particles as the vapor cools downstream of the thermodenuder. The enhanced re-condensation at 35% engine load is probably the result of higher concentrations of particulate elemental carbon, which provides more surface area, relative to the walls, for condensation of vapors.

The diesel particle mass spectra (middle and bottom plots in Figures 27-30) are similar for CA and FT fuel at all engine loads and thermodenuder temperatures. The most noticeable difference is that the *m/z* 83 peak becomes slightly larger than *m/z* 81 for both fuels at 20% load and 300^{o}C thermodenuder temperature, and for CA fuel at 35% load and both thermodenuder temperatures. This probably indicates that the lower volatility fraction of the oil is slightly enriched in cycloalkanes, which are more readily vaporized at the higher engine temperatures achieved at higher engine loads, and at the higher thermodenuder temperatures.

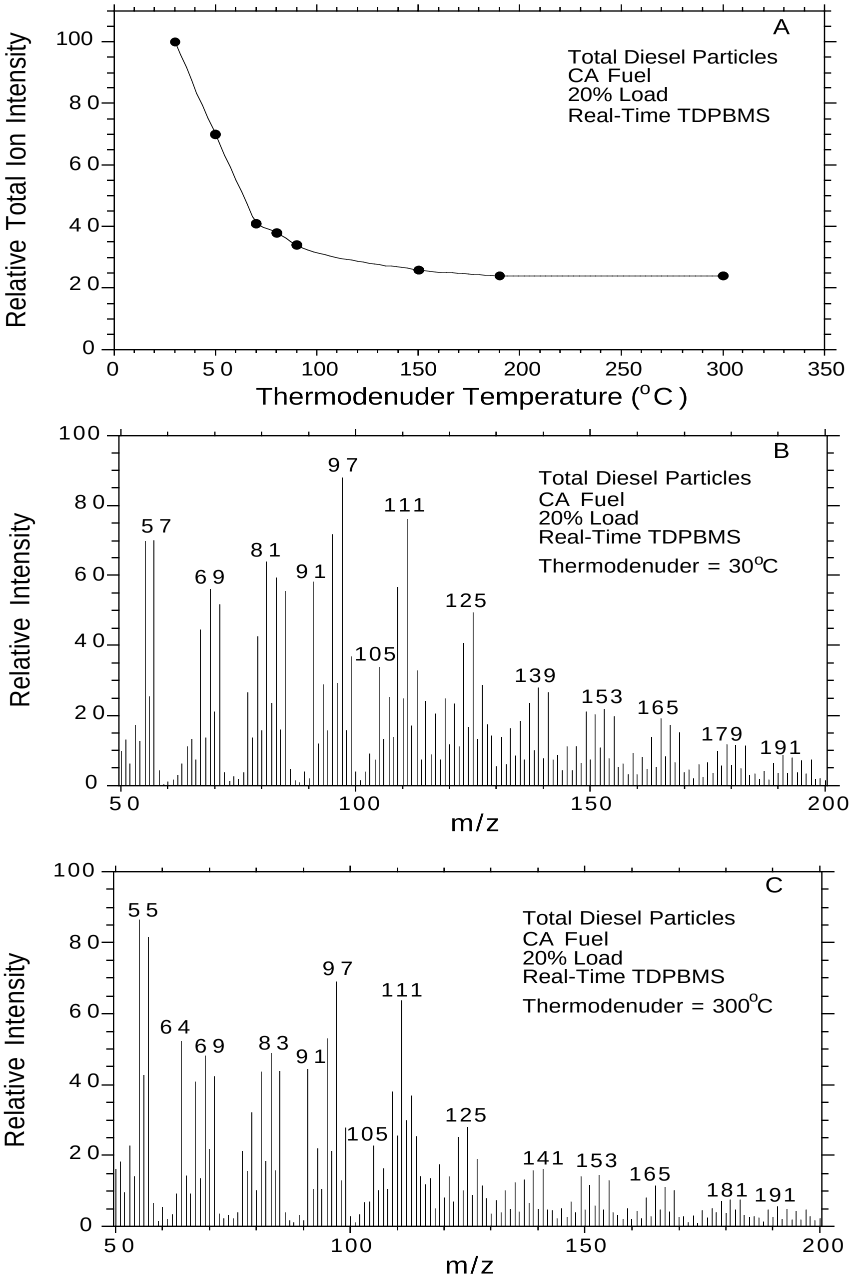

Figure 27. Real-Time TDPBMS of total diesel particles obtained from the Cummins engine with CA fuel at 20% load, after passing through a thermodenuder: (A) total ion signal for *m/z* 45-290, (B) 30°C thermodenuder temperature, and (C) 300°C thermodenuder temperature.

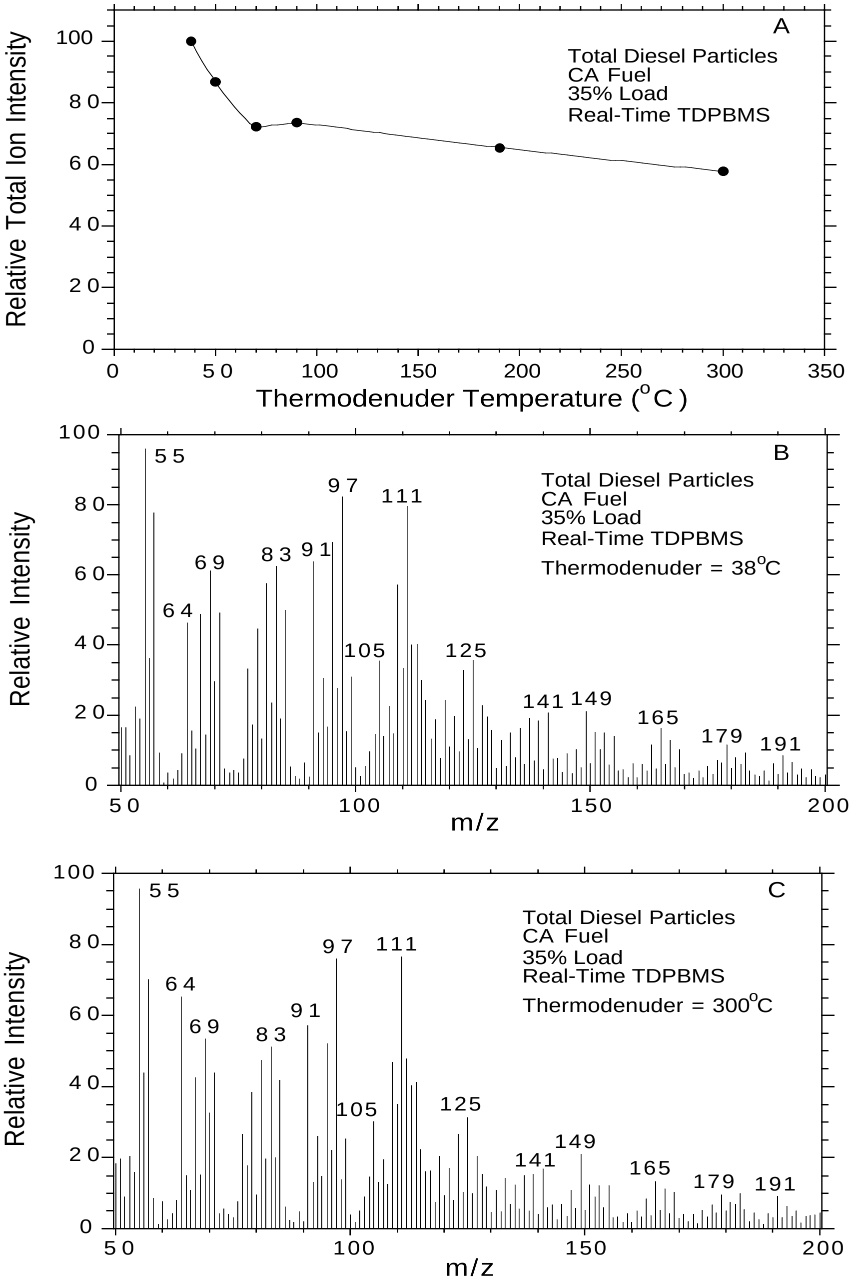

Figure 28. Real-Time TDPBMS of total diesel particles obtained from the Cummins engine with CA fuel at 35% load, after passing through a thermodenuder: (A) total ion signal for *m/z* 45-290, (B) 30°C thermodenuder temperature, and (C) 300°C thermodenuder temperature.

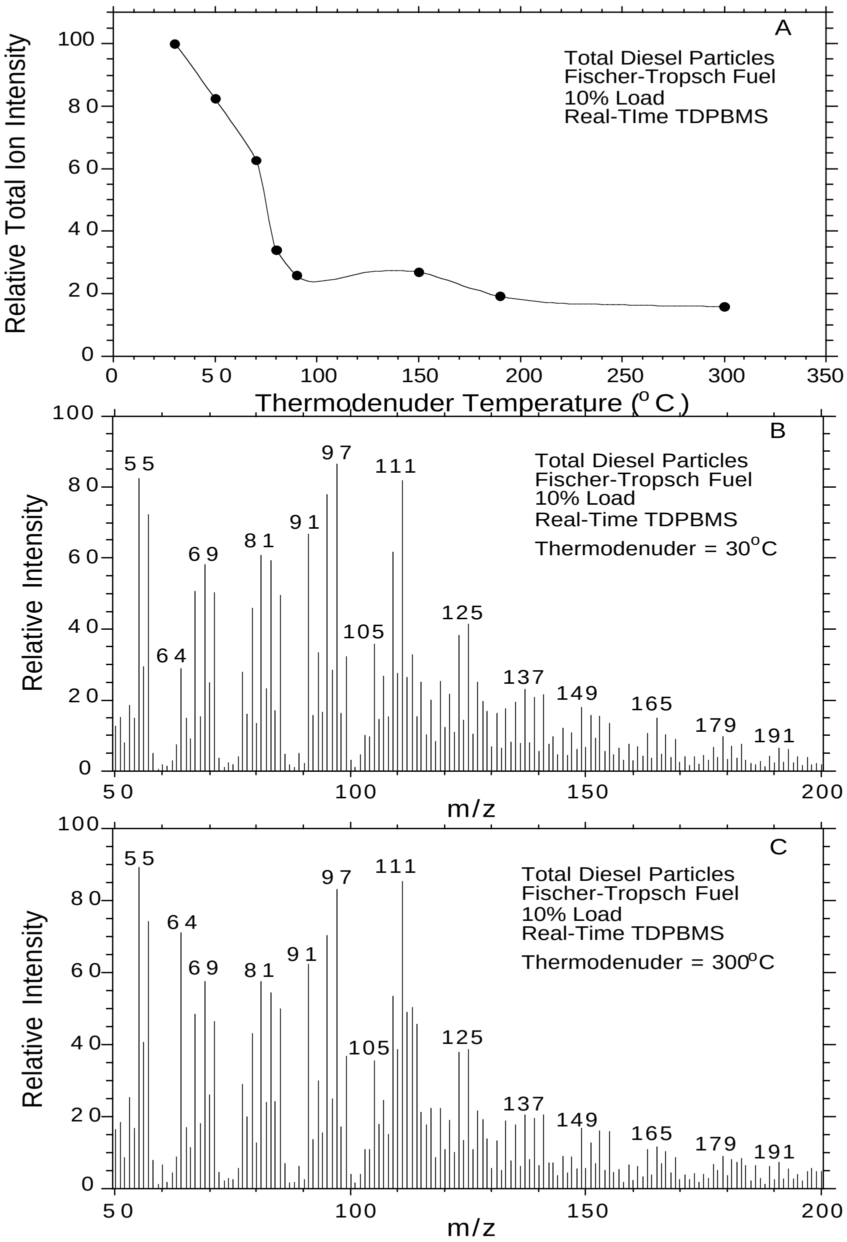

Figure 29. Real-Time TDPBMS of total diesel particles obtained from the Cummins engine with Fischer-Tropsch fuel at 10% load, after passing through a thermodenuder: (A) total ion signal for *m/z* 45-290, (B) 30°C thermodenuder temperature, and (C) 300°C thermodenuder temperature.

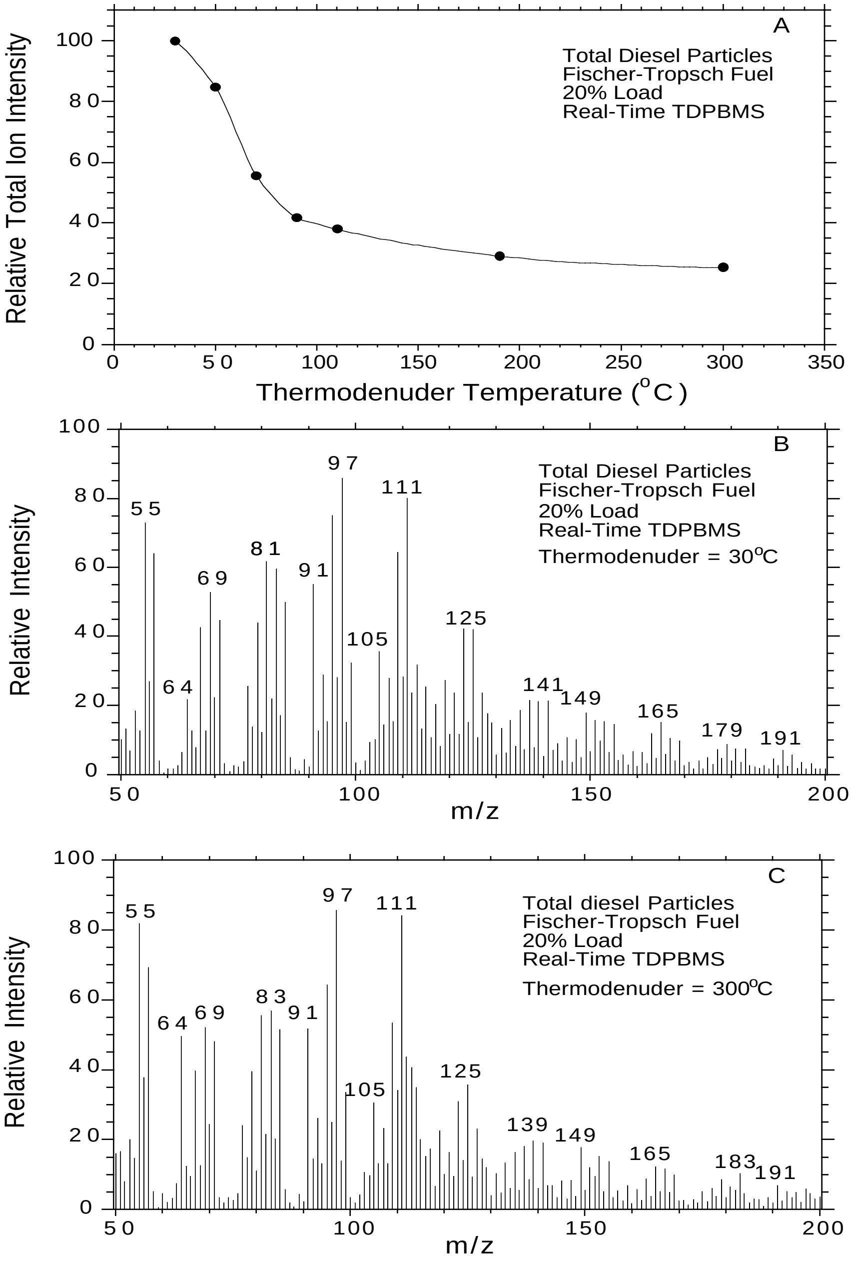

Figure 30. Real-Time TDPBMS of total diesel particles obtained from the Cummins engine with Fischer-Tropsch fuel at 20% load, after passing through a thermodenuder: (A) total ion signal for *m/z* 45-290, (B) 30°C thermodenuder temperature, and (C) 300°C thermodenuder temperature.

One surprise is the large peak at *m/z* 64 that appears only in the thermodenuder experiments, and increases with temperature. This is almost certainly due to the SO_2^+ ion. It is apparently not associated with sulfuric acid, since the mass spectrum in Figure 7 shows that it should then be accompanied by a peak approximately twice its size at *m/z* 98. This peak may be due to SO_2 that adsorbs to the denuder and is then released, especially at higher temperatures. The concentration would have to be quite high for it to reach the mass spectrometer, so it may enter adsorbed on soot particles.

6.2.3.6. Results of TDMA Analyses

6.2.3.6.1. Volatility of Diesel Particles

Figures 31-33 show results of volatility experiments performed when the engine was operated with CA fuel at 20% load. Three pairs of plots are presented for three different initial particle sizes. Figure 21 is for particles analyzed by the RTDMA, which had an initial size of 70 nm (determined by RDMA-1). The size-selected particles were heated in the particle heater at various temperatures, and then re-sized by RDMA-2. A linear y-axis scale is used in Figure 31A while a logarithmic y-axis is used in Figure 31B. Figures 32 and 33 are for volatility data obtained with the NTDMA for initial particle sizes of 30 and 12 nm (determined by NDMA-1), respectively.

As shown in Figure 31, particles with an initial diameter of 70 nm exit the heater with a diameter of 69 nm when the heater is set at ~30 °C (room temperature). This discrepancy, in which the diameter measured by DMA-2 was smaller (by as much as 5%) than the diameter selected by DMA-1, was consistently observed when using either the NTDMA or RTDMA at room temperature with diesel particles and with very low volatility alkane standards. The DMA-1/DMA-2 discrepancy was less than 1% when standard sodium chloride particles were analyzed, but for some unknown reason a slight discrepancy appears with other particles. When 70 nm diesel particles were heated at 70°C, the distribution shown in Figure 31 shifted to smaller sizes and the peak moved to ~65 nm due to evaporation of volatile components. When the heater temperature was increased to 90 °C, the distribution broadened, with a peak remaining at 65 nm and a new mode appearing at smaller sizes. The appearance of this second mode indicates there were two types of 70 nm particles present in the exhaust aerosol (i.e., an external mixture). The mode that appeared at smaller sizes as the heater temperature was raised was associated with more volatile particles. The particles that shrank slightly to ~65 nm and then stopped were probably composed of an ~65 nm non-volatile soot core coated by volatile organic matter. We will hereafter refer to these two modes as “more volatile” and “less volatile” particles. At 110 °C, the “more volatile” particles shrank further while the others remained at ~65 nm, leading to two distinctive peaks in the size distribution. The concentration ratio of the “less volatile” particles compared to the “more volatile” particles was calculated to be ~4 for these initially 70 nm particles. As the temperature was further increased, “more volatile” particles continued to shrink, until at ~300°C they became smaller than the lowest detectable size (Dp ~ 9 nm) of the CPC used in the RTDMA. At this point they disappeared, and the only remaining particles were those which had a non-volatile core. It is worth noting that the distribution of non-volatile cores in the “less volatile” particles was highly skewed and extended down to 14 nm (Figure 31B).

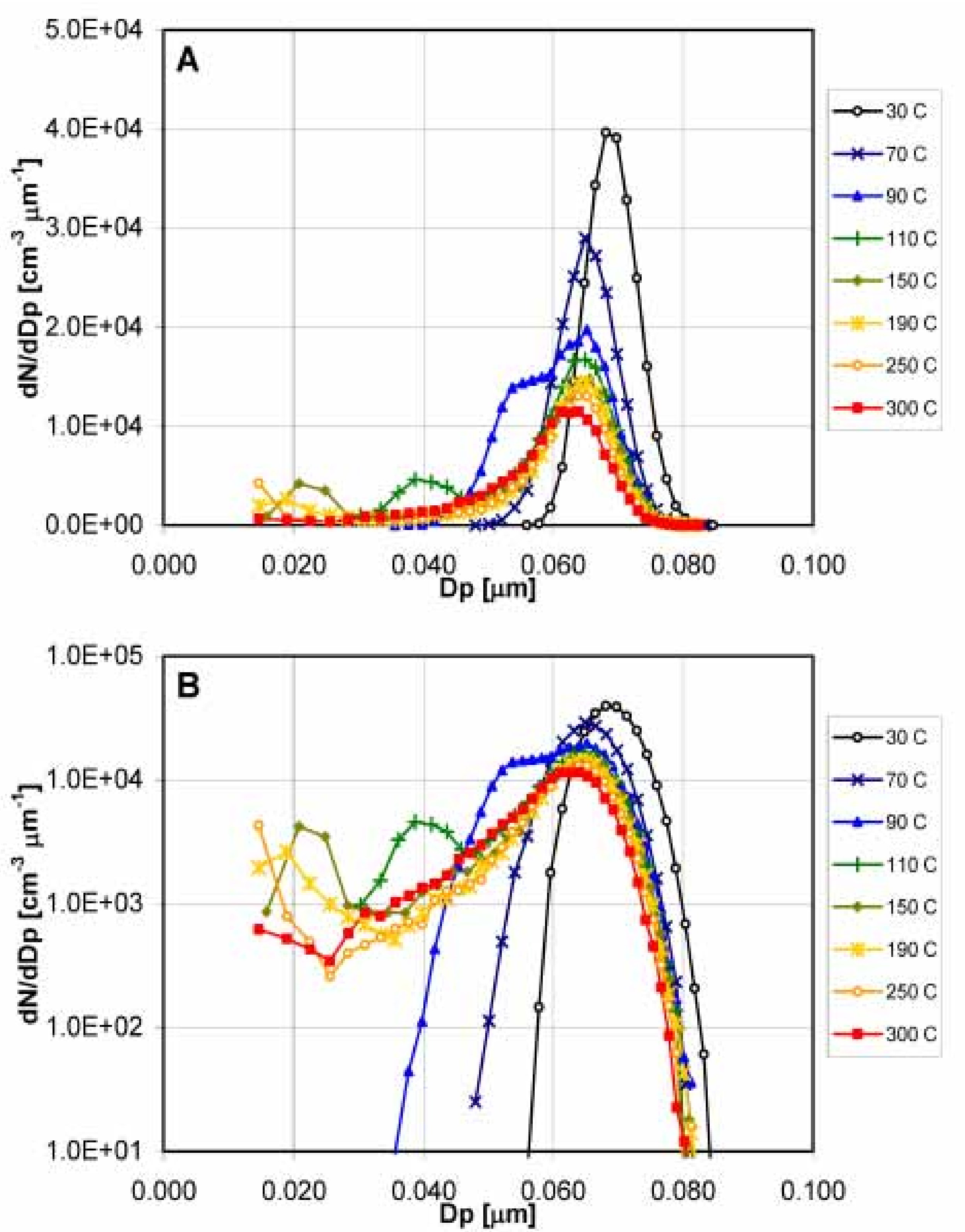

Figure 31. Evaporation profiles of 70 nm diesel particles from the Cummins engine with CA fuel at 20% load, obtained using the NTDMA. Size distributions are plotted using a (A) linear and (B) logarithmic y-axis.

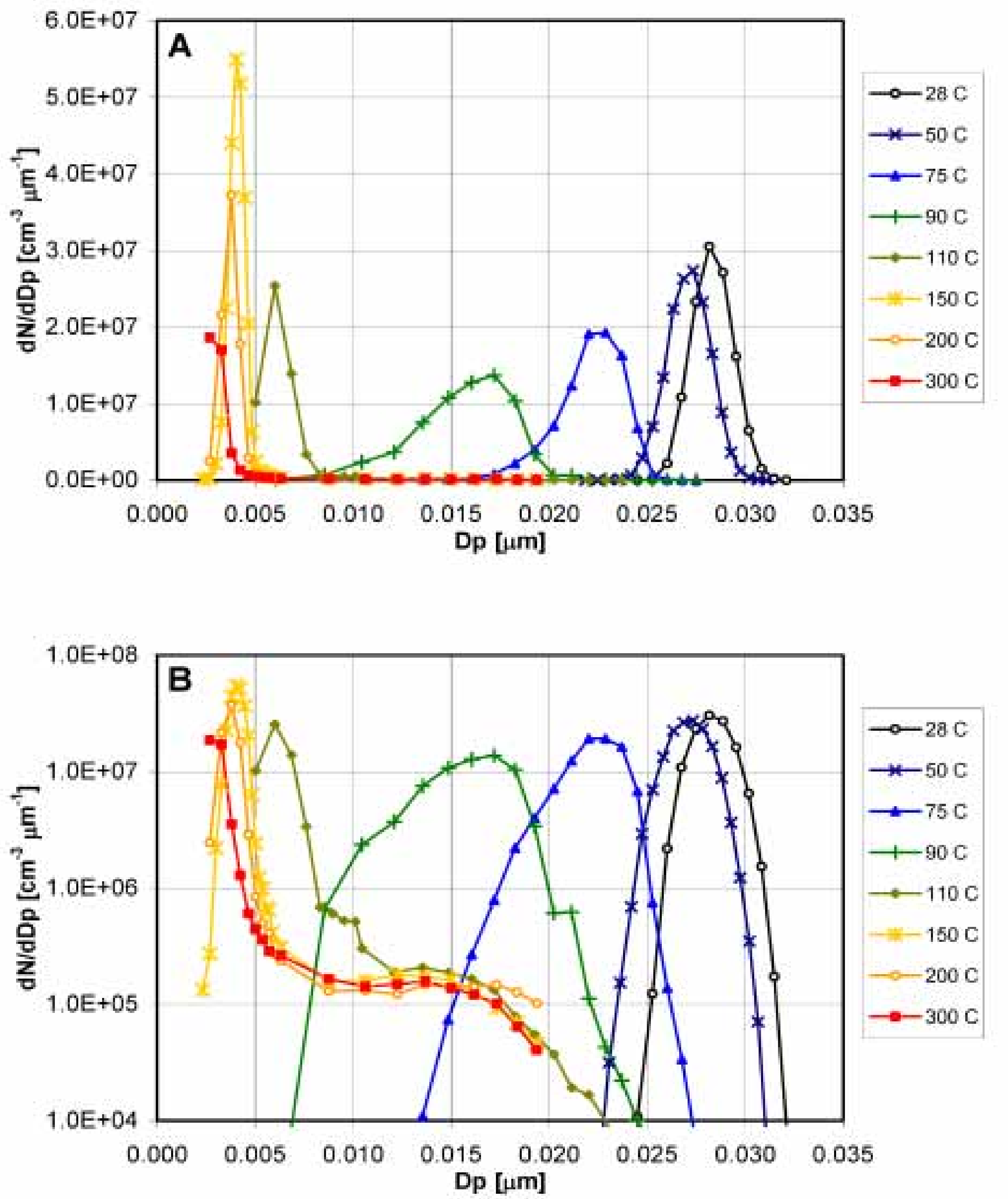

Figure 32. Evaporation profiles of 30 nm diesel particles from the Cummins engine with CA fuel at 20% load, obtained using the NTDMA. Size distributions are plotted using a (A) linear and (B) logarithmic y-axis.

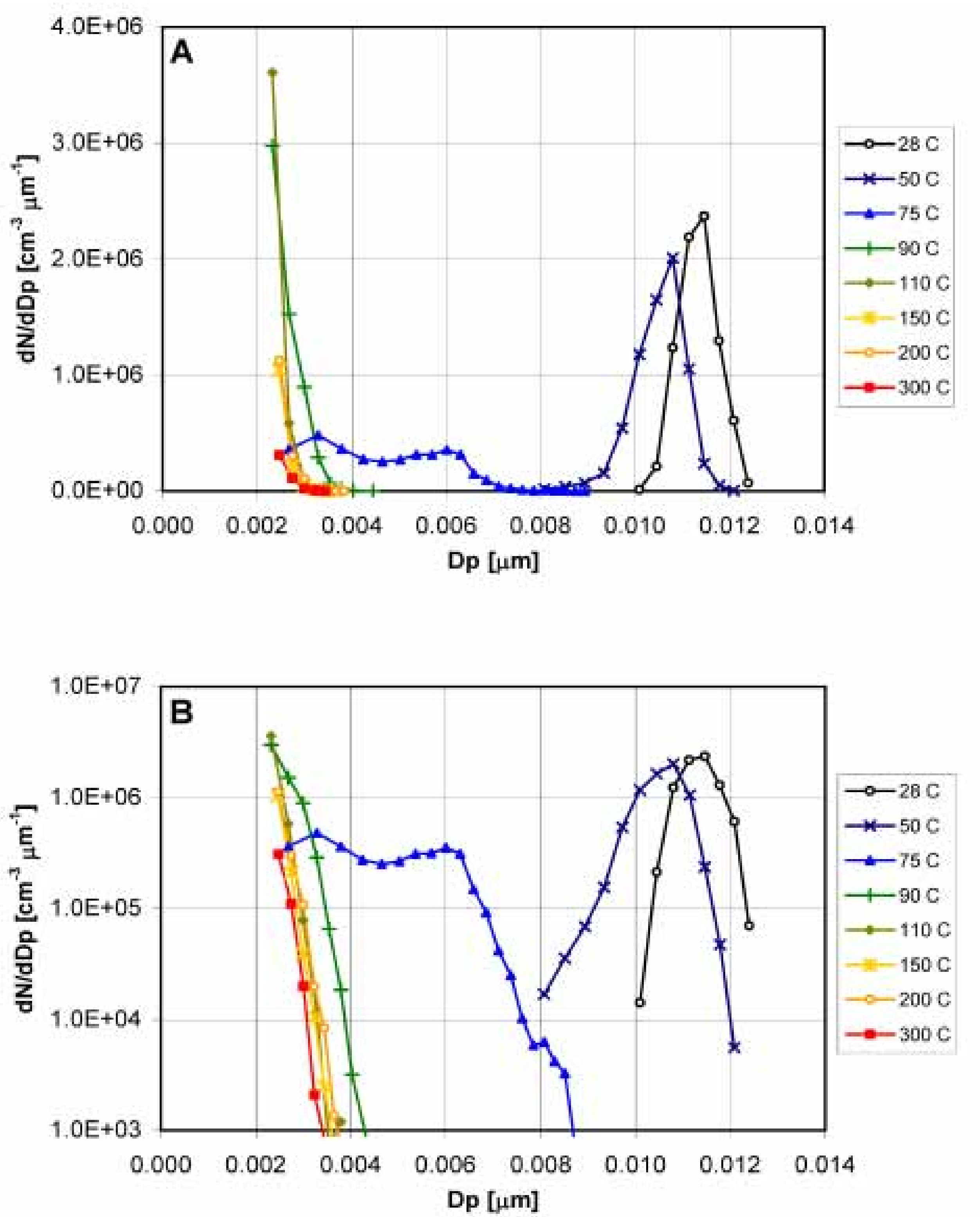

Figure 33. Evaporation profiles of 12 nm diesel particles from the Cummins engine with CA fuel at 20% load, obtained using the NTDMA. Size distributions are plotted using a (A) linear and (B) logarithmic y-axis.

Particles with initial diameters of ~30 nm also exhibited external mixing (Figure 32). The two volatility modes, due to the coexistence of the "more" and "less" volatile particles, were seen at 110 °C and higher temperatures. The concentration of "more volatile" particles was approximately two orders of magnitude higher than that of the "less volatile" particles. The "more volatile" particles shrank to 4.2 nm at 150 °C, and 3.8 nm at 200 °C. At 300 °C, part of the size distribution of "more volatile" particles was below the minimum detectable size (Dp ~ 2.7 nm) of the CPC used with the NTDMA. Similar distributions were observed at 400 and 460 °C (the maximum heater temperature), but are not shown in the figure.Measurements on particles with initial diameters of 12 nm showed no evidence for a "less volatile" particle mode (Figure 33), indicating that "more volatile" particles dominated the particle concentration. At 90 °C and above, all particles shrank to 4 nm or smaller in diameter, but even at temperatures of 460 ^{o}C (not shown) some of these small particles were still detected. The steeply increasing concentration toward the 2.7 nm minimum detectable particle size indicates that the majority of the particles became smaller than 2.7 nm.

Figure 34 is a plot of the diameter changes (-ΔDp) measured for the "more volatile" particles with initial diameters of 12 and 30 nm, for different heater temperatures, engine loads, and fuels, and also for the initial diameter of 70 nm with the CA fuel at 20% load. The value of -ΔDp was calculated from the count mode diameter (i.e., the diameter at which the highest concentration was observed) determined using DMA-2 at 30 °C and at the elevated temperatures. Because of the aforementioned discrepancy between the DMA-1 and DMA-2 diameters at room temperature (~30 °C), the evaporation curves do not start at -ΔDp = 0. When only a single peak was observed at low heater temperatures (e.g., 30-70 °C) because of coincidence of the "more" and "less" volatile particle modes, the mode diameter of that single peak was used in the calculations. Note that the coincidence of the two modes at these temperatures suggests that the volatile components in the "more" and "less" volatile particles have similar volatilities. As seen in this figure, the "more volatile" particles of each initial size evaporated until a certain temperature was reached and then almost stopped completely. The evaporation profiles are remarkably similar, with the major differences being that the curves for the 30 nm particles level off at ~100-110 ^{o}C, whereas the curves for the 12 nm particles level off at ~80 ^{o}C. The curves for the 70 nm particles level off at about 150 ^{o}C. The similarity in the evaporation profiles implies that the volatilities of the compounds that composed the particles were similar, irrespective of the differences in engine load and fuel.

The leveling off of the evaporation curves means there were some particles left after most of the material had evaporated. Understanding this observation will require further experiments and analyses, but we can think of a few possible explanations. The residual particles may have been composed of very low volatility material, such as soot or metal oxides, which did not evaporate upon heating to 450 °C. They may also have been single molecules or molecular clusters of low-volatility organic compounds which were large enough to be detected by the DMA and CPC. It is unlikely that these are soot particles formed by pyrolytic charring of organic compounds in the heater tube since the temperatures at which the curves level off are ~80-110^{o}C, which are very low to induce pyrolysis.

To estimate the composition of the volatile components of diesel particles, we performed volatility experiments with laboratory-generated dotriacontane ($C_{32}H_{66}$ *n*-alkane) and engine oil (RTDMA only) aerosols. Dotriacontane was used because its volatility is similar to the average of the components of oil. Particles were generated as described in the methods section.

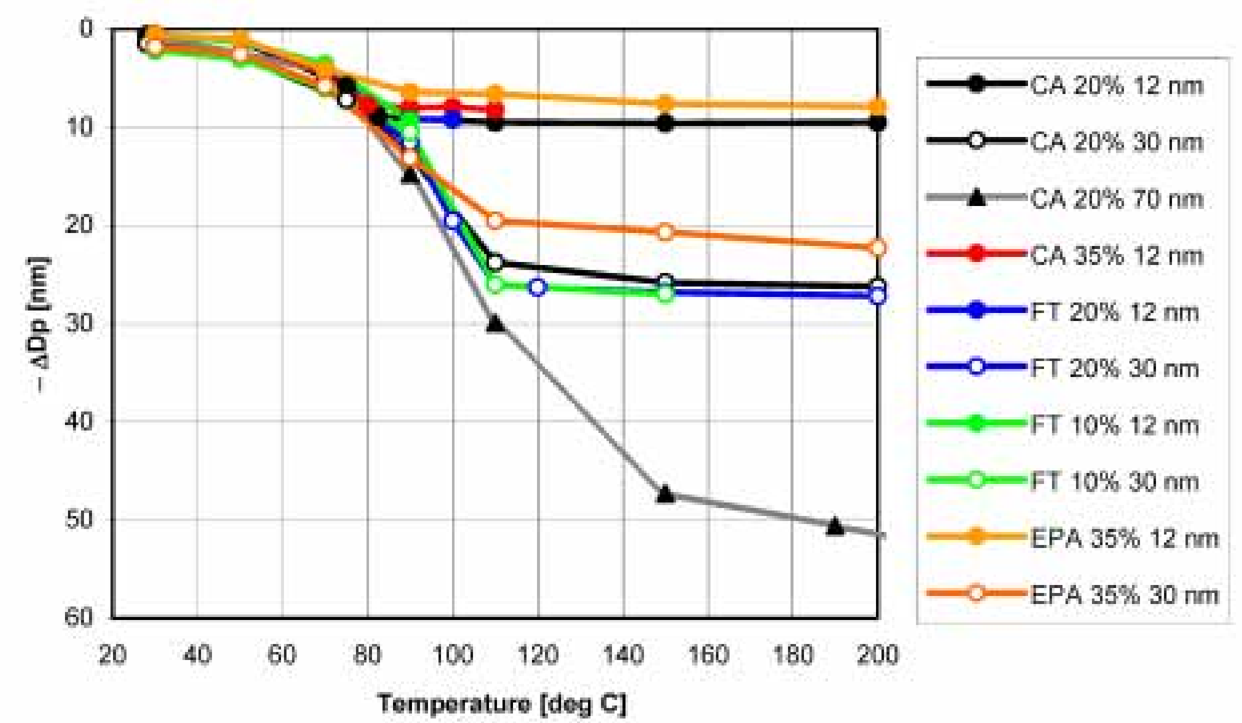

Figure 34. Evaporation profiles of nuclei-mode diesel particles from the Cummins engine with CA, Fischer-Tropsch, and EPA fuels at different engine loads. The data were obtained using the NTDMA. The initial particle sizes were 12 and 30 nm, and the y-axis shows the change from the initial size (-ΔDp).

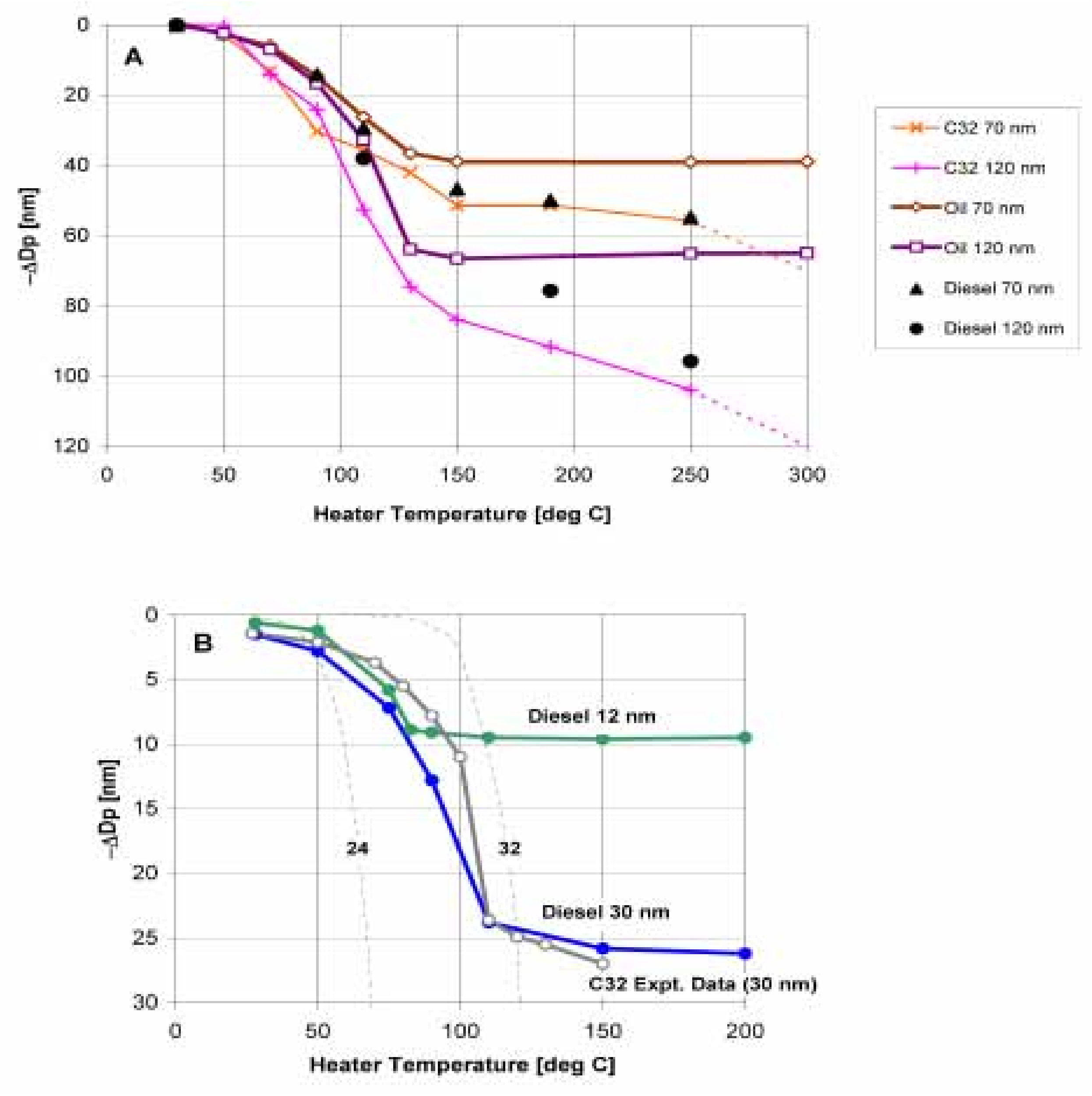

Figure 35. (A) Evaporation profiles of dotriacontane ($C_{32}H_{66}$), used oil, and diesel particles with initial sizes of 70 and 120 nm, obtained with RTDMA. The y-axis shows the change from the initial diameter ($-\Delta Dp$). The dashed lines for the C32 data after 250 °C represents disappearance of the particles below the limit of the CPC detector (~10 nm). (B) Evaporation profiles of diesel particles with initial sizes of 12 (green) and 30 nm (blue) and dotriacontane particles with an initial size of 30 nm (gray), obtained with NTDMA. The dashed lines are the calculated evaporation profiles of tetracosane ($C_{24}H_{50}$) and dotriacontane particles. For both plots, the diesel particles were sampled from the Cummins engine with the CA fuel at 20% load.

Figure 35A shows the changes in particle diameters measured in the RTDMA experiments for initial particle sizes of 70 and 120 nm, including data for the "more volatile" component of diesel particles obtained when the engine was operated with the CA fuel at 20% load. The evaporation profiles of dotriacontane and engine oil were similar between 30 and 130 °C, although dotriacontane was slightly more volatile. More importantly, however, the profile of the diesel particles (90, 110, and 150 °C) clearly overlapped the oil and dotriacontane curves, indicating that the volatility of the volatile components of the 70 and 120 nm diesel particles is similar to that of oil and dotriacontane. The oil contains some non-volatile particles which do not evaporate above 150 °C, whereas dotriacontane particles eventually disappeared from the measurable size range of RTDMA. This is indicated by the dashed line in the figure. The evaporation profiles of dotriacontane and engine oil were similar, indeed more similar than expected, since dotriacontane is a pure compound while engine oil is a complex mixture of hydrocarbons and additives of different volatilities. The oil would presumably give a less steep evaporation profile than dotriacontane. The similarity in the dotriacontane and oil profiles may imply that because of resolution limitations, the TDMA technique essentially measures an average volatility.

Another important feature in the evaporation profile of dotriacontane particles is that after the expected sharp decrease in size, the curve tails out to ~150 °C. This may be due to particle impurities that were less volatile than dotriacontane. It is also possible that the partial pressures of evaporated species in the heater reached sufficiently high values, relative to saturation vapor pressures, to reduce evaporation rates (38). Lastly, the vapor may have recondensed onto particles as they cooled downstream of the heater.

Results from the NTDMA experiments are shown in Figure 35B for "more volatile" 12 and 30 nm diesel particles obtained with CA fuel at 20% load, and laboratory-generated 30 nm dotriacontane particles. The evaporation profiles of 12-nm diesel particles up to 80 °C, 30-nm diesel particles up to 110 °C, and dotriacontane particles up to 110 °C are qualitatively similar. The slow evaporation of dotriacontane particles after 110 °C was possibly due to trace impurities which were less volatile than dotriacontane, build-up of evaporated species in the gas phase, or recondensation, as discussed above. Also shown in the figure are the evaporation profiles of dotriacontane and tetracosane ($C_{24}H_{50}$ *n*-alkane) calculated using a simple model for particle evaporation in the heater. In this model, the flow in the aerosol heater was assumed to be plug flow, and the temperature was assumed to be the same throughout the heater with a stepwise change to room temperature at the ends of the tube. The diameter change due to evaporation was calculated using the equation

$$\Delta Dp = -P/\rho_p(2M/\pi RT)^{1/2}\Delta t \tag{4}$$

which is applicable in the free-molecule regime, and where P, ρ, and M are the vapor pressure over a flat surface (temperature dependent), density (weakly temperature dependent), and molecular weight of dotriacontane or tetracosane, respectively. The partial pressure of the evaporating species in the gas phase is assumed to be zero. The vapor pressures were estimated using the method described by Lemmon and Goodwin (39), which is based on the law of corresponding states and uses the critical parameters (temperature and vapor pressure) of the *n*-alkanes. The Kelvin effect was not included in the calculation of the vapor pressure. The calculated evaporation profiles are shown as dashed lines in Figure 35B. The curve for tetracosane showed a steep drop starting at ~50 °C, while that for dotriacontane started to drop at ~100 °C. The model calculation for dotriacontane predicts a steeper evaporation profile than was observed in the experimental results. In addition, the experimental curve is shifted toward lower temperatures. This could be due to the model assumptions made for the flow and temperature profiles in the heater, and because we have neglected the Kelvin effect, which increases particle vapor pressures relative to bulk material. The evaporation profiles of the diesel particles had slopes similar to or slightly less steep than that of the experimental dotriacontane data. This may occur because diesel particles are a mixture of chemical compounds, although similar evaporation profiles were observed for dotriacontane and oil particles in the RTDMA experiments. Nevertheless, the observation that evaporation started at ~50 °C and ended at ~80 and ~110 °C for 12 and 30 nm particles, respectively, is probably best explained by the diesel particles being comprised of a mixture of compounds with volatilities between those of C24 and C32 alkanes. The gas chromatographic and TDPBMS analyses of fuel and oil described above showed that the major components of the fuel have volatilities equivalent to ~ C10-C24 alkanes, while those in oil are equivalent ~C22-C36 alkanes. Therefore, the volatile components of the nanoparticles are likely to be unburned oil.

6.2.3.6.2. External Mixing of the “More Volatile” and “Less Volatile” Particles

As demonstrated in Figures 31-33, the TDMA volatility measurements were able to separate the aerosol into “more” and “less” volatile particles. In this section the number concentrations for each type of particle are calculated by integrating the size distribution functions. Figure 36 shows the percentage of “more volatile” particles for different particle sizes with different fuels and engine loads. As expected, the percentage of “more volatile” particles decreased monotonically with increasing particle size. In addition, for a given particle size, the percentage of “more volatile” particles was less when the engine load was increased to 35%. This is consistent with a model of the diesel exhaust aerosol in which the nuclei mode is predominantly “more volatile” particles, while the accumulation mode is predominantly “less volatile” particles. This is one of the reasons why, when the engine load is increased and more organic compounds are combusted, the size of the nuclei mode decreases relative to the size of the accumulation mode.

6.2.3.6.3. Volume Fraction of the Volatile Components in “More” and “Less” Volatile Particles: Comparison of Mobility-Based and Mass-Based Analyses

The volume fraction, $F_{\text{volatile, mobility}}$, of volatile material in “more” and “less” volatile particles can be calculated using the volatility data and the equation

$$F_{\text{volatile, mobility}} = 1-(V_{\text{non-volatile}}/V_{\text{initial}}) = 1-(\pi Dp^3_{\text{non-volatile}}/6)/(\pi Dp^3_{\text{initial}}/6) \qquad (5)$$

where V_{initial} and Dp_{initial} are the volume and diameter before heating, and $V_{\text{non-volatile}}$ and $Dp_{\text{non-volatile}}$ are the volume and diameter of non-volatile cores after heating at temperatures above 110 °C. The volume calculated using equation (5) is the mobility-equivalent volume. The volume fractions obtained when the engine is run on CA fuel at 20% load are plotted in Figure 37 for different particle sizes. The “more volatile” particles were almost completely volatile.

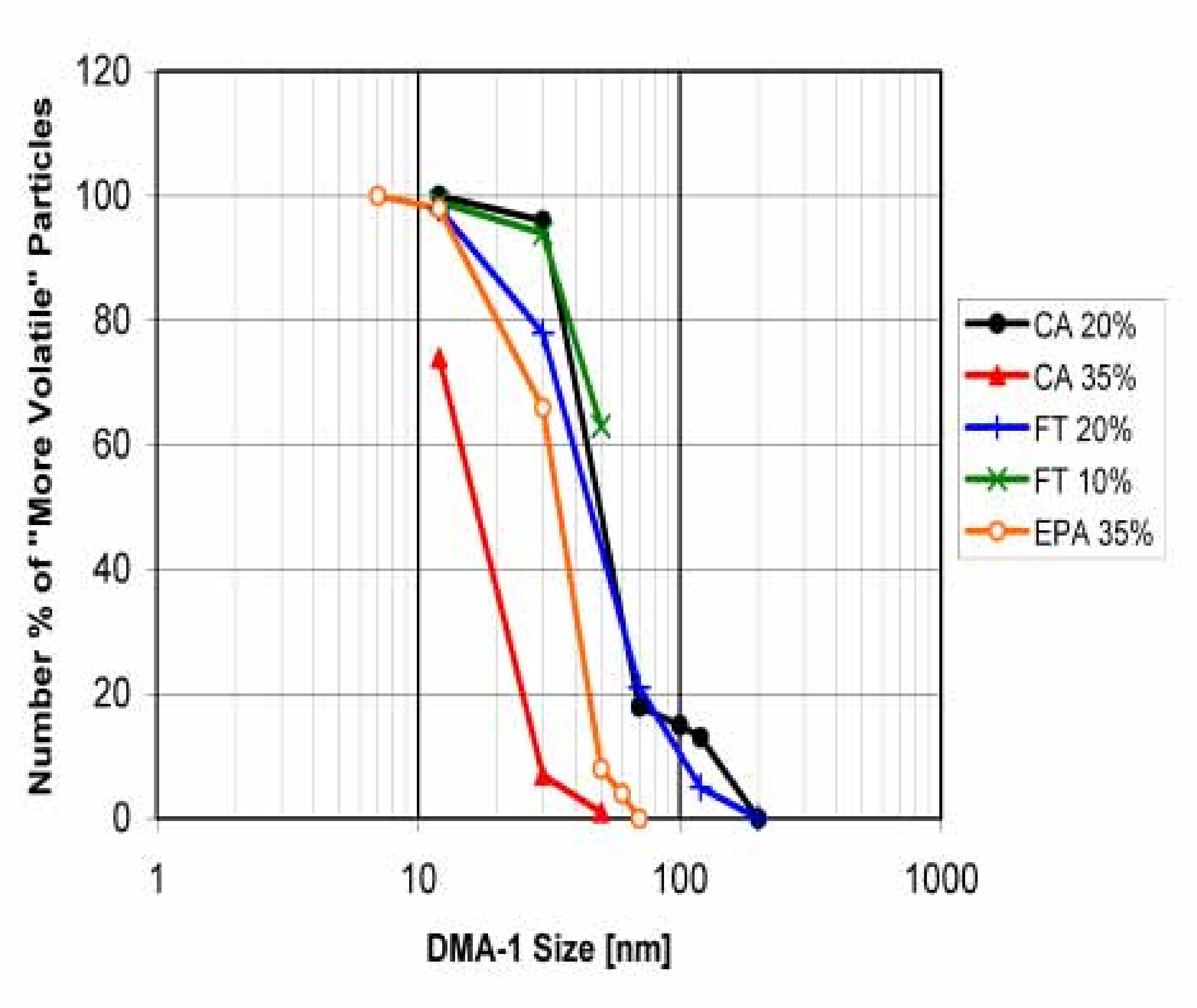

Figure 36. Percent number concentrations of “more volatile” particles for different initial sizes (DMA-1), calculated using the NTDMA and RTDMA volatility data. Particles were sampled from the Cummins engine with CA, Fischer-Tropsch, and EPA fuel at different engine loads.

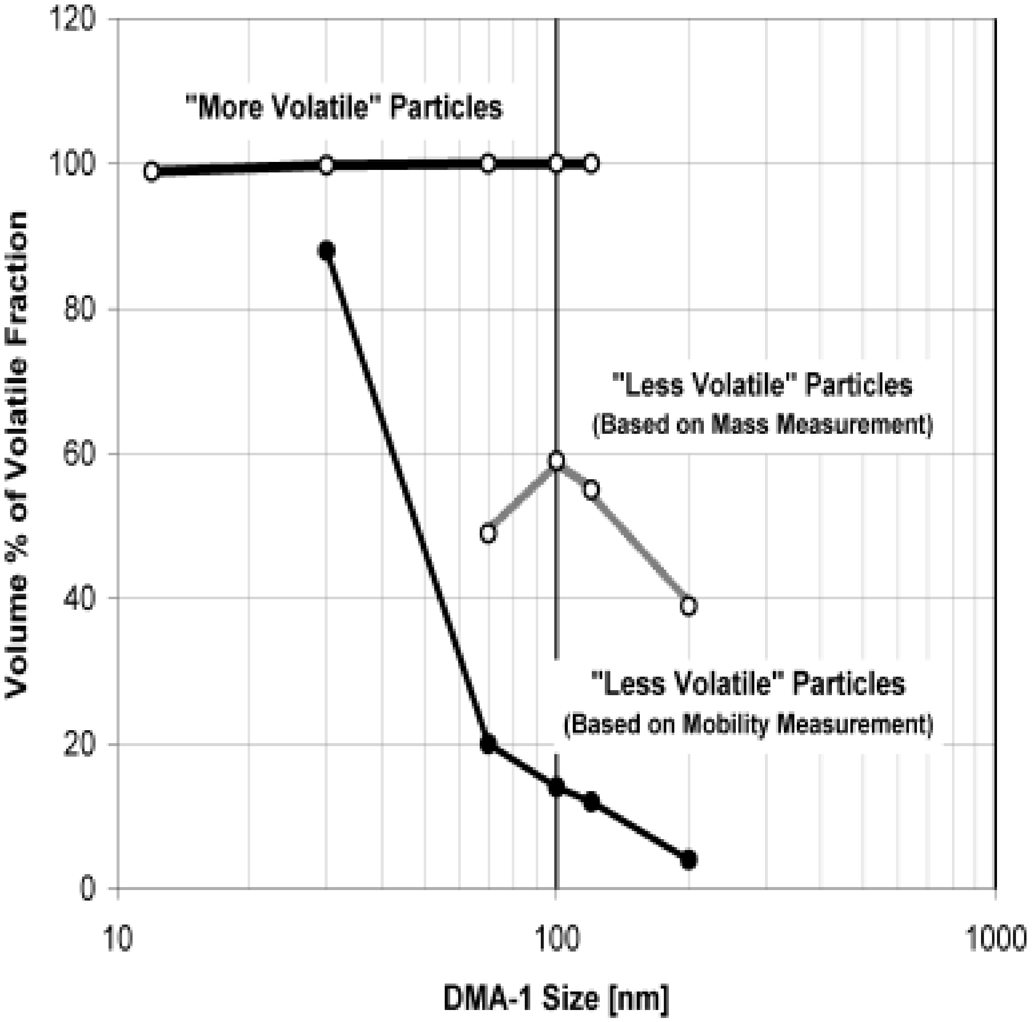

Figure 37. The volume percent of volatile material in less volatile and more volatile particles with different initial sizes (DMA-1). Values were calculated using the NTDMA, RTDMA, and RTDMA-APM volatility data for diesel particles from Cummins the engine with CA fuel at 20% load.

Assuming as an upper limit that these particles contained a 2.7 nm diameter non-volatile core (the actual mode diameter was not identified because of the 2.7-nm cut off of the NTDMA CPC), "more volatile" particles ≥ 12 nm (the smallest size analyzed) contained at least 99% volatile material. When combined with our previous conclusions regarding nanoparticle composition, it is estimated that for this fuel and load that lubricating oil composes at least ~95% of the "more volatile" particle volume.

On the other hand, the volatile fraction of the "less volatile" particles determined by the RTDMA varied significantly. The volatile fraction of the 30 nm particles was ~88%, while that of 70, 100, 120, and 200 nm particles was less than 20%, and decreased monotonically as the size increased. In order to further analyze the internal mixing state of the "less volatile" particles, in addition to the TDMA we also operated the APM analyzer for particle mass measurement (40). Because of the mass limit of the APM, we only analyzed particles with initial diameters of at least 70 nm. This experiment was performed because we were concerned that TDMA analysis based solely on particle mobility might not allow us to determine the internal mixing state of irregularly-shaped "less volatile" particles. For example, a soot particle which has pores between agglomerated primary carbon particles could hold a significant amount of volatile material in the interstitial space. The volatile components would evaporate upon heating and the true volume of the particle would decrease. This might not, however, result in a corresponding decrease in the mobility-based volume, because the mobility is not very sensitive to changes in the internal structure of irregularly-shaped particles. Indeed, we found that this was the case: the volume change determined by mass analysis was significantly larger than that determined by mobility analysis. For the CA fuel and 20% load, the evaporated mass as determined by the APM was 26%, 34%, 31%, and 19% for 70, 100, 120, and 200 nm particles, respectively. From these measurements, the true volume fraction of volatile components, $F_{\text{volatile, volume}}$, was estimated using the equation

$$F_{\text{volatile, volume}} = [1-(\rho_{\text{volatile}}/\rho_{\text{non-volatile}})(1-1/F_{\text{volatile, mass}})]^{-1} \tag{6}$$

where

$$F_{\text{volatile, mass}} = m_{\text{volatile}}/(m_{\text{volatile}} + m_{\text{non-volatile}}) \tag{7}$$

This equation can be derived from the relationship between volume, density, and mass of the volatile and non-volatile components, and the conservation of mass and volume. The quantity $F_{\text{volatile, mass}}$ is the mass fraction of volatile material calculated from the masses m_{volatile} and $m_{\text{non-volatile}}$ of volatile and non-volatile material determined from the evaporated mass measured by the APM. It is assumed that the densities of the volatile and non-volatile material are $\rho_{\text{volatile}} = 0.8$ g-cm^{-3} and $\rho_{\text{non-volatile}} = 2.2$ g-cm^{-3}, which are appropriate for alkanes and soot, respectively. The results are plotted in Figure 37. The true volume fraction of the volatile components were 40-60% in the size range studied, significantly higher than the fractions calculated from the mobility measurements. The volatile fraction had a local maximum at 100 nm, but we do not yet understand the reason for this. In addition, the behavior of the true volume fraction curve below 70 nm is not known.

6.2.3.6.4. Distribution of Volatile Components Across the Nuclei and Accumulation Modes

In the previous section, we estimated the fractions of volatile and non-volatile material present in single particles of a given size. In this section, we calculate the size-segregated volume contribution, across the nuclei and accumulation modes, of (a) volatile components in the "more volatile" particles, (b) volatile components in the "less volatile" particles, and (c) non-volatile components in the accumulation mode particles. The calculation combines the relative number concentrations of "more volatile" and "less volatile" particles (Figure 36) and the volume fractions of volatile components (Figure 37). Calculations are based on the mobility measurements for 12 and 30 nm particles and the mass measurements for particles ≥ 70 nm in diameter. Results are shown in Figure 38. Figures 38A and 38B show relative contributions and a volume-weighted size distribution of the absolute contributions of volatile, from both "more volatile" and "less volatile" particles and non-volatile components in "less volatile" particles. In Figure 38A, the expected trend is observed, in that the non-volatile volume fraction increased as the particle size increased, although there is again a local maximum at 100 nm. In Figure 38B, the blue curve is for dV/dlogDp, which was calculated by using the mobility diameter and assuming a spherical shape. The red curve is calculated by using the mass measurements for Dp ≥ 70 nm as described above. There is a significant discrepancy between the blue and red curves, which was caused by the irregular shapes of the accumulation mode particles. Note also that the absolute contribution of volatile components was distributed into two modes, one from the nuclei mode and the other from the accumulation mode, with seemingly comparable magnitude.

6.2.3.6.5. Hygroscopicity of Diesel Particles

Water uptake experiments were carried out with the engine running on CA (96 ppm S) and EPA (360 ppm S) fuels at 20% and 35% engine loads. This was to compare the effect of fuel sulfur content on the hygroscopicity of the diesel exhaust particles, and to shed a light on the potential role of sulfuric acid in particle nucleation (41, 42). According to the sulfuric acid-induced nucleation model, freshly nucleated particles would be enriched in sulfuric acid and water. Subsequent condensation of organic compounds onto the sulfuric acid core would reduce the fraction of sulfuric acid as the nuclei grow. Because sulfuric acid absorbs water, whereas uptake of water by organics should be negligible, it would be expected that smaller particles would be more hygroscopic than larger particles.

No water uptake was observed when the CA fuel was used at either engine load. When the EPA fuel was used, however, an increase in the particle size due to water uptake was observed with both the NTDMA and RTDMA. This indicated that the higher sulfur content of the EPA fuel increased the hygroscopicity, and hence changed the chemical composition of the nuclei-mode particles. The diameter growth factor, which is defined as the ratio of diameters Dp(wet)/Dp(dry), was obtained by measuring the size of particles downstream of the humidity conditioner under dry (6-7% RH) and wet (80% in RTDMA and 85% in NTDMA) conditions, and are plotted in Figure 39 for various initial particle sizes. Figures 39A and 39B are for the 20% and 35% engine load conditions, respectively. Data points at 30 nm and below were measured using the NTDMA and those at 50 nm and above were measured using the RTDMA.

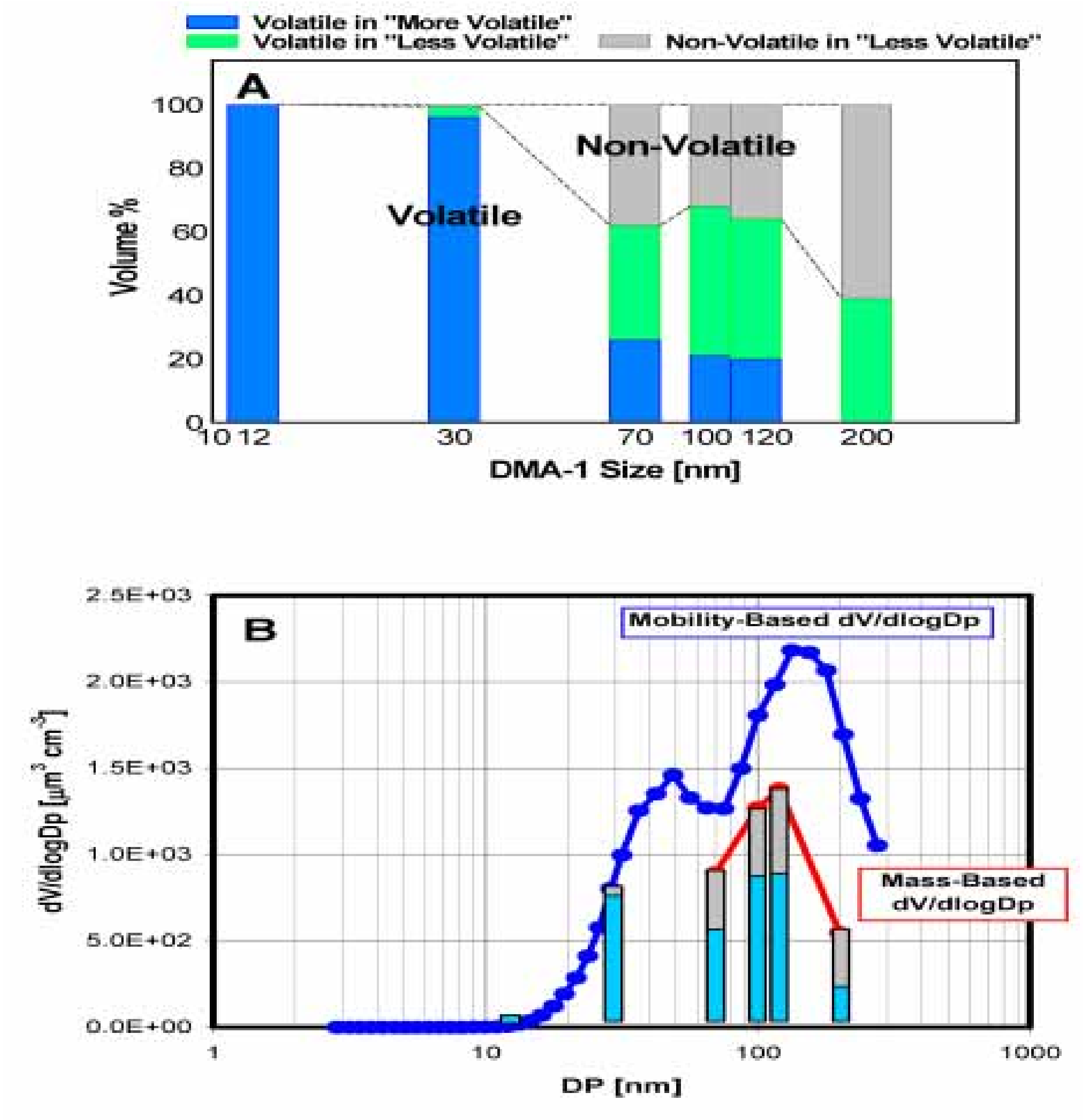

Figure 38. Distribution of the volatile fraction across the diesel particle nuclei and accumulation modes for CA fuel at 20% load. (A) The volume percent of volatile components in the nuclei and accumulation modes and of non-volatile components in the accumulation mode. (B) The volume distribution of the volatile components in the volume-weighted size distribution plot. The blue curve was calculated using volumes based on the mobility diameters and an assumed spherical shape. The red curve was calculated using volumes calculated from APM measurements and assumed material densities. The light blue portion of t he vertical bars indicates the volume fraction of volatile material at a given size. The bar data for 12 and 30 nm were calculated using measured mobilities.

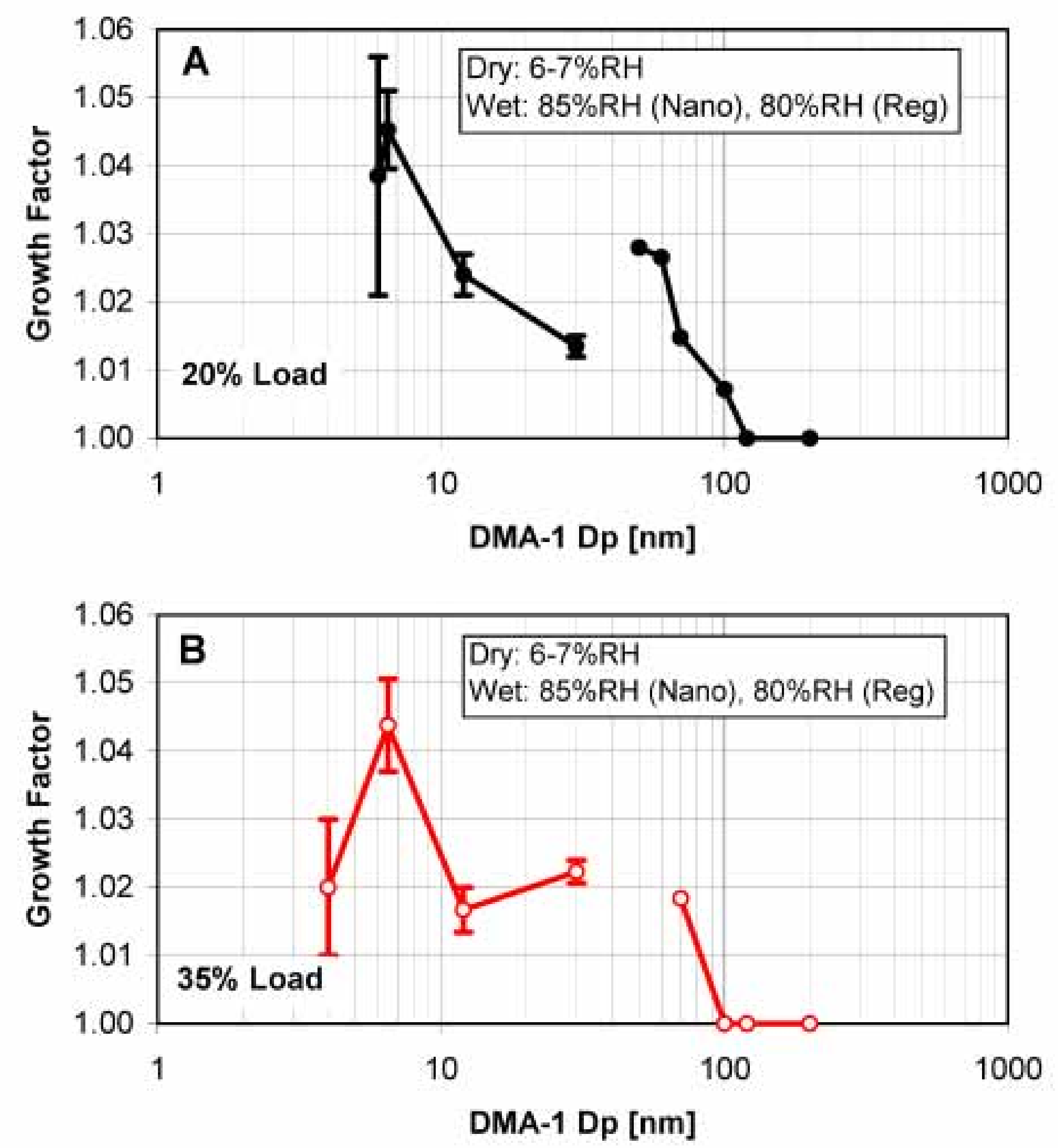

Figure 39. Hygroscopic growth factors measured for diesel particles with different initial sizes (DMA-1). Particles were sampled from the Cummins engine with EPA fuel at (A) 20% load and (B) 35% load. Data for Dp ≤ 30 nm were obtained using the NTDMA, and those for Dp ≥ 50 nm were obtained using the RTDMA.

Because of variability in the particle concentration and the small numbers of particles detected, NTDMA data suffered from errors in determining the mean diameter for each condition, especially below 10 nm. Large error bars below 10 nm represent uncertainties in calculating the growth factors. The plots of the NTDMA and RTDMA results have two things in common with respect to the size dependence of hygroscopicity: the highest growth factor was observed at 6.5 nm, and the growth factor decreased to zero (below detection limit) at ~100 nm. The overall trend is therefore that smaller particles were more hygroscopic, which is consistent with the sulfuric acid-induced nucleation model. There was no apparent dependence of hygroscopicity on engine load, even though formation of more sulfuric acid was expected at the higher load because of the higher combustion temperature.

It is worth noting that the growth factor for 4 nm particles at 35% load was significantly lower than that at 6.5 nm, despite the size dependence observed at other sizes. This was not due to the Kelvin effect, as will be discussed below. If all the particles were formed by the sulfuric acid nucleation mechanism, 4 nm particles should be the most hygroscopic. However, as described in the section on SMPS results and as shown in Figure 14, an additional intense peak was observed under this condition at about 4 nm. Because of the distinct appearance of this mode in the size distribution, the formation mechanism might be totally different from that of the larger particles, resulting in different hygroscopicities. For example, those particles might have been formed by nucleation of another low-volatility species, such as heavy organics, which are not as hygroscopic as sulfuric acid. The hygroscopicity of the 4 nm particles would then be significantly lower than that of the nuclei-mode particles ($D_p \geq 6.5$ nm).

Another point to note is that the growth factor increases between 30 and 50 nm at 20% load. It therefore appears that the hygroscopicity decreased as the particle size increased from 6.5 nm to 12 and 30 nm, then increased from 30 nm to 50 nm, and then decreased before going to zero. It is surprising that the size dependence of hygroscopicity would behave in this way, while the size distribution did not show any peculiar trends between 6.5 and 50 nm (Figure 14). One possible explanation might be that the ~0.5 s residence time in the NTDMA humidity conditioner was too short for 30 nm particles to completely grow to the equilibrium size, while the ~5 s residence time in the RTDMA humidity conditioner was long enough for 50 nm particles to equilibrate. An example of retarded water uptake was previously reported for sulfuric acid particles coated by a carboxylic acid film, and was attributed to slow mass transfer of water molecules across the organic surface layer (43). They observed noticeable decreases in growth factors when the reaction time was decreased from 10 to 6 s and when the thickness of the surface layer was increased. A similar effect may have played a role in our experiments, and adds uncertainty to the growth factors (especially for larger particles) determined by the NTDMA and perhaps also by the RTDMA. Understanding and evaluating this effect in our instruments will require further experiments.

As an aid in interpreting the observed growth factors, we estimated the physical size of the hygroscopic core. For this calculation we assumed that the core was made of sulfuric acid, that sulfuric acid was solely responsible for the observed growth while other components in the particles, such as organics, did not take up water, and that the hygroscopicity of sulfuric acid was not affected by the presence of the other species in the particles (Zdanovskii-Stokes-Robinson model; ref. 44). The volume fraction of sulfuric acid plus water (in equilibrium for non-zero RH) was calculated using the equation

$$V_{H2SO4 + H2O}(6\%)/V_{total}(6\%) = [(V_{total}(85\%)/V_{total}(6\%)) - 1]/[(V_{H2SO4 + H2O}(85\%)/V_{H2SO4 + H2O}(6\%)) - 1] \qquad (8)$$

where $V_{total}(85\%)/V_{total}(6\%)$ is the volume ratio of the diesel particles at the wet and dry conditions, which was calculated as the cube of their experimental growth factor, $(Dp(85\%)/Dp(6\%))^3$. $V_{H2SO4+H2O}(85\%)/V_{H2SO4+H2O}(6\%)$ is the volume ratio of pure sulfuric acid droplets at 85% and 6% RH, respectively, obtained from literature (e.g., ref. 45). The Kelvin effect, which reduces the relative humidity experienced by particles because of the elevated saturation vapor pressure, was included in this calculation. The diameter of the diesel particles was used to calculate the ratio of the water vapor pressure at the particle's surface to that over a flat surface ($P_{particle}/P_{flat\ surface}$), and the effective relative humidity was calculated by dividing the measured RH by this vapor pressure ratio. Using this method, we estimated a volume fraction of sulfuric acid of ~10% for the 6.5-nm particles, which had a growth factor of 1.045 at both engine loads. This corresponds to a ~3 nm sulfuric acid/water core. In contrast to this, we can also estimate the maximum possible sulfuric acid volume fraction for 6 nm diesel particles in the CA fuel experiment. We concluded those particles were non-hygroscopic, which was based on the observation that the growth factor was less than 1.01. By following the same procedure, we estimate the growth factor of 1.01 at 6 nm corresponds to ~2% of the volume fraction. Growth factors were also used to calculate the volume fraction, equivalent particle diameter, and mass fraction of sulfuric acid (and water) for other conditions, and the results are summarized in Table 2. Calculation of mass fractions required the density of the non-hygroscopic fraction of the particle, which was assumed to be 0.8 g cm^{-3}. It is intended that the data in this table will be used in a future modeling study of diesel particle formation, but details will not be discussed here.

As was mentioned earlier, the calculated volume fraction of sulfuric acid in particles at 35% load was lower for 4 nm than for 6.5 nm, even though the Kelvin effect was taken into account. This indicates that the 4 nm particles were less hygroscopic than the 6.5 nm particles. The calculated values may have considerable error, especially for the accumulation mode particles (i.e., Dp ≥ 100 nm in the 20% load data and Dp ≥ 70 nm in the 35% load data), for a few reasons. One is that the large non-volatile core (which is presumably soot) takes up a large fraction of volume and will not grow at a high relative humidity. This reduces the measured growth factor even if the remaining volume has a composition similar to that of smaller particles without a core. Calculated mass fractions may also be inaccurate because the density (0.8 g cm^{-3}) assumed for the non-hygroscopic volume might be too low.

The calculated sulfuric acid mass fractions and equivalent particle diameters at 0% RH in the size range from 30 to 70 nm were about 2-5% and 7-17 nm, respectively, in agreement with previously reported values. In Phase 1 of this study, the mass fraction and equivalent diameter of sulfuric acid were estimated using TDPBMS data to be 1.2-5.3% and 7-12 nm for 41 nm (mass median diameter; MMD) particles, and 0.7-2.3% and 8-13 nm for 58 nm MMD particles, respectively (16, 17). In another study, Shi and Harrison (41) estimated a sulfuric acid mass fraction of ~6% for 30-73 nm particles collected by impaction and subjected to offline sulfate analysis.

Table 2. Volume fraction, equivalent diameter, and mass fraction of sulfuric acid in diesel particles, calculated using hygroscopic growth factors.

DMA-1 Size [nm]	TDMA Used	Growth Factor	$H_2SO_4 + H_2O$ (6-7%RH)		H_2SO_4 only (0%RH)	
			Volume Fraction	Equivalent Diameter [nm]	Mass Fraction	Equivalent Diameter [nm]
20% load						
6 nm	Nano	1.039	8%	3	11%	2
6.5 nm	Nano	1.045	10%	3	12%	3
12 nm	Nano	1.024	4%	4	5%	3
30 nm	Nano	1.014	2%	8	2%	7
50 nm	Regular	1.028	4%	17	5%	14
60 nm	Regular	1.027	4%	20	5%	17
70 nm	Regular	1.014	2%	19	3%	16
100 nm	Regular	1.007	1%	22	1%	18
120 nm	Regular	1				
35% load						
4 nm	Nano	1.020	5%	2	7%	1
6.5 nm	Nano	1.044	9%	3	12%	3
12 nm	Nano	1.017	3%	4	4%	3
30 nm	Nano	1.022	3%	9	4%	8
70 nm	Regular	1.018	3%	21	4%	17
100 nm	Regular	1				

7. CONCLUSIONS

The Nano-DMA/TDPBMS and TDMA analyses of diesel particles from the Caterpillar and Cummins engines have yielded important new information on the size-dependent composition of diesel particles, their mixing characteristics, and particle formation processes. These studies have clearly demonstrated the power of the Nano-DMA/TDPBMS and TDMA techniques for diesel particle analysis. This study does not address issues related to exhaust dilution and its effects on particle size distributions, or the relationship between diesel particles generated in the laboratory and those from on-road vehicles. The major conclusions that can be drawn from these data for the specific experimental conditions studied here include:

1) The TDPBMS is a valuable tool for analyzing the chemical composition of total diesel particles, and, when coupled with the Nano-DMA, diesel nanoparticles. Through the use of mass-spectral matching techniques it can be used to obtain quantitative information (in real-time for total particles and near real-time for nanoparticles) on the contributions from major particulate sources, including unburned oil and fuel, oxidized organic combustion products, and sulfuric acid. As is the case for any technique, however, the TDPBMS has its limitations. No information is obtained on individual organic compounds, or nonvolatile soot or metal oxides.

For source apportionment of the volatile component of particulate engine exhaust (i.e., organics and sulfuric acid), which has only a few potential sources, this approach offers advantages over the traditional use of GC-FID and GC-MS analyses, and real-time single particle techniques. TDPDMS is much easier and more rapid than GC-FID or GC-MS analysis, and TDPBMS sampling is more accurate than impactor or filter methods. As we have shown here, the TDPBMS can sample particles containing compounds at least as light as ~C15 without significant evaporative losses. On the other hand, it is well known that filter and impactor samples are subject to serious artifacts from volatilization and adsorption, and therefore cannot be used to collect representative samples of particles containing semi-volatile compounds. Use of impactors is even more problematic for nanoparticle collection, as it is difficult to collect sufficient sample for analysis, and studies have shown that the mass collected on even greased Nano-MOUDI stages are dominated by particle bounce from upper stages. Denuders can improve the quality of filter samples for large diesel particles, but are also subject to artifacts and have not yet been thoroughly characterized for complex organic samples. They have generally not been used by the combustion community. Use of GC-FID or GC-MS total ion chromatograms to apportion fuel and oil components collected by impactor or filter samplers is therefore not reliable. Use of speciated GC-MS analysis for particle source apportionment is similarly affected by sampling problems. In addition, one must remember that the use of organic molecular tracers is based on the analysis of a very small fraction of the total diesel particulate organic matter (typically less than 10%) which can be identified. Conversely, TDPBMS analysis is based on all the organics, including the 90% or more of the material (branched and cyclic hydrocarbons) that is unresolved by GC-MS.

Single-particle mass spectrometers have the same real-time analytical capabilities as TDPBMS, but are not as well-suited for organic analysis. The multiphoton laser desorption/ionization method most commonly used in these instruments is far more destructive than thermal desorption/electron ionization, and generally fragments organics so thoroughly as to remove most of the useful mass spectral information. Multi-laser methods using single-photon VUV ionization offer the promise of less destructive analysis, but are not yet sufficiently well developed. The laser-based methods could be useful for analyzing the refractory soot and metal oxide components, but because of the extensive fragmentation, it is generally difficult to identify small amounts of soot in the presence of a significant organic component.

2) The TDPBMS samples compounds at least as volatile as ~C15 hydrocarbons with little loss from evaporation, and therefore does not suffer from the volatilization and adsorption artifacts associated with impactor or filter sampling methods commonly used to collect particles for off-line GC-MS or GC-FID analysis. In addition, the use of the Nano-DMA for nanoparticle size selection provides nanoparticle samples that are not affected by artifacts, such as the particle bounce phenomenon that currently makes Nano-MOUDI samplers unreliable for nanoparticle collection.

3) The Nano-TDMA, Regular-TDMA, and Regular-TDMA-APM are valuable tools for measuring the volatility and hygroscopicity of diesel nanoparticles and larger diesel particles. The measurements provide information on particle mixing properties, sulfuric acid content, and the volatility of organic components, which can be used to determine compound carbon numbers. The Nano-TDMA capability for measuring nanoparticle volatility fills an important gap in the TDPBMS capabilities, since TPTD analysis is not a reliable method for measuring the volatility of small nanoparticle samples. This is due to adsorption of evaporating compounds onto vaporizer soot deposits. Because the inhalation and deposition behavior of nanoparticles is determined by particle mobility rather than aerodynamic properties, mobility-based measurements are especially well-suited to diesel nanoparticle studies. By coupling mobility selection with the APM mass measurement, information on the relationship between mobility size and aerodynamic size can be obtained. For example, the Regular-TDMA-APM measurements showed that the volatile fraction of diesel particles was larger than that which was estimated by mobility-based TDMA measurements.

4) TDPBMS analyses indicate that the organic component of total diesel particles is comprised primarily of unburned lubricating oil. The oil contribution is estimated to be greater than 70% in all studies, a lower limit which is determined by the worst-case resolution of the mass spectral matching technique. In cases where resolution is improved through use of Fischer-Tropsch fuel or TPTD analysis, the oil contribution is estimated to be at least 95%.

5) TPTD profiles of oil and total diesel particles indicate that the oil in particles derives primarily from evaporation from the cylinder walls, although there may also be a significant component from atomization.

6) Nano-DMA/TDPBMS analyses and Nano-TDMA volatility measurements indicate that the organic component of diesel nanoparticles is comprised almost entirely of unburned lubricating oil.

7) Nano-TDMA analyses indicate that the volatility of nanoparticles does not change with fuel or engine load, indicating that the organic composition does not depend significantly on these parameters.

8) TDPBMS analyses employing a thermodenuder show little or no change in the organic composition of total diesel particles with component volatility, indicating that the major compound classes (alkanes, cycloalkanes, and aromatics) are distributed relatively uniformly across the volatility spectrum.

9) TDPBMS analyses of total diesel particles and nanoparticles indicate that the contribution of oxidized organic combustion products and PAHs, and sulfuric acid (also analyzed by Nano-TDMA), are only minor diesel particulate components. Oxidized organic combustion products and PAHs are known to be present in small quantities in large diesel particles (from GC-MS analyses by others), but no previous information is available for diesel nanoparticles.

10) Nano-TDMA, Regular-TDMA, and Regular-TDMA-APM volatility measurements indicate that two types of particles of different volatility are externally mixed across the nuclei and accumulation modes. The chemical components are distributed between two particle types: (a) “less volatile” particles, comprised of a significant non-volatile core (probably elemental carbon) and a volatile organic component, and (b) “more volatile” particles, containing predominantly organics and sometimes small amounts of sulfuric acid. The volatile components contribute more than 99% of the “more volatile” nanoparticle volume.

11) Nano-TDMA and Regular-TDMA measurements of water uptake indicate that diesel nanoparticles formed with high sulfur (360 ppm S) EPA Pump fuel contain small amounts of sulfuric acid, which may enhance nucleation. No sulfuric acid was detected in nanoparticles formed using lower sulfur (96 ppm S) CA fuel.

12) Nano-TDMA volatility measurements detect residual species a few nanometers in diameter when “more volatile” particles are evaporated at high temperatures. These may be non-volatile cores (soot or metal oxide), or single molecules or molecular clusters of low-volatility organic compounds. Because of the ~2.7 nm detection limit of the UCPC it is not possible at this time to determine the nature of these species, and therefore the percentages of non-volatile and completely volatile nanoparticle nuclei. We cannot, therefore, state with certainty the extent to which nanoparticle formation involves multicomponent homogeneous nucleation of volatile compounds or is initiated by the formation of non-volatile soot or metal oxide seeds < 2.7 nm in diameter.

The general model of diesel nanoparticle formation and chemistry that emerges from these results is that nucleation involves either a multicomponent mixture of some combination of low volatility organics, sulfuric acid, water, and ammonia, or formation of non-volatile nuclei of either elemental carbon or metal oxide. This still appears to be an open question, and both processes may be operating, depending on conditions. Once nucleation occurs, growth appears to involve condensation of organic compounds coming primarily from unburned lubricating oil. The resulting particles are an external mixture, some of which are nearly completely volatile (within detection limits), whereas others contain a significant non-volatile core. The resulting nuclei-mode particles are predominantly the "more volatile" particles, whereas the accumulation mode is predominantly the "less volatile" particles.

8. SUGGESTIONS FOR FUTURE RESEARCH

Although this research project has addressed a number of important questions regarding nanoparticle chemistry and formation processes, there is still much more work that could be done. In the course of these studies, we have gained a great deal of experience with a variety of new techniques that had not been previously used for diesel particle analysis. We are now more aware of the particular strengths and weaknesses of these techniques and will be able to employ them with even greater success in the future. We now have a demonstrated capability for obtaining mass spectra using the Nano-DMA/TDPBMS and volatility and water uptake profiles using the TDMAs and APM, for size-selected diesel nanoparticles as well as the total particle sample. These data provide information on organic composition and sources, sulfuric acid content, vapor pressures, volatile and non-volatile contributions to particle numbers and mass, as well as particle mixing characteristics. Through the use of mass spectrally distinct fuels and lubricating oils we can distinguish and quantify fuel and oil contributions to particle mass. The future use of synthetic oils could provide an even more powerful mass spectral marker for these analyses, and development of techniques for preparing standard particle mixtures of fuel and oil, and the use of statistical analysis methods would improve our mass spectral matching capabilities. Because the TDPBMS can analyze total diesel particles in real time, it should also be possible to use this approach to follow changes in organic composition during transient variations in engine conditions. Because of the widespread use of GC-MS analysis for engine emission studies, and the growing use of single-particle analysis methods, it would be valuable to perform an inter-comparison study using those techniques and various methods of particle collection (for GC-MS). While we have only applied our methods thus far to diesel engines, they could also be used in studies of gasoline or compressed natural gas engines. Important questions include, for example, the roles of organics, sulfuric acid, and non-volatile species in nucleation, the relative contributions of fuel and oil to particle mass, the importance of oil vaporization and atomization in particle formation, and the effect of shape and density on diesel particle measurements. We have also only studied particle formation over a very limited set of conditions, and in the future need to investigate the effects of higher engine loads, fuel and oil composition, and engine operation. Such studies would provide a much more complete understanding of the chemistry and mechanisms of particle formation in combustion systems, which is necessary for developing better approaches for controlling particulate emissions.

9. REFERENCES

(1) Pope, C. A.; Thun, M. J.; Namboodiri, M. M.; Dockery, D. W.; Evans, J. S.; Speizer, F. E.; Heath, C. W. *Am. J. Respir. Crit. Care Med.* **1995,** *151*, 669-674.

(2) Seaton, A.; MacNee, W.; Donaldson, K.; Godden, D. *Lancet* **1995,** *345*, 176-179.

(3) Kittelson, D. B. *J. Aerosol Sci.* **1998,** *29*, 575-588.

(4) Ferin, J.; Oberdorster, G.; Penny, D. P. *Am. J. Respir. Cell Mol. Biol.* **1992,** *6*, 535-542.

(5) Donaldson, K.; Beswick, P. H.; Gilmour, P. S. *Toxicol. Lett.* **1996,** *88*, 293-298.

(6) Oberdorster, G. *Inhal. Toxicol.* **1996,** *8*, 73-89.

(7) Donaldson, K.; Li, X. Y.; MacNee, W. *J. Aerosol Sci.* **1998,** *29*, 553-560.

(8) Marple, V. A.; Rubow, K. L.; Behm, S. M. *Aerosol Sci. Technol.* **1991,** *14*, 434-446.

(9) Kleeman, M. J.; Schauer, J. J.; Cass, G. R. *Environ. Sci. Technol.* **2000,** *34*, 1132-1142.

(10) McMurry, P. H. *Atmos. Environ.* **2000,** *34*, 1959-1999.

(11) Chen, D. R.; Pui, D. Y. H.; Hummes, D.; Fissan, H.; Quant, F. R.; Sem, G. J. *J. Aerosol Sci.* **1998,** *29*, 497-509.

(12) Tobias, H. J.; Ziemann, P. J. *Anal. Chem.* **1999,** *71*, 3428-3435.

(13) Tobias, H. J.; Kooiman, P. M.; Docherty, K. S.; Ziemann, P. J. *Aerosol Sci. Technol.* **2000**, *33*, 170-190.

(14) Tobias, H. J.; Ziemann, P. J. *Environ. Sci. Technol.* **2000,** *34*, 2105-2115.

(15) Tobias, H. J.; Docherty, K. S.; Beving, D. E.; Ziemann, P. J. *Environ. Sci. Technol.* **2000,** *34*, 2116-2125.

(16) Tobias, H. J.; Beving, D. E.; Ziemann, P. J.; Sakurai, H.; Zuk, M.; McMurry, P. H.; Zarling, D.; Waytulonis, R.; Kittelson, D. B. *Environ. Sci. Technol.* **2000,** *35,* 2233-2243.

(17) Ziemann, P. J.; McMurry, P. H. "Chemical Analysis of Diesel Nanoparticles Using a Nano-DMA/Thermal Desorption Particle Beam Mass Spectrometer", October 2000, Project No. E-43-4, Coordinating Research Council, Inc., Alpharetta, GA.

(18) Chen, D. R.; Pui, D. Y. H. *Journal of Nanoparticle Research* **1999,** *1*, 115-126.

(19) Liu, B. Y. H.; Pui, D. Y. H. *J. Colloid Interface Sci.* **1974,** *47*, 155-171.

(20) Knutson, E. O. *J. Aerosol Sci.* **1975,** *6*, 443-451.

(21) Wang, S. C.; Flagan, R. C. *Aerosol Sci. Technol.* **1990,** *13*, 230-240.

(22) Fuchs, N. A. *Geophys. Pura Appl.* **1963,** *56*, 185-193.

(23) Liu, P.; Ziemann, P. J.; Kittelson, D. B.; McMurry, P. H. *Aerosol Sci. Technol.* **1995,** *22*, 293-313.

(24) Liu, P.; Ziemann, P. J.; Kittelson, D. B.; McMurry, P. H. *Aerosol Sci. Technol.* **1995,** *22*, 314-324.

(25) Kinney, P. D.; Pui, D. Y. H.; Mulholland, G. W.; Bryner, N. P. *J. Res. Natl. Inst. Stand. Technol.* **1991,** *96*, 147-176.

(26) Rader, D. J.; McMurry, P. H. *J. Aerosol Sci.* **1986,** *17*, 771-787.

(27) Chen, D.-R.; Pui, D. Y. H.; Hummes, D.; Fissan, H.; Quant, F. R.; Sem, G. J. *J. Aerosol Sci.* **1997,** *29*, 497-509.

(28) Orsini, D. A.; Wiedensohler, A.; Stratmann, F.; Covert, D. S. *J. Atmospheric and Oceanic Technology* **1999,** *16,* 760-772.

(29) Ehara, K.; Hagwood, C.; Coakley, K. J. *J. Aerosol Sci*. **1996**, *27*, 217-234.

(30) Crable, G. F.; Coggeshall, N. D. *Anal. Chem.* **1958,** *30*, 310-313.

(31) Hinds, W. C. *Aerosol Technology*, 2nd ed.; John Wiley & Sons: New York, 1999.

(32) Piacente, V.; Fontana, D.; Scardala, P. *J. Chem. Eng. Data* **1994,** *39*, 231-237.

(33) Weast, R. C., Ed. *Handbook of Chemistry and Physics*; CRC Press: Boca Raton, FL, 1982.

(34) Fraser, M. P.; Cass, G. R.; Simoneit, B. R. T. *Environ. Sci. Technol.* **1998,** *32*, 2051-2060.

(35) Black, F.; High, L. *SAE Paper* 790422, 1979.

(36) Simoneit, B. *Atmos. Environ*. **1984**, *18*, 51-67.

(37) Rogge, W. F.; Hildemann, L. M.; Mazurek, M. A.; Cass, G. R.; Simoneit, B. R. T. *Environ. Sci. Technol.* **1993,** *27*, 636-651.

(38) Zhang, S.-H.; Seinfeld, J. H.; Flagan, R. C. *Aerosol Sci. Technol.* **1993,** *19*, 3-14.

(39) Lemmon, E. W.; Goodwin, A. R. H. *J. Phys. Chem. Ref. Data* **2000,** *29*, 1-39.

(40) McMurry, P. H.; Wang, X.; Park, K.; Ehara, K. *Aerosol Sci. Technol,* **2002,** *36*, 1-12.

(41) Shi, J. P.; Harrison, R. M. *Environ. Sci. Technol.* **1999,** *33,* 3730-3736.

(42) Khalek, I. A.; Kittelson, D. B.; Brear, F. *SAE Technol. Pap. Ser.* **2000,** 2000-01-0515.

(43) Xiong, J. Q.; Zhong, M.; Fang, C.; Chen, L. C.; Lippmann, M. *Environ. Sci. Technol.* **1998,** *32,* 3536-3541.

(44) Stokes, R. H.; Robinson, R. A. *J. Phys. Chem.* **1966,** *70,* 2126-2130.

(45) Liu, B. Y. H.; Levi, J. In *Generation of Aerosols and Facilities for Exposure Experiments,* K. Willeke. Ann Arbor Science**,** Ann Arbor, Michigan, 1980, pp. 317-336.

10. GLOSSARY OF ACRONYMS

APM: aerosol particle mass analyzer

CPC: condensation particle counter

DMA: differential mobility analyzer

GC-MS: gas-chromatography-mass spectrometry

MOUDI: microorifice uniform deposit impactor

Nano-MOUDI: nano-microorifice uniform deposit impactor

NDMA: nano-differential mobility analyzer

NSMPS: nano-scanning mobility particle sizer

NTDMA: nano-tandem differential mobility analyzer

RDMA: regular-differential mobility analyzer

RTDMA: regular-tandem differential mobility analyzer

RTDMA-APM: regular-tandem differential mobility analyzer-aerosol particle mass analyzer

SIM: selected ion monitoring

SMPS: scanning mobility particle sizer

TDMA: tandem differential mobility analyzer

TDPBMS: thermal desorption particle beam mass spectrometer

TPTD: temperature programmed thermal desorption

UCPC: ultrafine condensation particle counter

VRTDS: variable residence time dilution system